

CHARACTERIZATION OF FUNGAL GROWTH ON LENZING BEECH LOGS

C. Gradinger¹, A. Promberger³, M. Schwanninger^{2,4}, K. Messner⁵, and H. Sixta⁶

¹Competence Center Wood, 1060 Vienna, Austria,

²Competence Center Wood, 1190 Vienna, Austria,

³Competence Center Wood, 4860 Lenzing, Austria,

⁴BOKU - University of Natural Resources and Applied Life Sciences, 1190 Vienna,

⁵University of Technology Vienna, 1060 Vienna, Austria,

⁶Lenzing AG, R&D, 4860 Lenzing, Austria

Fungal attack is of great influence on the quality of beech wood stored on wood yards of the pulp and paper industry. Microbiological inspection of fungal species appearing on log surfaces of the Lenzing wood yard revealed numerous fruit bodies of two dominating fungi, which are common on hardwood. In order to display the impact of these fungal species on beech wood,

spectroscopic methods (FT-NIR) on controlled infected beech wood were performed and the production of ligninolytic enzymes of the respective species was recorded.

Keywords: *dissolving pulp, Fagus sylvatica L., FT-NIR, log storage, white rot fungi*

Introduction

The fast decay of certain hardwood species such as beech wood (*Fagus sylvatica* L.) during the storage of logs and chips is a well-known problem in the pulping industry [Smuldki, 1996, Sixta et al., 2004]. Wood logs, which have been stored in wood yards for a long time, are highly exposed to seasonal changes in humidity, temperature, and solar radiation. Humid environment and shady areas are ideal prerequisites for fungal attack. Inspection of the Lenzing wood yard showed that numerous fruit bodies of two different kinds occurred on longer stored logs.

Identification

Microbiological investigation of fruit bodies, growing densely on the cross sections of logs, was carried out by the use of special selective media [Hunt et al., 1971]. Fungal species were isolated and brought into pure culture. The resulting strains were used for all further investigations. For comparison of these isolates with a typical wood degrader, the

selective white rot fungus *Ceriporiopsis subvermispota*, which is well known from biopulping experiments [Messner et al., 1998, Akhtar et al., 2000], was used.

Enzyme production and NIR spectroscopy

Wood inhabiting fungi, which are able to depolymerise lignin, are known to produce lignin degrading enzymes like lignin-peroxidase, manganese-peroxidase and laccase. In order to compare the ability of lignin degradation of the identified isolates, the activity of manganese peroxidase and laccase was measured. For determining the amount of degradation, mass loss of beech wood chips, inoculated for several weeks with the respective isolates, was determined. Additionally, the effects of these isolates on lignin structure were verified by FT-NIR spectroscopy, which is known to be a rapid and powerful technique for the determination of wood components and the changes in wood structure [Schwanninger et al., 2004].

Experimental

Controlled infection

Cultures of the main identified isolates were grown on plates with 2.5 % malt extract agar and mixed in a commercial blender under sterile conditions with the additional nutrition source corn steep liquor (1 malt extract agar plate / 70 ml 2 % CSL (w/v)). Batches of 100 g beech wood chips (wet weight) with a dry content of 50 % were sterilized for 10 min at 121°C and inoculated with 50 ml of the mycelium suspension. Inoculated chips were incubated for 10 weeks at 28 °C. For determination of mass loss, chips were oven dried (105°C / 24h) before inoculation and weight, evacuated with tap water and prepared for inoculation as described above. Dry weight was calculated after inoculation again and mass loss was determined. For enzyme measurements, inoculated chips were milled to particles (see below). Sterilized chips with only corn steep liquor were used as a reference for all following experiments.

Enzyme production

Fungal manganese peroxidase and laccase activity was measured by means of a photometric assay with 2,2-Azino-bis-3-ethylenbenzothiazoline-6-sulfonic acid (ABTS) as substrate. 4 parallel batches of 3 g beech wood particles (3.5 mm, dry content 50 %) were steam sterilized and inoculated with the mycelium suspension (see above) to reach a total moisture content of 200 %. Batches were incubated for 3, 4, 5, 6, 7, 8, 9, 10, and 12 days. After incubation, wood particles were extracted with 20 mL 20 mM sodium-acetate buffer pH 5 for 1 hour at 4 °C. The activities of laccase and manganese-peroxidase (U/g wood dry weight) were determined in the wood extract as described elsewhere [Böhmer et al., 1998].

FT-NIR Spectroscopy

Sterile beech wood veneers (50 mm x 50 mm, Danzer Company, Austria) were soaked with a mixture of fungal mycelium and CSL (see above) and placed on water agar above sterile beech toothpicks to allow growth throughout the whole surface. After 3 weeks of incubation, all veneers were rinsed with distilled water and dried for 2 days at 50 °C. FT-NIR spectroscopy was performed according to [Schwanninger et al., 2003]. The relative lignin content was estimated by comparison of the 2nd derivative spectra at 5978 cm⁻¹, which is representative for lignin. Each veneer was measured 8 times with measure points evenly distributed throughout the surface. Untreated veneers as well as sterilized veneers with CSL only were used as reference. Mass loss of veneers was calculated as % loss of dry weight.

Results and Discussion

Logs in the wood yard revealed numerous fruit bodies of two dominating fungi, which could be identified as *Chondrostereum purpureum* and *Schizophyllum commune*. *S. commune* is known to be a common white rot fungus on wood, whereas *C. purpureum* is responsible for the so called silver leaf disease on fruit trees. The two species covered approximately 60 - 70 % of the stored logs and grew mainly on the cross sections, especially in wet areas, which were not directly exposed to sunlight and thus provide high humidity as an ideal prerequisite for intense fungal growth. Growth of these fruit bodies is progressing from the surface areas close to the cambium along the nutrient rich rays leading to discoloration of sapwood. Infection may be initiated by a high density of air-borne basidiospores, which enter the wood parenchyma cells via lesions resulting from, e.g. transport. When the logs were sectioned closely behind the original surface, a dense staining of the wood with a preferred orientation along the

rays was detected. Obviously, degradation of nutrient rich cell contents within parenchyma cell tissues and their reaction with metabolite products of bacteria and fungi leads to intense discoloration after only a few days [Koch et al., 2001].

To verify a possible delignifying potential of the two fungal species, ligninolytic enzyme activities in batches with controlled infected beech wood chips were determined spectrophotometrically. All fungal inoculated chips showed brown surface discoloration. No laccase and no manganese-peroxidase activity could be detected in the extracts of the two Lenzing isolates up to 12 days of inoculation. The lack of lignin degrading enzymes of *C. purpureum* and *S. commune* has already been reported elsewhere [Simpson et al., 2001; Boyle et al., 1992].

Mass loss (% of dry weight) of infected beech wood chips was determined from 4 parallel batches over a period of 10 weeks. With the reference strain *C. subvermispora*, mass losses up to 13 % were achieved after 10 weeks. In the case of *C. purpureum* and *S. commune*, after 10 weeks growth only 2 % mass loss occurred, which derives only from the degradation of extractives (figure 1).

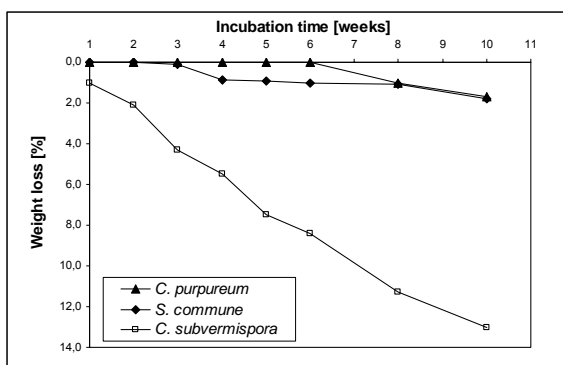


Figure 1. Time course of weight loss of beech wood chips after controlled infection with the fungal isolates, compared to the selective white rot fungus *C. subvermispora*.

Reflectance spectra from surfaces of three weeks inoculated beech wood veneers were

collected and changes of the amplitude of the lignin-associated band (5978 cm^{-1}) were followed in the 2nd derivative mode. Figure 2 clearly shows that the decrease of the lignin band in case of *C. purpureum* is negligible; *S. commune* degrades lignin only to a minor degree. In contrast, *C. subvermispora* shows a high decrease of the lignin-associated band. Furthermore, growth of *C. subvermispora* leads to a decrease of the “hemicellulose” band at 5800 cm^{-1} (1st overtone of the C-H stretching vibration) whereas only little decrease occurred with *S. commune* and almost no changes with *C. purpureum* inoculated veneers.

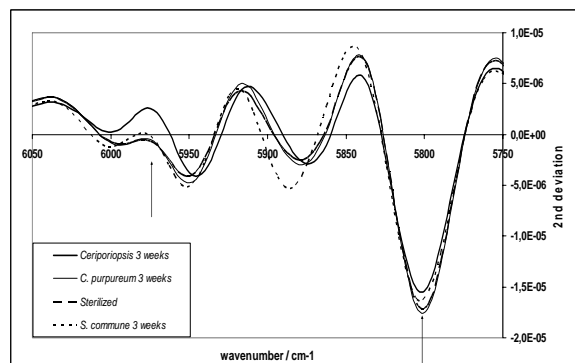


Figure 2. “Lignin band” (5978 cm^{-1}) and CH stretching vibration (“hemicellulose” band) at 5800 cm^{-1} (arrows) of 2nd derivative of NIR spectra of 3 weeks inoculated beech wood veneers compared to *Ceriporiopsis subvermispora* inoculated veneers and an untreated reference.

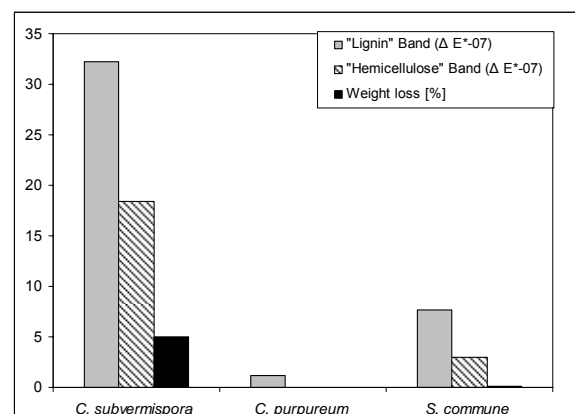


Figure 3. Depiction of weight loss and Delta lignin (5978 cm^{-1}) and hemicellulose band (5800 cm^{-1}) of the two isolates compared to the reference strain *C. subvermispora* after 3 weeks incubation.

Our spectroscopic investigations showed that growth of *C. purpureum* after 3 weeks obviously does not influence structural components like lignin and hemicelluloses, and only results in the formation of chromophores within infested parts of the wood, which are responsible for wood quality deterioration, especially in the case of bleaching performance. In the case of *S. commune*, lignin is only degraded to a very small extent; the hemicellulose content remains more or less unchanged. Wood, inhabited by this fungus, also shows brown discoloration within growth areas.

Conclusion

One of the two fungal species *C. purpureum* which has been found throughout the whole Lenzing wood yard does not degrade the wood structural components and therefore may have no influence on the pulp yield. We assume that this fungus grows exclusively along the nutrient rich rays, degrading only storage compounds located within the parenchyma cell lumina, which can be seen by following the small mass loss after 10 weeks of fungal treatment. The second identified isolate, *S. commune* seems to have only little influence on the wood lignin structure and nearly no hemicellulose is degraded. When regarding NIR spectra of wood, infected by this fungus, a slight decrease in the lignin associated band could be displayed although no lignin degrading enzymes were produced after 12 days incubation time. Also in this case, mass loss of wood treated with *S. commune* for 10 weeks is only 2 %. Therefore we can conclude that this fungal species, although it is known to be a white rot fungus, primarily uses easy to degrade storage compounds from wood before attacking the lignin structure after longer colonization. Degradation of nutrient rich cell contents like starch, proteins, or polyphenolic compounds during fungal growth leads to the formation of chromophore structures probably as a result of secondary reactions

with fungal metabolites [Koch et al., 2001]. These chromophores withstand the pulping process [Mc Cubbin, 1919]. The main effect of the two dominating fungi on the pulp quality obviously lies in the formation of chromophores within the wood structure thus reducing the brightness of the pulp.

Acknowledgements

Financial support was provided by the Austrian government, the provinces of Lower Austria, Upper Austria, and Carinthia as well as by the Lenzing AG.

References

- [1] Akhtar, M., G. M. Scott, R. E. Swaney and D. F. Shipley. 2000. Biomechanical pulping: a mill-scale evaluation. *Resources, Conservation and Recycling* 28, 241 – 252.
- [2] Böhmer, S., K. Messner, and E. Srebotnik. 1998. Oxidation of Phenanthrene by a Fungal Laccase in the Presence of 1-Hydroxybenzotriazole and Unsaturated Lipids. *Biochemical and Biophysical Research Communications* 244, 233 – 238.
- [3] Boyle, D. C., B. R. Kropp, and I. D. Reid. 1992. Solubilization and Mineralization of Lignin by White Rot Fungi. *Applied and Environmental Microbiology*, 58 (10), 3217-3224.
- [4] Hunt, R. S. and F. W. Cobb. 1971. Selective medium for the isolation of wood-rotting Basidiomycetes. *Canadian Journal of Botany* 49, 2064 – 2065.
- [5] Koch, G., J. Bauch, J. Puls und J. Welling. 2001. Ursachen und wirtschaftliche Bedeutung von Holzverfärbungen, *Interdisziplinäre Forschung am Beispiel der Rotbuche. Forschungsreport* 2, 30 – 33.
- [6] McCubbin, W. A. Discolored Pulp. *Pulp and Paper Magazine of Canada*, May, 15th 1919, 461-462.

- [7] Messner K., K. Koller, M.B. Wall, M. Akhtar, and G. Scott. 1998. In: Environmentally Friendly Technologies for the Pulp and Paper Industry. R.A. Young and M. Akhtar (eds.), John Wiley & Sons, 385-420.
- [8] Schwanninger, M., B. Hinterstoisser, C. Gradinger, K. Messner, and K. Fackler. 2004. Examination of spruce wood biodegraded by *Ceriporiopsis subvermispora* using NIR and MIR spectroscopy and Principal Component Analysis, paper in preparation.
- [9] Schwanninger, M., N. Gierlinger, J. Hanger, C. Hansmann, B. Hinterstoisser, and R. Wimmer. 2003. Characterization of thermally treated beech wood by UV-Microspectrophotometry, FT-MIR and FT-NIR Spectroscopy. Proceeding of the 12th ISWPC Madison, USA, June 9. -12. 2003; Vol. III, 55-58.
- [10] Simpson, R. M., R. Van Hekezen, F. Van Lune, D. Brewster, J.T. Christeller, and A.G. Spiers. 2001. Extracellular enzymes of *Chondrostereum purpureum*, causal fungus of silverleaf disease. Horticulture and Food Research Institute of New Zealand, Palmerston North, N. Z.; Proceedings of the New Zealand Plant Protection Conference.
- [11] Sixta H., A. Promberger, G. Koch, C. Gradinger and K. Messner. 2004. Influence of beech wood quality on bisulfite dissolving pulp manufacture. Part 1: Influence of log storage on pulping and bleaching. *Holzforschung* 58, 14-21.
- [12] Smuldki, S., 1996. Wood Destroying Fungi in Residential Construction, Building Materials and Wood Technology.

TOPOCHEMICAL CHARACTERIZATION OF LIGNINS AND PHENOLIC EXTRACTIVES IN WOOD CELL WALLS

Gerald Koch

Institute for Wood Biology and Wood Protection,
Federal Research Centre of Forestry and Forest Products,
D-21031 Hamburg, Germany
e-mail: g.koch@holz.uni-hamburg.de

The topochemical distribution of lignin and phenolic extractives in woody tissue was determined at a cellular level using scanning UV microspectrophotometry (UMSP). This improved analytical technique enables direct imaging of lignin distribution within individual cell wall layers with a resolution of $0.25 \mu\text{m}^2$. The technique is based on the ultraviolet illumination of semi-thin transverse sections ($1\mu\text{m}$ thickness) of the woody tissue which can be related semi-quantitatively to the concentration of lignin within the cell wall. For demonstration, selected softwood (*Picea abies*), and hardwood (*Fagus sylvatica*)

sections were scanned at a defined wavelength and evaluated with the APAMOS software. This approach allows the distribution pattern of lignin and aromatic compounds within the cell wall to be visualised simultaneously. The method was found to be ideally suited for the study of lignification during wood formation, the detection of phenolic extractives, the removal of lignin during pulp processes, and other applications in chemical technology of wood.

Key words: *lignin distribution, phenolic extractives, scanning UV microspectrophotometry, topochemistry*

Introduction

The synthesis and deposition of lignin is an important biochemical and morphological transformation in plant cell walls during maturation. Lignin can be described as a highly complex polymer consisting of phenylpropane units linked together by a variety of carbon-oxygen and carbon-carbon bonds. The complex structure of lignin arises from its biosynthesis, in which the last step is a nonenzymatic, random recombination of phenoxy radicals of coniferyl, sinapinyl, and *p*-coumaryl alcohols [1]. Variations in the chemical reactivity of lignin are based on the proportions of the three structural units. Whereas coniferous lignin consists mainly of guaiacylpropane (4-hydroxy-3-methoxyphenylpropane) units (G), hardwood lignins also contain up to 50% syringyl (3,5-dimethoxy-4-hydroxyphenyl) groups (S), and compressive wood lignins

up to 40% *p*-hydroxyphenylpropane (H) units. Up to 30% of the latter also occur in grass lignins [2]. In wood cell walls these basic monomers build up a three dimensional polymer wrapping the aggregated cellulose and hemicelluloses chains and filling up most of the microvoids between them. The monomer composition and ultrastructural distribution of lignin within the cell walls are responsible for various wood properties and affect the reactivity under chemical treatments (e.g. pulping) or during biodegradation of woody materials. Therefore, the knowledge of the qualitative and (semi-) quantitative distribution of lignin within individual cell wall layers is of great interest.

Furthermore, the topochemical characterization and distribution of phenolic extractives are important for the

study of wood properties. Depending on the quantity and the type of compound, which are specific to the wood genus and species to some extent, the phenolic extractives affect the chemical, biological, physical, and optical properties of the wood to varying degrees [3].

In order to provide a better understanding of (i) the lignin distribution during wood formation, (ii) the course of delignification during pulping, and (iii) the discoloration of wood in the living tree and during processing, the topochemical distribution of lignin and phenolic extractives were investigated on a subcellular level by using scanning UV microspectrophotometry.

This improved cellular analytical technique enables direct imaging of aromatic compounds within individual cell wall layers and also offers a variety of graphical and statistical analyses with a resolution of $0.25 \mu\text{m}^2$ [4]. In comparison to the conventional UV microscopic point measurements, the topochemistry of lignin can be depicted as two- or three-dimensional image profiles. The present study gives examples which demonstrate the applicability of scanning UV microspectrophotometry to the investigation on wood topochemistry.

Materials and Methods

For the basic microspectrophotometric investigation of the subcellular lignin distribution in softwoods and hardwoods, small wood blocks ($1 \times 1 \times 5 \text{ mm}^3$) of selected species of spruce heartwood (*Picea abies* [L.]) and beech sapwood (*Fagus sylvatica* [L.]) were prepared [4]. In addition, industrial wood chips from spruce were used for the topochemical characterization of lignin removal during a standardised bisulphite pulping [5]. The cooking processes were interrupted at intervals of 30 minutes for determining the progress of delignification on a subcellular level. The collected chips were immediately washed in deionised water and small blocks ($1 \times 1 \times 5 \text{ mm}^3$) were

dissected from inner parts of the chips. For the topochemical characterization of phenolic extractives small wood blocks ($1 \times 1 \times 5 \text{ mm}^3$) of discoloured tissue from industrially steamed and kiln-dried beech sawn timber were selected [6].

All samples were serially dehydrated in a graded series of acetone, impregnated with Spurr's epoxy resin [7] through a series of acetone/resin mixtures, followed by immersion in pure resin. For the investigation of low molecular phenolic extractives in beech heartwood a direct impregnation with pure Spurr's resin under vacuum was chosen instead. For this special impregnation the specimens were freeze-dried and immediately embedded with Spurr's epoxy resin under mild vacuum with several cycles of evacuation and ventilation [8].

The embedded blocks were trimmed to provide a face of approximately 0.5 mm^2 . Ultrathin sections ($1 \mu\text{m}$) were cut with a diamond knife mounted in a LKB Bromma ultramicrotome. The sections were then transferred to quartz microscope slides, immersed in a drop of non-UV absorbing glycerine, and covered with a quartz cover slip.

The analyses were carried out using an UV microspectrophotometer (UMSP 80, Zeiss) equipped with a scanning stage enabling the determination of image profiles at defined wavelengths using the scan program APAMOS[®] (Automatic-Photometric-Analysis of Microscopic Objects by Scanning (Zeiss)). For the detection of the lignin distribution of softwoods and hardwoods wavelengths of 280 nm and 278 nm, respectively, were selected. The scan programme digitises rectangular fields with a local geometrical resolution of $0.25 \mu\text{m}^2$ and a photometrical resolution of 4096 grey scale levels which are converted in 14 basic colours to visualise the absorbance intensities. The scans can be depicted as two- or three-dimensional image profiles including a

statistical evaluation (histogram) of the semi-quantitative lignin distribution [9]. The sections were also conventionally subjected to point measurements with a spot size of $1 \mu\text{m}^2$ between 240 nm and 400 nm wavelength using the program LAMBDA SCAN[®] (Zeiss). This program evaluates the UV absorbance spectra of the lignified cell walls and accessory compounds in tissues.

Results and Discussion

UV scanning profiles of lignin distribution in wood cell walls

Scanning UV microspectrophotometry enables direct imaging of the lignin distribution within individual cell wall layers and incorporates advances on the previous UV microscopy investigations of lignin topochemistry. Figures 1 and 2 show typical two- and three-dimensional UV image profiles of lignin distribution within individual cell wall layers of a spruce tracheid and a beech fibre. The grey scales indicate different intensities of UV absorbance at $\lambda_{280 \text{ nm}}$ and $\lambda_{278 \text{ nm}}$. The high resolution ($0.25 \mu\text{m}^2$ per pixel) enables a high differentiation of the UV absorbance within the individual cell wall layers.

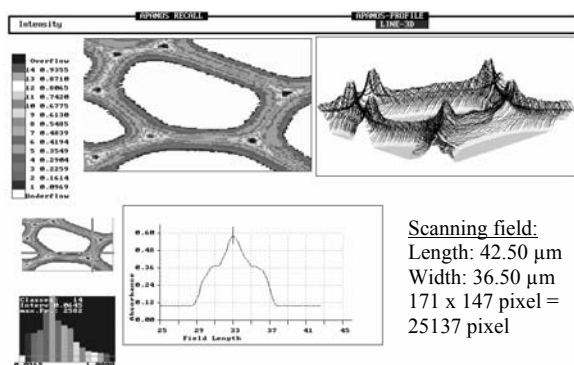


Figure 1. UV microscopic image profiles of an individual tracheid of *Picea abies* scanned with a geometrical resolution of $0.25 \mu\text{m}^2$. The grey scales indicate the different UV-absorbance values at a wavelength of 280 nm.

The image profiles of spruce tracheids (figure 1) are characterised by a high UV absorbance at the cell corners and compound middle lamellae ($\text{abs}_{280\text{nm}}$ 0.61

to 0.87) as compared to the adjacent S2 layers with a lower, slightly varying lignin distribution ($\text{abs}_{280\text{nm}}$ 0.35 to 0.54). As found by Fergus [10] the average lignin content in the compound middle lamella is about twice that in the S2 of the tracheids. For detailed illustration, the scanning area is presented as a three-dimensional image as well as line image profile. In the three-dimensional profile, the compound middle lamella region stands out as a highly absorbing band which broadens towards a heavily lignified area at the cell corners. An example of a line image profile depicted by the marked cross line is shown in detail. The compound middle lamella of the scanned spruce tracheid is recorded as a pronounced peak while the S2 layers are characterised by a lower level plateau on either side of the compound middle lamella. These graphical presentations allow a refined evaluation of the topochemical distribution of lignin within the cell walls. An unambiguous statistical presentation of the data is an additional asset.

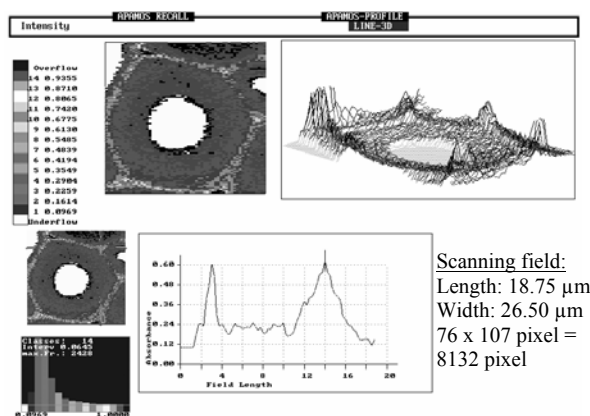


Figure 2. UV microscopic image profiles of an individual fibre of *Fagus sylvatica* scanned with a geometrical resolution of $0.25 \mu\text{m}^2$ at a wavelength of 278 nm.

The scanned beech fibre (figure 2) shows a different absorbance level as compared to the softwood tracheids (compare figure 1). In particular, the broad S2 layer reveals a lower absorbance with values of $\text{abs}_{278\text{nm}}$ 0.16 to 0.29. The uniform level of absorbance in this wall layer corresponds to earlier results reported by Saka [11], who

predicted lignin distribution across the width of the whole S₂ should be homogeneous. The compound middle lamella is distinguished by higher absorbance values as compared to those of the spruce tracheids.

Topochemistry of bisulfite pulping

In a comparative study, the delignification of spruce tracheids during bisulfite pulping was analysed on a subcellular level by scanning UV microspectrophotometry [5]. In figure 3 representative UV micrographs of pulped spruce latewood tracheids at the beginning of cooking are shown. The UV microscopic study reveals that delignification starts in the region of the pit canals and proceeds homogeneously across the entire S₂ [12, 13, 14]. The beginning of delignification becomes evident as local areas of the S₂ with significantly reduced absorbance values (abs_{280nm} 0.1 to 0.2). As a specific feature, a partial delignification of the radial compound middle lamella can be detected at this cooking stage. Jayme and Torgersen [15] assume that the cooking liquor penetrates the radial middle lamella from the pit system, whereas the tangential middle lamella is not yet penetrated at this early cooking stage. At the end of the pulping process, the tissue reveals a homogenous delignification throughout the cell wall. Only parts of the cell corners can be distinguished by the UV scanning technique, showing low absorbance values in the range of $\log Abs_{280nm}$ 0.3. Due to the shape of the tracheids, the radial cell walls are characterised by higher absorbance values caused by the shorter distance between the cell corners in radial direction [5].

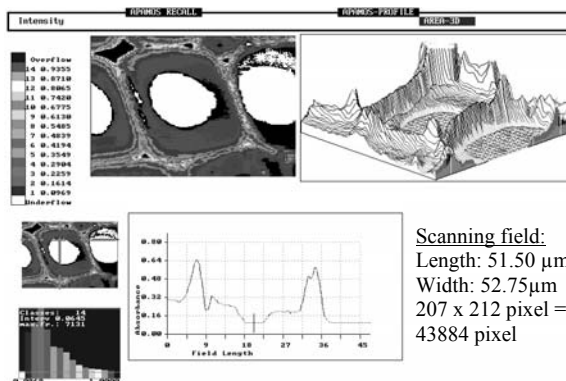


Figure 3. UV-microscopic image profiles of bisulfite pulped *Picea abies* latewood tracheids (Cooking stage 60 min). The grey scales indicate the different UV-absorbance values at a wavelength of 280 nm.

Topochemical detection of phenolic extractives in discoloured beechwood tissue

Scanning UV microspectrophotometry can also be used to detect and quantify aromatic compounds associated with the woody tissue [6]. The presence of extractives can easily be visualised as spherical conglomerations of high absorbance as compared with the surrounding tissue. In figure 4 the local deposition of extractives in the lumina of ray parenchyma cells of beech heartwood is emphasized by a significantly higher absorbance (abs_{280nm} 0.68 to 1.00) as compared to the cell wall associated lignins. The phenolic compounds are generally synthesised by parenchyma cells *in situ* and are highly condensed, making it impossible for them to penetrate into the interfibrillar spaces of the cell walls [16]. The adjacent fibres do not seem to be impregnated, as evidenced by lower absorbance levels in these cells. The scanned fibres and parenchyma cells show the typical absorbance profile originating from the lignification of the different cell wall layers as presented in figure 2. In contrast to wood species with an obligatory heartwood formation, the cell walls of beech fibres are not impregnated, and the deposited phenolic extractives in the cell lumina do not contribute to decay resistance [17].

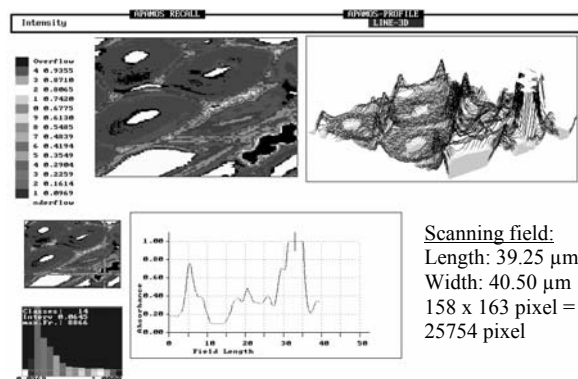


Figure 4. UV microscopic image profiles of *Fagus sylvatica* tissue measured at $\lambda_{278\text{nm}}$ showing the deposition of phenolic extractives (arrows) in lumina of ray parenchyma cells

Localisation of lignin in cell walls by point analysis

The lignification of individual cell wall layers was also studied by the evaluation of the UV absorbance spectra in a wavelength range of 240 to 400 nm. In figure 5 typical UV absorbance spectra of individual cell wall layers and phenolic extractives in beech heartwood are presented. The UV spectra of the compound middle lamellae and S2 show the typical absorbance behaviour of a hardwood lignin with a distinct maximum at 278 nm and a local minimum at about 250 nm [18, 19]. The cell wall layers of the vessels are generally characterised by higher absorbance values than that of the fibres. This behaviour is based on the different chemical constitution of lignin in both cell types. Fergus [18] and Terashima [20] proved that the lignin located in vessel cell walls consists predominantly of the strongly absorbing guaiacyl type units, while the fibre cell wall lignin contains more syringyl units showing a lower UV absorbance at increasing OCH_3/C_9 ratio [21]. In comparison, the UV spectra of spruce tracheids show generally higher absorbance values compared to the hardwood fibre and vessels. A pronounced absorbance maximum at 280 nm usually indicates the presence of the strongly absorbing guaiacyl-lignin [21, 22].

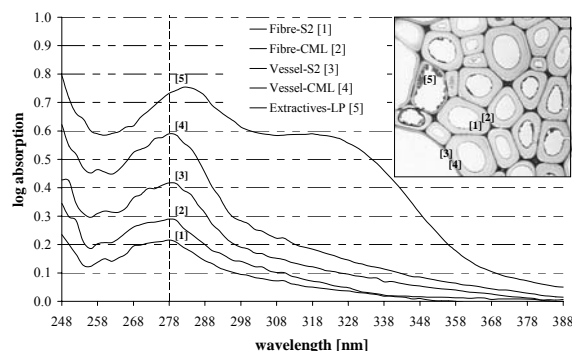


Figure 5. Representative UV absorbance spectra of individual cell wall layers and cell lumen deposited phenolic compounds in the woody tissue of *Fagus sylvatica* (S2-secondary wall, CML-compound middle lamella, L-longitudinal parenchyma).

The detected phenolic extractives in the ray parenchyma cells of beech heartwood have much higher absorbance values ($\text{abs}_{280\text{nm}}$ 0.75 and 0.95) than cell wall associated lignins ($\text{abs}_{280\text{nm}}$ 0.20 and 0.38). Furthermore, their absorbance maxima display a bathochromic shift to a wavelength of 284 nm and slight shoulder at a wavelength range of 320 nm. This spectral behaviour can be explained by the presence of chromophoric groups, e.g., conjugated double bonds. The higher degree of conjugation stabilises $\pi-\pi^*$ transitions resulting in absorbance bands shifted to higher wavelengths [23] which can be detected by UV microspectrophotometry. However, the technique does not allow a detailed chemical identification of the condensed phenolic extractives [6].

The selected examples demonstrate that UV microspectrophotometry is ideally suited to study the topochemical distribution of lignin and phenolic extractives on a subcellular level. In particular, the application of the scanning technique enables a direct imaging of lignin distribution and provides fundamental information on the topochemistry of lignin [4, 24]. Using this technique, fine differences in the lignification of individual cell wall layers and their delignification during pulping processes can be analysed. The technique can be used for a wide range

of applications in wood biology and chemistry.

References

- [1] K. Freudenberg: Constitution and biosynthesis of lignin. Springer-Verlag, Berlin (1968).
- [2] K.V. Sarkanen, H.L. Hergert: Classification and Distribution. In: K.V. Sarkanen and C.H. Ludwig (ed.), Lignins, Occurrence, Formation, Structure and Reactions. Wiley Interscience, New York (1971) 43-49.
- [3] D. Fengel, G. Wegener: Wood. Chemistry, Ultrastructure, Reactions. de Gruyter, Berlin, New York (1989).
- [4] G. Koch, G. Kleist: Application of scanning UV microspectrophotometry to localise lignins and phenolic extractives in plant cell walls. *Holzforschung* 55 (2001) 563-567.
- [5] G. Koch, B. Rose, R. Patt, O. Kordsachia: Topochemical investigations on delignification of *Picea abies* [L.] Karst. during alkaline sulfite (ASA) and bisulfite pulping by scanning UV microspectrophotometry. *Holzforschung* 57 (2003) 611-618.
- [6] G. Koch, J. Puls, Bauch: Topochemical characterisation of phenolic extractives in discoloured beechwood (*Fagus sylvatica* L.). *Holzforschung* 57 (2003) 339-345.
- [7] A.R. Spurr: A low viscosity epoxy resin embedding medium for electron microscopy. *J. Ultrastruct. Res.* 26 (1969) 31-43.
- [8] G. Kleist, U. Schmitt: Evidence of accessory components in vessel walls of Sapelli heartwood (*Entandrophragma cylindricum*) obtained by transmission electron microscopy. *Holz Roh- u. Werkstoff* 57 (1999) 93-95.
- [9] G. Koch, C. Grünwald: Application of UV microspectrophotometry for the topochemical detection of lignin and phenolic extractives in wood fibre cell walls. In: U. Schmitt, P. Ander, J. Barnett, A.M. Emons, P. Saranpää and S. Tschegg (ed.), Wood Fibre Cell Walls: Methods to Study their Formation, Structure and Properties. COST E-20, published by OPOCE, EC, Brussels (2004) 121-131.
- [10] B.J. Fergus, A.R. Procter, J.A.N. Scott, D.A.I. Goring: The distribution of lignin in sprucewood as determined by ultraviolet microscopy. *Wood Sci. Technol.* 3 (1969) 117-138.
- [11] S. Saka, D.A.I. Goring: Localization of lignins in wood cell walls. In: T. Higuchi (ed.), Biosynthesis and biodegradation of wood components. Academic Press, New York (1988) 51-62.
- [12] A.R. Procter, W.Q. Yean, D.A.I. Goring: The topochemistry of delignification in kraft sulphite pulping of spruce wood. *Pulp Paper Magaz., Canada* 68 (1967) 445-460.
- [13] P. Whiting, D.A.I. Goring: The topochemistry of delignification shown by pulping middle lamella and secondary wall tissue from black wood. *J. Chem. Technol.* 1 (1981) 111-122.
- [14] U. Schmitt, A.P. Singh, O. Kordsachia, E. Pöhler: The topochemistry of delignification of *Pinus radiata* during ASAM pulping. In YS. Kim (ed.) *New Horizons in wood Anatomy*. Chonnam National University Press (2000) 189-197.
- [15] G. Jayme, H.F. Torgersen: Topochemie der Delignifizierung beim Aufschluss von Fichtenholz nach dem Sulfit- und Sulfatverfahren. Teil I: Ultraviolett-mikroskopische Untersuchungen an teilweise delignifizierten Fichtenholz. *Holzforschung* 21 (1967) 110-116.
- [16] W.E. Hillis: Heartwood and tree exudates. Springer Verlag, Berlin (1987).

- [17] G. Kleist, J. Bauch: Cellular UV microspectrophotometric investigation of Sapelli heartwood (*Entandrophragma cylindricum* Sprague) from natural provenances in Africa. *Holzforschung* 55 (2001) 117-122.
- [18] B.J. Fergus, D.A.I. Goring: The location of guaiacyl and syringyl lignins in birch xylem tissue. *Holzforschung* 24 (1970) 113-117.
- [19] K. Takabe, S. Miyauchi, R. Tsunoda, K. Fukazawa: Distribution of guaiacyl and syringyl lignins in Japanese beech (*Fagus crenata*): variation within annual ring. *IAWA Bulletin* 13 (1992) 105-112.
- [20] N. Terashima, K. Fukushima, K. Takabe: Heterogeneity in formation of lignin. VIII. An autoradiographic study on the formation of guaiacyl and syringyl lignin in *Magnolia kobus* DC. *Holzforschung* 40 (1986) 101-105.
- [21] Y. Musha, D.A.I. Goring: Distribution of syringyl and guaiacyl moieties in hardwoods as indicated by ultraviolet microscopy. *Wood Sci. Technol.* 9 (1975) 45-58.
- [22] T. Fujii, K. Shimizu, A. Yamaguchi: Enzymatic saccharification on ultrathin sections and ultraviolet spectra of Japanese hardwoods and softwoods. *Mokuzai Gakkaishi* 33 (1987) 400-407.
- [23] O. Goldschmid: Ultraviolet spectra. In: K.V. Sarkanen and C.H. Ludwig (ed.), *Lignins, Occurrence, Formation, Structure and Reactions*. Wiley Interscience, New York (1971) 241-266.
- [24] T. Röder, G. Koch, H. Sixta: Application of confocal Raman spectroscopy for the topochemical distribution of lignin and cellulose in plant cell walls of beech wood (*Fagus sylvatica* L.) compared to UV microspectrophotometry. *Holzforschung* 58 (2004) 480-482.

CONFOCAL RAMAN SPECTROSCOPY – APPLICATIONS ON WOOD SAMPLES*

Thomas Röder and Herbert Sixta

Department Zellstoff-Forschung, Lenzing AG, Werksstrasse 1, A-4860 Lenzing, Austria
Phone: (+43) 07672-701-3082; Fax: (+43) 07672-918-3082; E-mail: t.roeder@lenzing.com

* This work was presented during the 6th International Symposium "Alternative Cellulose - Herstellen, Verformen, Eigenschaften" 1st-2nd September 2004, Rudolstadt, Germany

Confocal Raman Spectroscopy in combination with a 785 nm or 830 nm laser is a useful tool to analyse wood samples because of the low excitation probability of fluorescence of these lasers. This technique provides chemical information with high spatial resolution and was therefore used to determine the lignin and cellulose content in wood cell

walls. In addition composites of melamine formaldehyde and wood were analysed. It could be demonstrated that Melamine formaldehyde (MF) partly permeated into wood cell walls.

Keywords: *confocal Raman, lignin, melamine formaldehyde, wood*

Introduction

15 years ago Raman spectroscopy has largely been used for academic purposes. One of the main reasons was the appearance of fluorescence which covers the Raman spectra due to its higher intensity (up to 10^6 times). However, most of the fluorescent compounds have no electronic absorption bands in the near infrared. Therefore, often FT-Raman with a 1064 nm light source is used. 785 nm-lasers combine largely fluorescence prevention with high spatial resolution of dispersive Raman spectroscopy in comparison to FT-Raman. [1]

Especially the investigation of wood samples needs sufficient fluorescence suppression or prevention, respectively. Raman microspectroscopy is a promising technique to study both lignin and cellulose simultaneously [2]. The obtained vibrational spectra of the wood contain contributions from all of its major constituents. Cellulose and hemicelluloses, both being carbohydrate polymers, have similar σ -bond frames (arrangements of single bonds), and thus their spectra are

expected to be similar [3]. However, lignin, which represents a heterogeneous polymer with π -contributions (aromatic structures), produces different spectra. By applying confocal Raman spectroscopy the vibrational information is combined with spatial resolution. In the confocal technique [4], the excitation laser is focussed on a small area (spot size 2 μm) of the sample through a microscope objective. The detected Raman scattering signal is limited by a pinhole to the area surrounding the focus. The smaller the pinhole, the better is the depth resolution, but at the expense of signal intensity.

Experimental

Wood

Samples (measuring about 5 mm x 5 mm x 10 mm) of beech sapwood from the same stem section were taken without dehydration and embedding, freshly cut with a sliding microtome (Reichert) into 10 μm sections, and stored in a water-glycerol mixture. The wet sections were

transferred to glass microscope slides, washed in deionised water, dried in air, and fixed to avoid motion during measurement. The Raman measurements were performed with a HoloLab Series 5000 Modular Raman Spectrometer (HL5R) from Kaiser Optical Systems Inc. (USA) equipped with f/1.8 optics, transmission grating, multichannel CCD array detector (optimised for NIR), and a 785 nm diode laser (400 mW) coupled via single mode fibre to the microscope (approximately 10 mW on the sample). Between microscope and detector, a confocal fibre with a pinhole of 20 μm was used. With the 100X objective the lateral resolution was about 1-2 μm .

Wood melamine composites

Specimens (30 mm x 12 mm x 10 mm (radial x tangential x longitudinal) were prepared from spruce (*Picea abies* L. [Karst.]). After complete water saturation followed by a dehydration with methanol (4 x 2 hours), resin infiltration was done by simply immersing in melamine (MER, AMI™), which was dissolved with methanol to a weight percentage of 50:50. After 3 days of immersion the samples were dried overnight at 60°C and cured at 180°C for 30 min. For Raman microscopy 10 μm thick transverse sections were cut from the same samples by a rotary microtome. The sections were transferred to glass microscope slides and fixed to avoid motion during measurement. The measurements were done with the spectrometer above, despite the use of a more powerful 785 nm-laser (500 mW, Toptica Photonics AG, Martinsried, Germany) with approximately 80 mW on the sample.

Results and discussion

The resolution in confocal Raman spectroscopy is limited by diffraction depending on the wavelengths. To avoid fluorescence, a 785 nm laser was used. In

this configuration analysis of wood samples is possible.

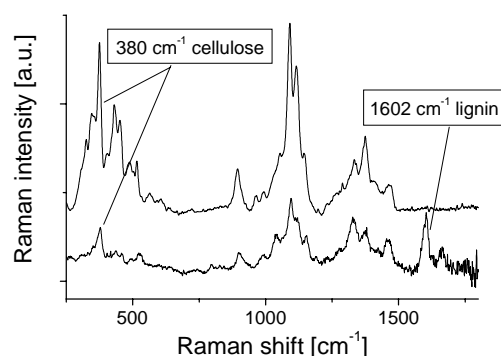


Figure 1. Raman spectra of beech wood (bottom) and of beech wood pulp (top).

The lignin and cellulose distribution in individual cell wall layers could be measured. The lignin content was determined by the signal of the aromatic ring stretching around 1602 cm^{-1} (peak area between 1593 cm^{-1} and 1614.5 cm^{-1}) and the cellulose content by the signal around 1092 cm^{-1} and 1123 cm^{-1} (peak area between 1074 cm^{-1} and 1134 cm^{-1} , figure 1) [5].

The maximum lignin content was shown to be located in the cell corner (figure 2b), whereas the cellulose content revealed a minimum there. The distribution of lignin and cellulose across a fibre cell wall is given in Figure 2a as obtained from measurements with a sampling time of 30 s. The cellulose content decreased in the middle lamella and increased in the S2 layer. Additional information about the hemicellulose content could not be gained, since the spectra of hemicelluloses and cellulose cannot be separated.

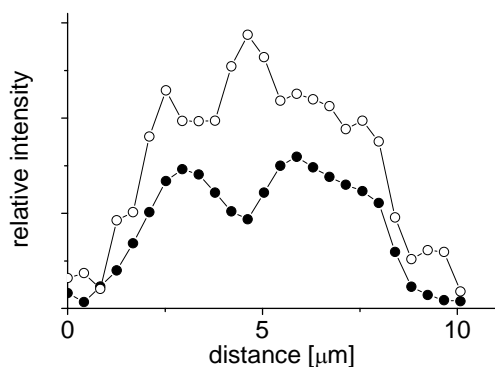


Figure 2a. Distribution of lignin (—●—) and cellulose (—○—) in the cell wall. [6]

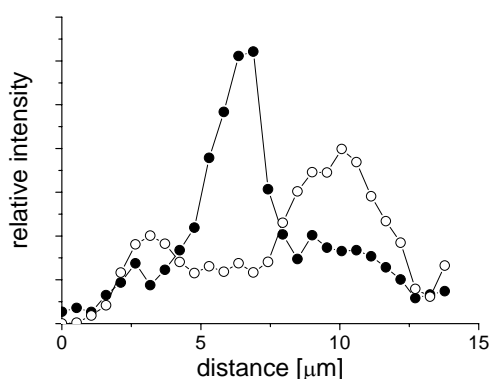


Figure 2b. Distribution of lignin (—●—) and cellulose (—○—) in a cell corner. [6]

These results were expected due to basic knowledge about wood structure. The high spatial resolution of this method allows the investigation of, for instance, composites of wood with polymers. Melamine-formaldehyde (MF) is one of the hardest and stiffest isotropic polymeric materials [7] used in decorative laminates, moulding compounds, adhesives, coatings and other products.

Lumen filled with MF was assumed to have a MF content of 100%. A sharp and intense band was observed at 975cm^{-1} (figure 3, top), attributed to the triazine ring nitrogen radial in-phase vibration [8]. From the Raman bands of pure MF resin only the intense ring vibration band at 974cm^{-1} was found in the MF treated spruce cell walls (figure 3). All other bands also occurred in the untreated

reference samples and can be assigned to cellulose, hemicelluloses and lignin [3]. At 965cm^{-1} , a small band attributed to cellulose was overlapped by the strong 974cm^{-1} melamine peak of the treated samples. By dividing the melamine peak area (993.9cm^{-1} to 949.5cm^{-1}) of pure resin in the lumen through the peak area of melamine within the cell wall a relative concentration was calculated.

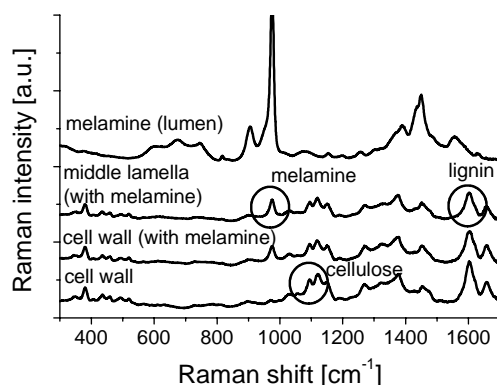


Figure 3. Raman spectra of melamine treated spruce wood in comparison to untreated sample (bottom).

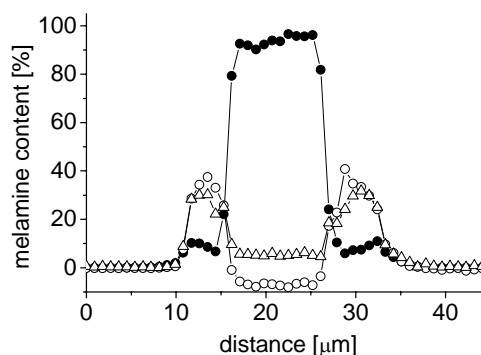


Figure 4. Distribution of melamine (—●—), and cellulose (—△—), and lignin (—○—) in a spruce wood cell. [9]

Melamine concentration was also “corrected” by subtracting the cellulose band area from the reference. Figure 4 shows the calculated melamine content of the line scan through a spruce wood cell. In addition, the Raman intensities of a cellulose ($1079\text{--}1107\text{cm}^{-1}$) and lignin band ($1568\text{--}1636\text{cm}^{-1}$) are lined out to verify the position within the cell wall (figure 4). The

averaged MF concentration detected within the cell wall of this section was 11.5%.

Conclusions

Fluorescence suppression by newly developed lasers with near-infrared wavelengths combined with a higher spatial resolution than FT-Raman and IR spectroscopy account for growing applications of dispersive Raman spectroscopy. Reaching from wood over pulp to regenerated cellulose fibres, dispersive Raman spectroscopy can be used to determine content, modification, or structural properties in substances along the "resource chain wood".

Lignin distribution in wood cell walls could be determined as well as the cellulose distribution. The maximum of lignin in the cell wall was found in the cell corners, where cellulose content revealed its minimum. Melamine-formaldehyde (MF) and wood formed stable composites with up to 11.5% MF in the wood cell wall.

Acknowledgements

We want to thank K. Wimmer and N. Gierlinger (BOKU Vienna, Austria) for the melamine samples, G. Koch (BfH Hamburg, Germany) for the microtome cuts of the beech wood samples, J. Moosbauer (Lenzing AG, Austria) and T. Rosenau (BOKU Vienna, Austria) for helpful discussions.

References

- [1] B. Schrader, Infrared and Raman Spectroscopy. Methods and Applications. (B. Schrader ed.), VCH Verlagsgesellschaft mbH Weinheim, Germany, 1995
- [2] Bond, J.S. and R.H. Atalla, 1999. A Raman Microprobe Investigation of the Molecular Architecture of Loblolly Pine Tracheids. *In: Proceedings of the 10th international symposium on wood and pulping chemistry, main symposium; 1999 June 7-10; Yokohama, Japan. Atlanta, GA: TAPPI Press. Vol. 1: 96-101*
- [3] U.P. Agarwalv and S.A. Ralph. 1997. FT-Raman Spectroscopy of Wood: Identifying Contributions of Lignin and Cabohydrate Polymers in the Spectrum of Black Spruce (*Picea mariana*). *Applied Spectroscopy 51*, No. 11. 1648-1655
- [4] N. J. Everall, *Applied Spectroscopy* 2000, 54, No. 6. 773-782
- [5] U.P. Agarwal, 1999. An Overview of Raman Spectroscopy as Applied to Lignocellulosic Materials. *In: Argyropopoulos, Dimitris S., comp., ed. Advances in lignocellulosics characterization. Atlanta, GA: TAPPI Press: Chap. 9: 201-225.*
- [6] T. Röder, G. Koch, H. Sixta, Application of Confocal Raman Spectroscopy for the Topochemical Distribution of Lignin and Cellulose in Plant Cell Walls of Beech Wood (*Fagus sylvatica* L.) compared to UV Microspectrophotometry, *Holzforschung* 2004,58, 480-482.
- [7] Hagstrand, P.O., Mechanical analysis of melamine-formaldehyde composites. Ph.D. thesis, Chalmers University of Technology, 1999
- [8] Larkin, P. J., Makowski , M. P., Colthup, N. B., Flood, L. A. (1998) *Vibrational Spectroscopy* 17: 53-72
- [9] N. Gierlinger, C. Hansmann, T. Röder, H. Sixta, W. Gindl, R. Wimmer, Comparison of UV- and confocal Raman microscopy to measure the melamine-formaldehyde resin content within cell walls of impregnated spruce wood, *Holzforschung*, in press

INVESTIGATION OF STORAGE CONDITIONS ON BEECH WOOD LOGS AND CHIPS AND ITS INFLUENCE ON THE PRODUCTION OF DISSOLVING SULFITE PULP

Andrea Promberger¹, Hedda K. Weber¹, Andreas Stockinger¹, and Herbert Sixta²

¹ Competence Center Wood, Area 6, 4860 Lenzing, Austria, Werkstrasse 1

² Lenzing AG, BU Pulp ZF, 4860 Lenzing, Austria, Werkstrasse 1

The storage of wood is of great importance in the pulping industry for the production of dissolving pulp. Extended storage is manifested in the deterioration and discoloration of the wood, which is mostly combined with some wood loss. The resulting costs are essential factors in the pulping process.

Beech wood logs have been stored for one year under dry conditions, submerged in water and irrigated, respectively. Afterwards, dissolving pulp was produced according to the acidic Mg-bisulfite pulping process. This was the basis for the evaluation of the wood quality after storage. The results were correlated with pulp from freshly cut beech wood.

Additionally, the chip storage in silos was closely investigated because of the newly equipped wood yard in Lenzing. In particular, the storage time and the

CO₂ development, which is a side effect of the chip storage, were explored. Laboratory experiments were performed and compared to the chip samples from the production line as well as fresh beech wood. Furthermore, a plant trial was performed to gain better information about the wood chip storage and the quality changes during the storage period in the day-to-day production.

The water-stored wood logs showed a very good pulping performance being comparable to that of fresh beech wood. Dry stored wood, however, showed a very poor delignification and a decrease in brightness. This is attributed to highly condensed structures, which were determined with UV-microspectrophotometry.

Keywords: *beech wood, storage, irrigation, chip silo, sulfite dissolving pulp*

Introduction

The quality of wood is a very important aspect in the production of dissolving pulp. In the case of Lenzing, where the studies took place, primarily beech wood is used for the production of pulp by the acidic Mg-sulfite process.

The beech logs are mainly harvested in the non-growing season. This results in an extended storage period of several months before the wood is introduced into the process. The different storage methods severely influence the wood quality and the best conditions have to be found in order to guarantee a minimal quality loss. As shown

before, this seasonal variation of the wood supply significantly affects the delignification and the optical properties of both the pulp and the viscose fibers [1]. Therefore, reinforced bleaching conditions have to be applied to compensate lower brightness, which in turn results in higher bleaching costs.

The unprotected storage of hardwood logs is accompanied by a fast decay, which affects the yield and the properties of the sulfite pulp [2]. The effect strongly depends on the type and degree of the decay as well as on the conversion process and the

resulting final product. The demand for brighter paper from mechanical pulps and the environmental awareness are affecting the bleaching conditions and make it more important to fully utilize the potential of the raw material wood [3]. The importance of fresh wood has also grown for the pulping processes in general [4]. For example, the use of rotten wood increases the amount of chemicals required in Kraft pulping [5]. Mainly fungi are responsible for the decrease in wood quality during storage. Generally, brown rot fungi depolymerize cellulose, which results in decreased fiber strength, while white rot fungi degrade lignin with fewer effects on the strength. Both types of rot degrade hemicellulose and decrease pulp yield [6, 7].

Beech wood (*Fagus sylvatica* L.) is reported to be primarily attacked by white-rot fungi, such as *Trametes versicolor*, *Pleurotus ostreatus*, *Lentinus edodes*, only to name a few [8]. Recently, *Chondrostereum purpureum* and *Schizophyllum commune*, were identified as the two main fungal species growing on the surface of the beech logs in Lenzing [9, 10].

In addition to the long term storage of wood logs the chip storage is of great importance serving as the short term buffer in the production line. It was found that the storage time of beech wood chips significantly influences the optical properties of the pulp [11]. The chip storage of beech wood for only four weeks resulted in a doubling of the kappa number of the unbleached pulp in the course of viscose pulp production by the sulfite process [12]. After the introduction of a silo storage system for wood chips at the wood yard in Lenzing the maximum storage time without any quality loss had to be determined. Therefore, several process parameters like temperature, humidity, time etc. were examined.

Furthermore a microbiological characterization identified *Phanerochaete chrysosporium*, a white rot fungus to be present in the chip silo [13].

Experimental

Raw material: Freshly cut beech wood (*Fagus sylvatica*) was used for all log and chip storage experiments. The long term storage was performed for one year as following:

The logs were divided into three piles. One pile was submerged in the Ager river (WET), one was continuously irrigated with water (IRR) and the third one was stored without further treatment (DRY) on fortified ground.

The fresh beech wood (FRESH) was used as a reference. All wood samples were stored at -18°C immediately after chipping. The chip storage experiments were performed with the fresh beech wood in plastic buckets with a lid in a climate chamber for 2 to 20 days. Each bucket was used for one cooking experiment. The climate chamber parameters were adjusted to 85% humidity and 40°C in order to mimic the production setup. Additionally, the chips from the production silo stored for 2 days as well as for several months were used for comparison. Furthermore, mill trials were performed storing the chips for 3 days and 6 days, respectively.

The acidic Mg-bisulfite pulping experiments were carried out in a 10L-digester according to reference [14].

The wood and pulp samples were analyzed by standard methods. An aliquot of the sample was taken to measure the dry content according to ISO 638-1978. The extractives content of the samples were determined with the following solvents: dichloromethane, acetone, and ethanol analog to the methods DIN 54354, ISO 624 with Soxhlet extraction and gravimetric determination of the dissolved residue. The hot water extraction was performed according to Tappi T207 om -93 and the Klason lignin isolation according to Tappi T 222 os-74 in addition to the acid soluble lignin, which is determined by the UV- VIS spectrometry [15].

The ash content was analyzed at 850°C combustion temperature. The cation

determination including Fe, Ca, Mn, Mg, Si, Ni, Cu was performed by ICP after microwave digestion.

The alkali resistances were analyzed according to ISO 699 / ZM IV/39/67, the carbohydrate composition by total hydrolysis and HPLC separation with AX/EC-PAD detection, the copper number according to ZM IV/8/70 and the carboxylic groups according to *Das Papier* 1965, 19 (1). The UV-microspectrophotometry was performed by Koch, BFH Hamburg [16].

The prepared wood meal (0.5g) (FRESH, WET, IRR, DRY) was stored in sealed headspace vials at 20°, 30°, and 40°C respectively for 0 to 5 days for the CO₂-measurements. The gas phase was analyzed with a headspace (HP-7694) coupled with a GC-MS (Thermoquest-Finnigan GC-Q) and equipped with a J&W GS-GASPRO column (30m x 0.32mm PLOT technology).

Results and Discussion

The analyses of the main wood components in the beech wood logs stored for one year (WET, IRR, DRY) are given in table 1 and are compared to the reference (FRESH). Whereas the changes in the extractives content are significant, the other parameters of the wood samples lay within the natural variation.

Parameters		FRESH	WET	IRR	DRY
DCM	%	0.20	0.19	0.16	0.14
Ethanol	%	1.7	0.6	0.6	0.5
Acetone	%	1.0	0.4	0.4	0.3
Hot water	%	2.7	1.8	1.9	1.9
Glucan	%	41.6	41.9	41.7	41.0
Xylan	%	17.9	17.8	18.0	19.0
Mannan	%	1.3	0.5	0.5	1.1
Arabinan	%	0.5	0.5	0.4	0.3
Galactan	%	1.2	0.6	0.5	0.4
Klason	%	21.1	21.4	20.0	20.7
Acid soluble	%	3.1	3.3	4.1	3.3
Ash content	%	0.34	0.38	0.41	0.32

Table 1. Wood analysis of the main components in fresh and stored wood logs.

The results of the continuous sampling of the stored logs over the storage period

reveal a significant course in the extractives content starting with an increasing release followed by a fast deterioration of the storage substances, particularly in dry stored beech wood as given in figure 1.

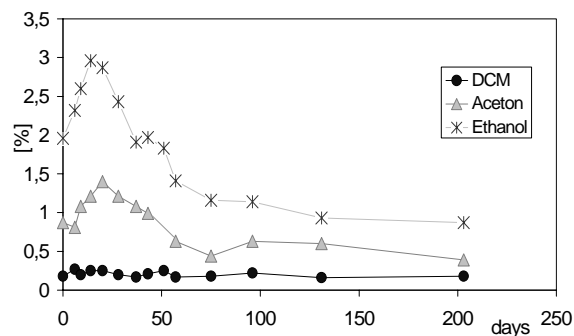


Figure 1. Development of extractives in dry stored beech wood logs over the storage period of time (days)

The samples WET and IRR, however, show only a continuous decrease in the hydrophilic extractives (not shown). These were most likely washed out, whereas the hydrophobic extractives remain constant and were comparable to the values of the dry stored sample.

A variation in the extractives was also observed for the wood chips. The change was caused by the faster deterioration of the storage substances, which were easier accessible because of the larger surface.

Also a rather quick change in the wood color was determined, which could be correlated with the quality of the cooking performance: The delignification selectivity decreased with the increase of the discoloration of the wood chips, which was caused by oxidative reactions of the extractives [17]. These results were verified with the chip storage experiments and the pulp mill trials, which are discussed below. The main interest of the investigation was the performance of the stored wood in the pulping process. Therefore, all stored samples were digested by the acidic Mg-bisulfite process and the produced pulps were analyzed.

Especially the log storage yielded interesting results. Again the fresh beech wood was used as the reference.

Surprisingly, the delignification selectivity of the two wet stored wood samples was excellent and well comparable to the fresh beech wood as illustrated in table 2.

Sample	Visc.	Bright.	Kappa	V/K value
	ml/g	% ISO	#	ml/g
FRESH	700	65	4.4	159
WET	700	67	4.4	160
IRR	700	63	5.2	135
DRY	700	50	7.7	91

Table 2. Viscosity/Kappa ratio of differently stored beech wood samples at the target CED viscosity of 700ml/g

Even the irrigated wood showed a very good delignification performance. In contrast, the pulp product from the dry stored wood had the lowest brightness values and the highest kappa-numbers, resulting in the worst delignification performance.

The results of the chip storage experiments and the chips of the silo were compared with respect to their pulping performance. Again the fresh beech wood was used as the reference. The climate chamber (cc) samples (2d cc and 20d cc) and the silo samples were cooked at two different H-factors.

Despite the expectations of a gradually decreasing performance of the stored beech wood chips, all but one sample showed no negative storage effect (figure 2).

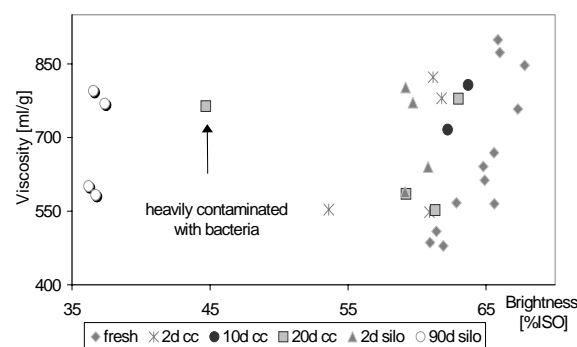


Figure 2. Delignification as correlation of viscosity to brightness of differently stored beech wood chips from the climate chamber and the silo

The delignification of the silo samples had as expected a slight and a high decrease for the 2d and 90d stored sample, respectively. The sample from the climate chamber (20d cc), which did not follow this trend, was discolored and heavily contaminated with bacteria on the chip surface. It gave a bad result concerning the brightness and delignification performance. Although the growth of micro-organisms was limited to the chip surface, we assume that the bad pulping performance was caused by this infestation. For example the fungus *C. purpureum* along with other surface growing micro-organisms can build up barriers for the cooking liquor with their hyphae and, therefore, inhibit the impregnation and penetration of the wood. Conclusively, this could result in a higher amount of residual lignin and chromophoric structures.

We assume that during the experiment the lids of the buckets were airtight excluding the 20d cc sample. This resulted in an oxygen limitation because of the respiratory activity of micro-organisms present. The atmosphere in the buckets did not suffice for a continuous growth of the various micro-organisms before long. All analysis buckets as well as the contaminated sample were reopened during that storage time and changed their color quickly, whereas the unopened samples kept their original color.

A pulp mill trial was performed with an extended storage of the wood chips in the silo for 3 and 6 days, respectively. The unbleached pulps were compared with the previously produced batch under comparable conditions. The trial data are presented in table 3.

These experiments revealed that the decrease of the brightness seemed to be high within the first 3 days but no further changes were observed for this parameter after another three days of storage. The

variation of the kappa number, however, doubled between the 3rd and 6th day of storage. We presume that the high impact of these storage experiments on the pulp quality originated from a great quantity of fresh beech wood present in the silo, which has a higher concentration of extractives as described before. Additionally, the high outside temperatures during these experiments promoted the unwanted oxidation and condensation reactions in the silo [19].

Storage time	$\Delta Kappa$	$\Delta Brightness$	$\Delta Visc.$
	% Δ	% Δ	% Δ
3 days	+ 10,9	- 5,3	+ 12,3
3 days	+ 17,5	- 7,3	+ 4,0
6 days	+ 30,4	- 7,0	- 4,3
6 days	+ 31,6	- 5,1	+ 10,6

Table 3 Percentile variation of the plant trial of 3d and 6d chip storage in the silo in relation to the prior pulp batch

These results are comparable to the quality decrease described by Etzhöld [18], although his investigation was made with outdoor piles over a longer period of time. Another practical aspect in the silo storage is the massive development of CO₂ in the silo, which can reach high concentrations depending on the storage time, temperature, wood quality, silo operation mode, and several other parameters.

As already mentioned the CO₂-development is dependent on the storage temperature of the wood chips (figure 3). A higher temperature resulted in an increasing CO₂-concentration. We assume that the development of CO₂ has two different sources, on one hand the increased microbial activity with the risen temperature and on the other hand the accelerated enzymatic oxidation of the extractives in the parenchyma cells at elevated temperatures as described by Koch [20], [17].

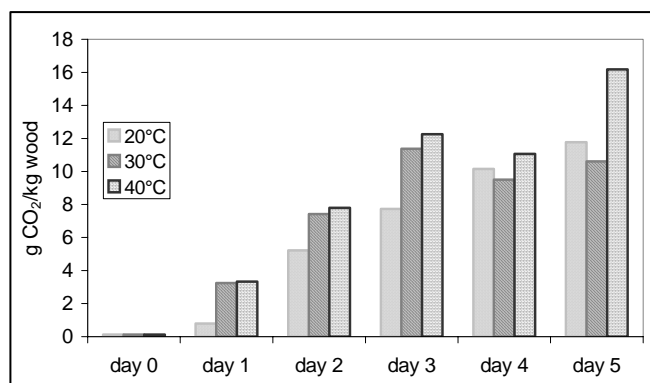


Figure 3. Cumulative CO₂ concentration deriving from freshly cut beech wood chips at different temperatures

Since the CO₂ development also closely correlated with the concentration of the extractives, it can be clearly stated that wood with high extractives content e.g. fresh beech wood produces more CO₂ than dry stored wood (figure 4).

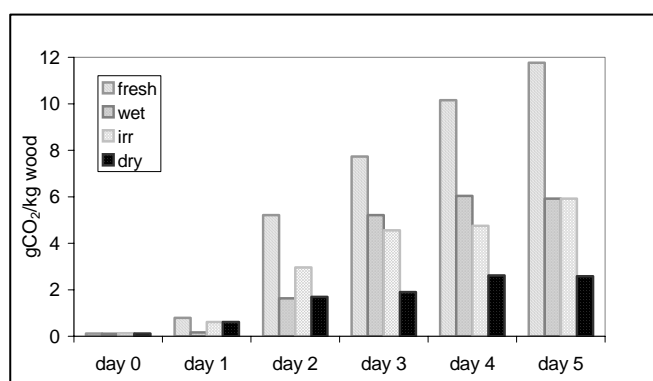


Figure 4. Cumulative CO₂ concentration in 1 year wet, irrigated and dry stored beech wood in comparison to fresh beech wood.

Conclusion

The characteristic in the different storage forms was accompanied by the variation of the extractives content, which is also very important concerning the CO₂-development.

The delignification was also influenced by the storage conditions of the logs and chips. The wet and irrigated samples had a better and faster delignification performance compared to the dry stored wood. The mill

trials gave a decreasing performance with increasing chip storage time.

The brightness results showed the same trend as those from the delignification. The wet and irrigated wood was comparable to the fresh samples, whereas the dry sample had a higher content of residual chromophores, highly condensed structures, which were found and further investigated by Koch with UV-microspectrophotometry [21]. These substances are most likely polyphenols, which are accumulated in the cell lumina [14]. This result is also in accordance to the blocked cell lumina reported by Hägglund and Lange [22].

Finally we can state that the lower degree of delignification including the [17] presence of highly condensed structures in the unbleached pulp negatively effected the bleaching process by demanding a higher amount of bleaching chemicals. A wet storage of the beech wood logs is definitely of advantage for the pulping process of dissolving pulp as well as a short storage time of the chips in the silo especially during the warm season.

Acknowledgement

Financial support was provided by the Austrian government, the provinces of Lower Austria, Upper Austria and Carinthia as well as by the Lenzing AG. We also express our gratitude to the Johannes Kepler University, Linz, the University of Natural Resources and Applied Life Sciences, Vienna, and the Lenzing AG for their in kind contributions. We also want to thank Dr. Gerald Koch from the BFH Hamburg, Germany for the UV-microspectrophotometric measurements

References

[1] Sixta, H.; Promberger, A.; Koch, G.; Gradinger, C.; Messner, K.; In *International Symposium on Wood Based Materials; Wood composites*

and Chemistry; Robert Stingl, ed.; Inst. of Wood Science and Technology: Vienna, 2002; Vol. 4, pp. 455.

- [2] Rydholm, S. A.; *Pulping Processes*, Wiley Interscience: New York 1965.
- [3] Varhimo, A.; Tuovinen, O.; In *Mechanical Pulping*, Sundholm J., ed.; FAPET/Tappi: Helsinki, 1999, pp. 67.
- [4] Söderstam, G.; Öman, M.; Olofsson, J.; In *STFI Renseri konferens*; STFI: STFI Stockholm, 1998.
- [5] Henningsson, B.; *Biodeterioration Materials* 1972, 2, 336.
- [6] Hunt, K.; *Pulp Paper Can.* 1978, 79, T194.
- [7] Procter, A. R.; *Pulp Paper Can.* 1973, 74, 62.
- [8] Faix, O.; Bremer, J.; Schmidt, O.; Stevanovic, J.; *J. Anal. Appl. Pyrolysis* 1991, 21, 147.
- [9] Promberger, A.; Sixta, H.; Gradinger, C.; Messner, K.; In *223rd ACS National Meeting*; American Chemical Society: Orlando, USA, 2002, pp. CELL 110.
- [10] Gradinger, C., Personal Communication.
- [11] Lenz, J.; Fuhrmann, F.; Peter, W.; Geppert, K.; *Lenzinger Berichte* 1981, 51, 10.
- [12] Fischer, K.; Schmidt, I.; *Zellstoff und Papier* 1977, 11, 344.
- [13] Gradinger, C.; K.Messner; Promberger, A.; Sixta, H.; In *12th International Symposium on Wood and Pulping Chemistry*; University of Wisconsin, Madison, Department of Forest Ecology and Management: Madison, USA, 2003; Vol. 3, pp. 27.
- [14] Sixta, H.; Promberger, A.; Koch, G.; Gradinger, C.; Messner, K.; *Holzforschung* 2004, 58, 14.
- [15] Sjöström, E.; Alén, R.; *Analytical Methods in Wood Chemistry, Pulping and Papermaking*, Springer Verlag: Heidelberg 1999.
- [16] Koch, G.; Kleist, G.; *Holzforschung* 2001, 55, 563.

- [17] Koch, G.; Bauch, J.; Puls, J.; Welling, J.; *ForschungsReport* 2001, 2, 30.
- [18] Etzhold, C.; Kretschmar, G.; Öchsner, W.; Wiessner, P.; *Zellstoff und Papier* 1974, 5, 131.
- [19] Promberger, A.; 2004, Doctoral thesis, University of Technology Graz, Graz
- [20] Koch, G.; Bauch, J.; Puls, J.; Schwab, E.; Welling, J.; *Holzzentralblatt* 2000, 6, 1.
- [21] Koch, G.; Puls, J.; Bauch, J.; *Holzforschung* 2003, 57, 339.
- [22] Hägglund, E.; Lange, P. W.; Über den Sulfitaufschluß von weißfaulem Buchenholz, Report, Schwedisches Holzforschungsinstitut: Stockholm, 1950.

PRODUCTION OF SPRUCE DISSOLVING PULP WITH THE PREHYDROLYSIS-ALKALINE SULFITE PROCESS (PH-ASA)

O. Kordsachia, S. Roßkopf, R. Patt

Institute for Wood Chemistry and Chemical Technology of Wood and
Department of Wood Science, Section Chemical Technology of Wood
Leuschnerstraße 91
D-21031 Hamburg
e-mail: o.kordsachia@holz.uni-hamburg.de

Introduction

Kraft and soda/AQ pulping are well-established technologies for paper pulp production. With preceding acid hydrolysis (PH) the kraft process is also used for dissolving pulp production. The simple soda process is preferentially applied to nonwoods, but as PH-Soda/AQ process also appropriate for production of dissolving pulps from hardwoods. The alkaline sulfite pulping process with addition of anthraquinone and methanol (ASAM) was developed initially as an alternative to the kraft process for the production of paper pulps. With a prehydrolysis stage, this process can also be used to produce high-grade dissolving pulps [1-4]. Up to now, this process has not been implemented on an industrial scale mainly due to problems caused by the presence of methanol in this process. It requires an explosion proof digester house and methanol recovery facilities. We have tried to eliminate methanol without losing the distinct advantages of the ASAM pulping process. Without methanol, the extent of delignification is considerably reduced. This loss in delignification efficacy can be compensated for by changing the Na_2SO_3 :NaOH ratio and the mode of NaOH addition. A high percentage of sodium sulfite in the total chemical charge - as applied in ASAM cooking - provides the process with high selectivity in lignin removal. With increased sodium hydroxide percentage delignification is improved at the expense of selectivity. A high charge of sodium hydroxide results in an enhanced

carbohydrate degradation, especially in the initial cooking phase. It was possible to demonstrate that the results of alkaline sulfite/AQ pulping with increased NaOH percentage in the total chemical charge can be substantially improved when the NaOH charge is split: one part is added to the impregnation liquor and another part is added when the maximum cooking temperature has been reached. In softwood pulping this NaOH splitting has a twofold effect: the pulp viscosity increases and simultaneously delignification is extended. With this so-called ASA process we were able to obtain results similar to those achieved in ASAM pulping [5]. This was the starting point for our investigations on ASA pulping with prehydrolysis for production of dissolving pulps.

Optimization of different alkaline dissolving pulp processes

In order to explore the potential of the ASA process for production of dissolving pulp grades, softwood (spruce) was chosen as raw material, because it is more difficult to pulp than hardwood. This study comprised three parts: first the modified AS/AQ process with prehydrolysis stage (PH-ASA) was optimized, then the cooking results were compared with those obtained with other processes carried out for comparison under standardized conditions, and finally a PH-ASA pulp was bleached in a TCF sequence.

For all cooks industrial spruce chips from a German pulp mill were used. The chemical composition of the extract-free raw material was analyzed according to Puls et al. [6]. After total hydrolysis the monomer sugars detected by HPLC were calculated into cellulose and the different hemicelluloses according to Janson [7]. The lignin content was determined by applying the Klason method. Table 1 shows the chemical composition of the spruce chips.

Cellulose	44.8 %
Glucomannan	16.6 %
Xylan	7.3 %
Lignin	28.1 %

Table 1. Chemical composition of spruce chips

Prehydrolysis ASA pulping

In earlier investigations we optimized the conditions of prehydrolysis with weak sulfuric acid and of cooking for PH-ASAM pulping of spruce [1-4]. Based on this knowledge, the prehydrolysis conditions for PH-ASA cooking were fixed. Only the H₂SO₄ charge, the most important hydrolysis factor, was varied. Liquor to wood ratio, heating up time, maximum temperature, and treatment time at T_{max} were kept constant. In ASA cooking, those cooking conditions were applied which have been proven optimal for spruce ASA paper pulps [5]. Only a few parameters, like the alkali ratio (Na₂SO₃:NaOH), the NaOH splitting ratio and the cooking time, were varied systematically.

Prehydrolysis and cooking were carried out in two separated steps. The prehydrolysis stage was performed in an indirectly steam-heated 30 l-digester with forced liquor circulation charging always 4500 g o.d. wood. The prehydrolyzed chips were washed with cold water, dewatered and cold stored till further use in cooking. The ASA cooks were carried out in a 71 MK-digester with liquor

circulation. The charge of prehydrolyzed spruce chips was 600 o.d. wood minus the yield loss during the prehydrolysis stage. Unless otherwise stated in the tables or figures, the standard conditions listed in table 2 were applied in prehydrolysis and cooking.

In the first set of experiments, the H₂SO₄ charge in the prehydrolysis step was varied between 0.3 and 0.5 %/o.d. wood. In the subsequent ASA cooking stage the alkali ratio was 60:40. All other parameters were as listed in table 2.

Prehydrolysis	
H ₂ SO ₄ (%/o.d. wood)	0.3
Liquor to wood ratio	4:1
Maximum temperature (°C)	140
Time to T _{max} (min)	15
Time at T _{max} (min)	120
Cooking	
Chemical charge (%/o.d. wood)	27.5
Na ₂ SO ₃ /NaOH ratio	70:30
NaOH splitting	25:75
AQ charge (%/o.d. wood)	0.1
Liquor to wood ratio	4:1
Maximum temperature (°C)	170
Time to T _{max} (min)	75
Time at T _{max} (min)	180

Table 2. Prehydrolysis and cooking conditions

The sulfuric acid charge had a strong effect on the severity of hydrolysis. The yield loss in prehydrolysis with 0.3 % H₂SO₄ was only 12.2 %. The losses increased to 15.4 and 16.4 % with 0.4 and 0.5 % H₂SO₄ charge, respectively. Apparently, only a part of the hemicelluloses is already dissolved in the prehydrolysis stage. In an earlier investigation, we found that most of the hardwood xylans are already dissolved in the prehydrolysis stage, whereas softwood hemicelluloses are only partially degraded during prehydrolysis and most of them are dissolved in the following cooking stage [3].

An increased sulfuric acid charge impaired the pulping results considerably; in particular the pulp viscosity was affected (table 3). The higher kappa numbers attained after prehydrolysis with higher H₂SO₄ charge can be explained by enhanced lignin condensation, as it is known that softwood lignin tends to condensate easily under those conditions. With 0.3 % sulfuric acid the by far best cooking results were obtained with highest viscosity and lowest kappa number at only marginally reduced R₁₀ and R₁₈ values. However, even with the mildest prehydrolysis conditions, the pulp viscosity was below 1000 ml/g, due to the severe cooking conditions, especially the high NaOH percentage in the total chemical charge.

H ₂ SO ₄ (%)	Kappa no.	Visc. (ml/g)	Total yield (%)	Rej. (%)	Brightness (%)	R ₁₀ (%)	R ₁₈ (%)
0.3	17.7	959	39.5	2.4	31.3	95.2	95.7
0.4	20.5	878	39.2	2.4	28.3	95.4	95.8
0.5	20.1	832	39.2	1.5	29.7	95.4	95.9

Table 3. Impact of H₂SO₄ charge in prehydrolysis on PH-ASA cooking
 PH: 140 °C, 120 min.
 ASA: 27.5 % chemicals, alkali ratio 60:40, NaOH splitting 25:75, 170 °C, 120 min at T_{max}

Alkaline sulfite pulping offers the option to change the alkalinity of the cook by variation of the Na₂SO₃:NaOH ratio. Less NaOH in the cooking liquor reduces the alkaline attack on carbohydrates and thus increases the viscosity. In the second set of cookings the alkali ratio was varied between 65:35 and 80:20. The prehydrolysis was done with a H₂SO₄ charge of 0.3 %. The conditions and results are shown in Figure 1.

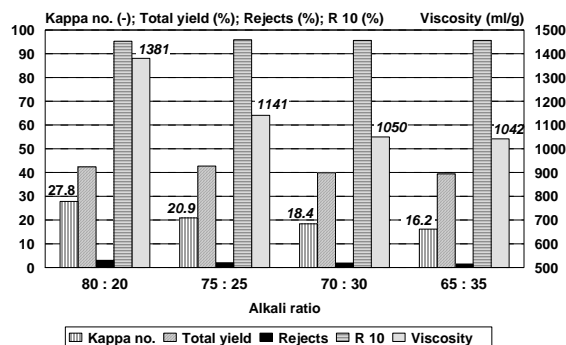


Figure 1. Effect of alkali ratio on PH-ASA cooking
 PH: 0.3 % H₂SO₄, 140 °C, 120 min.
 ASA: 27.5 % chemicals, NaOH splitting 25:75, 170 °C, 120 min heating up, 180 min at T_{max}

The results in Figure 1 demonstrate that the Na₂SO₃:NaOH ratio has a strong impact on extent and selectivity of delignification. At an alkali ratio of 80:20, a pulp with high yield and viscosity but also high kappa number was obtained. With decreasing percentage of Na₂SO₃ the delignification was considerably improved at the expense of selectivity. With an alkali ratio of 70:30 a kappa number below 20 was attained at still high viscosity of 1050 ml/g. Therefore, we decided to apply this alkali ratio in further trials.

Since tentative investigations on ASA cooking after prehydrolysis with 0.5 % sulfuric acid had shown that, in accordance with cookings without prehydrolysis, NaOH splitting improves selectivity considerably, the impact of the NaOH splitting ratio was investigated in detail, starting with a mild prehydrolysis (0.3 % H₂SO₄). Based on the results achieved with paper pulps, the NaOH splitting ratio was varied in the most beneficial range between 50:50 and 25:75 (Figure 2).

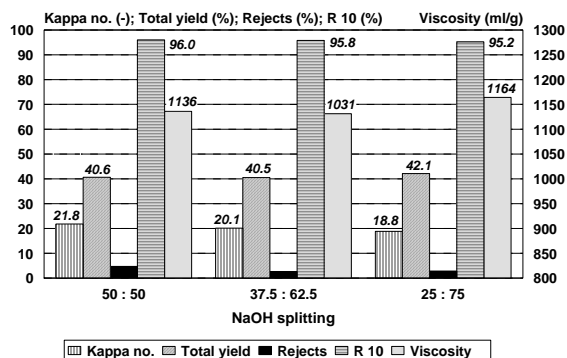


Figure 2. Effect of the NaOH splitting ratio on cooking results

PH: 0.3 % H₂SO₄, 140 °C, 120 min.
 ASA: 27.5 % chemicals, alkali ratio 70:30, 170 °C, 180 min at T_{max}

Also in the case of PH-ASA pulping, an alkali splitting, i.e. a lower alkalinity of the impregnation liquor, improves the selectivity of the cook. When less alkali is added at the beginning of the cook, the extent of cellulose degrading reactions is restricted. Moreover, lignin sulfonation, and thus lignin dissolution, is promoted by NaOH splitting because of the higher percentage of sodium sulfite in the total chemical charge in the initial cooking phase. Consequently, an alkali splitting of 25:75 resulted in higher yield and viscosity and, simultaneously, in a lower lignin content (Figure 2).

The kappa number to viscosity relationship for PH (0.3 % H₂SO₄)-ASA cooks carried out at different Na₂SO₃:NaOH ratios is shown in Figure 3. As pointed out before, the alkali ratio is the main influencing factor on this relationship. Delignification to a low kappa number is inevitably accompanied by a drastic reduction in pulp viscosity. It was also not possible to increase selectivity by lowering the maximum temperature from 170 to 165 °C. A significant improvement of the process selectivity can only be achieved by reducing the severity of the prehydrolysis stage. Presumably even milder hydrolysis conditions are sufficient to achieve a high α-cellulose content because of the efficient hemicelluloses dissolution in the ASA

cooking stage. This is obviously a further potential for process optimization.

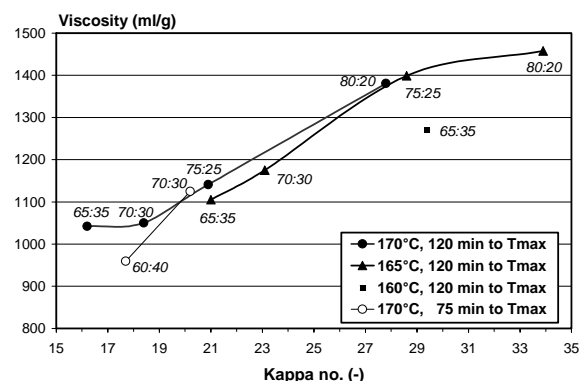


Figure 3. Kappa number to viscosity relationship in PH-ASA cooking with different alkali ratio
 PH: 0.3 % H₂SO₄, 140 °C, 120 min.
 ASA: 27.5 % chemicals, NaOH splitting 25:75, 180 min time at T_{max}.

Prehydrolysis Soda/AQ pulping

The same prehydrolyzed spruce wood samples used in ASA cooking to investigate the impact of different sulfuric acid charges on the cooking results were taken for PH-soda/AQ pulping. This approach has the advantage that the cooking results are not affected by different results of the prehydrolysis stage, and the results of the different cooking methods are directly comparable.

The soda/AQ cooks were also performed in the 7 l MK digester with same amounts of prehydrolyzed raw material. 25 % NaOH per o.d. wood were charged in the cooking stage and maximum temperature was 165 °C, which means 5 °C lower than in standard ASA cooking. The other parameters are given in table 2 and 4.

H ₂ SO ₄ (%)	Kappa no.	Visc. (ml/g)	Total yield (%)	Rej. (%)	Bright-ness (%)	R ₁₀ (%)	R ₁₈ (%)
0.3	19.4	557	38.6	0	25.4	92.8	95.1
0.4	21.5	483	38.0	0	26.8	92.7	96.0
0.5	20.0	467	37.0	0	27.4	92.8	96.1

Table 4. Impact of H₂SO₄ charge in prehydrolysis on PH-soda/AQ cooking
 PH: 140 °C, 120 min.
 Soda/AQ: 25 % NaOH, 0.1 % AQ, 165 °C, 75 min heating up, 180 min cooking time

The results presented in table 4 show that it is also possible with the PH-soda/AQ process to produce pulps with low kappa numbers around 20. The prehydrolysis treatment improves delignification considerably. A standard soda/AQ process is not able to delignify spruce wood to such an extent. However, this extensive delignification is only possible at the expense of pulp viscosity, which is reduced to a level which is critical for most uses of dissolving pulp, considering that bleaching will further reduce the DP of the cellulose. All soda/AQ pulps have a fairly low purity represented by R_{10} values. The difference between R_{18} and R_{10} exceeds 3 %. This indicates that these PH-soda/AQ pulps contain a lot of short chained carbohydrates which have a different solubility in 10 or 18 % NaOH [8]. Pulp brightness is also very low, and it can be assumed that this pulp will have a poor bleachability. As in ASA pulping a prehydrolysis treatment using 0.3 % H_2SO_4 /o.d. wood yields the best pulp, in particular with regard to pulp viscosity.

It is generally accepted that PH-soda/AQ pulping is not a suitable process for dissolving pulp production from softwoods. Further cookings at 160°C have shown that the pulp viscosity can be improved to some extent. However, it is necessary to stop delignification at a kappa number well above 30 to reach reasonable viscosities. But the target of these reference cooks was the production of pulps with low kappa number suitable for TCF bleaching.

Prehydrolysis Kraft pulping

As in PH-soda/AQ cooking the raw material prehydrolyzed with 0.3, 0.4 and 0.5 % sulfuric acid was used in the kraft references. Again, the cooking conditions were kept constant. The active alkali charge was 24 %/o.d. wood, calc. as NaOH, at a sulfidity of 30 %. The cooks

were performed at 170 °C and cooking time was 60 min (table 5).

H_2SO_4 (%)	Kappa no.	Visc. (ml/g)	Total yield (%)	Rej. (%)	Brightness (%)	R_{10} (%)	R_{18} (%)
0.3	24.5	840	39.9	0.1	24.5	94.3	95.3
0.4	25.5	716	39.2	0.1	29.5	94.5	96.2
0.5	25.3	686	38.2	0.1	30.4	93.5	95.3

Table 5. Impact of H_2SO_4 charge in prehydrolysis on PH-kraft cooking

PH: 140 °C, 120 min.

Kraft/AQ: 24 % active alkali (as NaOH), 30 % sulfidity, 170 °C, 75 min heating up, cooking time 60 min

Due to the short cooking time, higher kappa numbers were obtained compared to ASA cooking. Nevertheless, the PH-kraft pulps had lower pulp viscosities than the PH-ASA pulps, which also decreased with increasing sulfuric acid charge.

Compared to the PH-ASA pulps, the R_{10} values are lower and the difference between R_{18} and R_{10} is greater, which indicates that the PH-kraft pulps contain more degraded cellulose. The yield of the kraft reference cooks is fairly high, but it has to be considered that the residual lignin content of all kraft pulps is higher than that of the corresponding ASA and soda pulps.

Prehydrolysis ASAM pulping

In ASAM pulping of the prehydrolyzed spruce chips, a total chemical charge of 25 %/o.d wood was applied. The ASAM cooks were performed in a 71 rotating digester designed for higher maximum pressure with addition of methanol (15 % v/v of the cooking liquor) and AQ (0.1 %/o.d. pulp). The Na_2SO_3 :NaOH ratio was 80:20 and cooking time 150 min at 180 °C. The cooking results are shown in table 6.

H ₂ SO ₄ (%)	Kappa no.	Visc. (ml/g)	Total yield (%)	Rej. (%)	Bright- ness (%)	R ₁₀ (%)	R ₁₈ (%)
0.3	18.3	1147	40.0	1.0	40.1	95.3	96.6
0.4	22.7	1097	40.1	2.1	35.6	95.3	96.3
0.5	26.0	1087	40.1	1.6	36.1	95.7	95.6

Table 6. Impact of H₂SO₄ charge in prehydrolysis on PH-ASAM cooking

PH: 140 °C, 120 min.

ASAM: 25 % chemicals, alkali ratio 80:20, 0.1 %

AQ, 15 % v/v methanol, 180 °C, 75 min heating

up, 150 min cooking time

The results obtained in these cooks are very close to those of PH-ASA pulping. Both processes yielded excellent dissolving pulps with high purity, high viscosity, and low kappa number.

In the ASAM cooks all cooking chemicals were added at the beginning of the cook. The cooking results can be improved by NaOH splitting as well, but to a lesser extent than in ASA cooking, where more sodium hydroxide is charged.

As in the other pulping processes the best pulp properties, especially with regard to the kappa number to viscosity ratio, were obtained with 0.3 % sulfuric acid in the prehydrolysis stage. All ASAM results confirm earlier findings [1-4].

Of all processes investigated, ASAM yielded the highest pulp brightness. As shown in a previous study, the bleachability of PH-ASAM softwood pulps is excellent and, therefore, bleaching can be performed in a TCF sequence [2]. Of course the technical performance of the ASAM process is more complicated due to the presence of methanol and the high cooking temperature required. These are the reasons why we have been developing the prehydrolysis ASA process, which yields similar results except for pulp brightness. The lower brightness of the PH-ASA pulps might be caused by more intense lignin condensation due the absence of methanol. In that case, it would be much more difficult to bleach the pulp

to high brightness. Therefore, we have tested the bleachability of these ASA pulps in detail (see chapter 3).

Comparison of different alkaline dissolving pulp processes

A comparison of the results of the different processes investigated is given in Figure 4 and 5. The screened pulp yield from all processes is almost at the same level when the different residual lignin contents of the pulps are considered (Figure 4). ASAM and ASA pulping, performed at moderate alkalinity, yielded similar results. It was possible to achieve high pulp viscosity at low residual lignin content without affecting the pulp purity. The serious carbohydrate degradation provoked by the stronger alkaline processes is reflected in fairly low pulp viscosities and, as shown before, by the greater differences between the R₁₀ and R₁₈ values. Both cooking processes, in particular the PH-soda/AQ, must be stopped at much higher kappa numbers in order to produce pulps with higher viscosities required for higher-valued applications.

The carbohydrate composition of the dissolving pulps from the different processes differs as well (Fig. 5). Again the superiority of alkaline sulfite pulping is evident. In ASA and ASAM the cellulose is attacked and dissolved to a minor extent, and the resulting pulps contain fewer hemicelluloses. The ASAM pulp has the highest purity, but the carbohydrate composition of the ASAM and the ASA pulp differs only slightly.

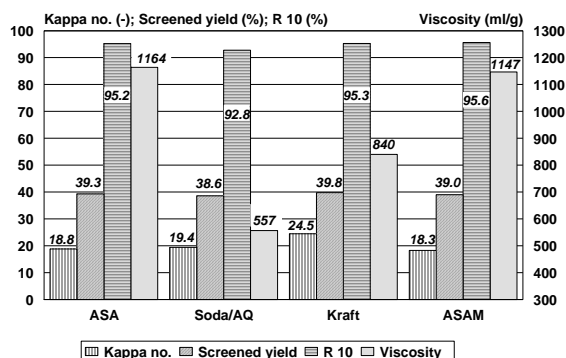


Figure 4. Comparison of the different spruce dissolving pulps prepared with a charge of 0.3 % H₂SO₄ in the prehydrolysis stage

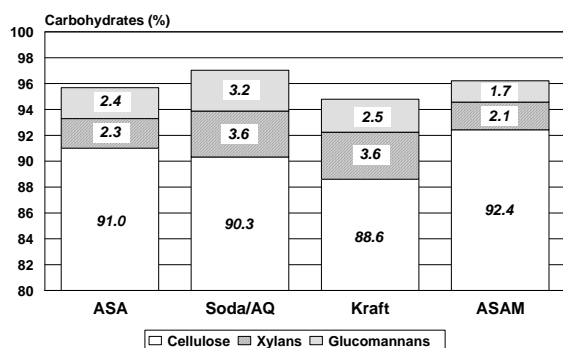


Figure 5. Carbohydrate composition of the dissolving pulps

TCF bleaching of PH-ASA pulp

Bleaching of dissolving pulps is primarily a purification process. Dissolving softwood pulps produced in alkaline cooking processes are generally bleached conventionally with chlorine containing bleaching agents or in ECF sequences because the use of chlorine dioxide improves the cleanliness of the pulp effectively while preserving the pulp viscosity. Moreover, disturbing inorganic compounds are effectively removed in D stages due to the acidic conditions. However, from an environmental point of view, closed mill operation is the ultimate goal. This is facilitated when chlorine-free bleaching agents are exclusively applied in TCF sequences.

The initial idea was to start TCF bleaching of PH-ASA softwood pulp at low kappa

number in the range of around 20 in order to facilitate the bleaching process with oxygen based chemicals, which are much less selective than chlorine dioxide. As shown before in Figure 3, the final phase of PH-ASA pulping is not very selective and the reduction of the kappa number from above 30 to below 20 was associated with a drastic loss in viscosity by almost 400 ml/g. Therefore, the question arose if it would not be better to carry out this final delignification in the oxygen stage instead. Dissolving pulps show much better response to oxygen delignification than paper pulps, and high delignification rates can be achieved with moderate conditions.

It was therefore tested in a preliminary investigation which kappa number would be the best to start oxygen delignification. We took four unbleached PH-ASA pulps, covering a kappa number range from 19 to 34, and subjected them to oxygen bleaching. The target kappa number after the oxygen stage was 5-6. The NaOH charge was varied depending on the kappa numbers of the unbleached pulps, all other conditions were kept constant. The bleaching conditions and results are listed in table 7.

<i>unbleached</i>				
Kappa no.	18.8	23.1	27.8	33.9
Viscosity (ml/g)	1164	1175	1381	1458
Brightness (%ISO)	32.6	33.0	35.2	33.3
<i>O stage</i>				
NaOH charge (%)	2.5	2.5	3.5	3.5
Kappa no.	5.2	5.7	5.8	7.6
Viscosity (ml/g)	933	866	926	978
Brightness (% ISO)	48.8	46.0	44.9	47.1

Table 7. Oxygen delignification of PH-ASA pulps with different starting kappa numbers
Bleaching conditions: 0.6 % MgSO₄, O₂ pressure 0.6 MPa, 10 % consistency, 120 min, 98°C

Oxygen delignification resulted in a leveling of the great differences in pulp viscosity. It was not possible to preserve the viscosity gain of the pulps with high kappa number, which means that oxygen

delignification did not show better selectivity than the final phase of ASA cooking.

The very high extent of delignification achieved in the oxygen stage, ranging from 72 to almost 80 %, demonstrates that PH-ASA softwood pulps respond very well to oxygen delignification and, in principle, high unbleached kappa numbers can be accepted. However, in the case of the pulp with the highest kappa number of 34, it was not possible to attain the targeted low kappa number below 6, necessary for chlorine-free final bleaching.

The best kappa number to viscosity ratio after oxygen delignification was obtained with the lowest unbleached kappa number of 19 (table 7). Thus, we concluded that an unbleached kappa number pulp below 20 would be the best starting point for TCF bleaching in an O/Q/OP/Z/Q/P sequence.

To prepare enough pulp for the bleaching trials, an additional PH-ASA cook was performed using optimized conditions. In order to avoid a too high reject content in ASA cooking due to the only moderate alkalinity of the cooking liquor, the heating up time was extended to 120 min. All other conditions were the same as given in table 2. In this case, however, both stages, prehydrolysis and cooking, were carried out consecutively in the 30 l-digester charging 4500 g of spruce chips. Between both stages the chips were washed with cold water. Similar results as in the corresponding cook with smaller wood charge were obtained (table 8).

	unbleached	O stage
Kappa no.	19.4	5.7
Viscosity (ml/g)	1195	939
Brightness (% ISO)	31.7	44.7

Table 8. Results of oxygen bleaching of ASA pulp with a starting Kappa number of 19.4
Bleaching conditions: 2.5 % NaOH, 0.6 % MgSO₄, O₂ pressure 0.6 Mpa, 10 % cons., 120 min, 98 °C

In oxygen delignification of this pulp the same conditions were applied as before for the pulp with the lowest kappa number (see table 7). Compared to the preliminary trials, the slightly increased kappa number of the unbleached sample resulted in a marginally higher kappa number at the same viscosity. After the oxygen stage, and after each of the other bleaching stages, the pulp was thoroughly washed with deionized water.

The first chelation stage (Q₁) with 0.2 % DTPA/o.d. pulp, carried out to remove transition metal ions, resulted in a brightness increase by 7 % ISO. This chelation stage was followed by a peroxide reinforced oxygen stage (OP). Based on the results of preliminary trials, performed with small pulp charges to find optimal conditions, a bigger pulp charge was subjected to OP bleaching. Only 1 % alkali and 0.5 % peroxide per o.d. pulp were sufficient to reduce the kappa number from 5.6 to 3. With only small viscosity losses the brightness increased from 51.8 to 68.5 % ISO (table 9).

	Q ₁ stage	OP stage
Kappa no.	5.6	3.0
Viscosity (ml/g)	939	881
Brightness (%ISO)	51.8	68.5

Table 9. Results of Q and OP stages

Bleaching conditions:

Q₁: 0.2 % DTPA, pH 5.2, 3 % cons., 30 min, 50 °C

OP: 1.0 % NaOH, 0.5 % H₂O₂, 10 % cons., 0.3 %

MgSO₄, Opress: 0.6 Mpa, 120 min, 98 °C

Prior to high consistency ozone treatment, the pH was adjusted with sulfuric acid to 3.0, dewatered to 40 % consistency and fluffed in a refiner. Once more preliminary trials were performed to optimize this stage. The ozone charge was increased in 0.05 % steps from 0.2 to 0.5 %. Depending on the ozone charge, kappa numbers between 1.7 and 0.3, viscosities between 732 and 599 ml/g, and brightnesses between 76.9 and 86.5 % ISO were obtained. Based on these results, a charge of 0.45 % ozone was chosen to bleach a

bigger pulp charge because with this ozone charge a kappa number below 0.5 was achieved, necessary for successful final peroxide bleaching (table 10).

	Z stage	P stage
Kappa no.	0.5	0.1
Viscosity (ml/g)	622	593
Brightness (%ISO)	86.3	91.2

Table 10. Results of Z and P stages

Bleaching conditions:

A: pH 3.0, 3 % cons., 50 °C, 30 min

Z: 0.45 % O₃, 40 % cons., 50 °C

Q₂: 0.1 % DTPA, pH 5.2, 3 % cons., 30 min, 50 °C

P: 0.5 % H₂O₂, 0.8 % NaOH, 10 % cons., 120 min, 70 °C

For TCF bleaching of dissolving pulps an intermediate ozone treatment of the pulp is essential to remove lignin as far as possible. No other chlorine free bleaching agent is able to do this to the same extent. However, compared to chlorine dioxide, ozone has a rather low selectivity toward lignin degradation and the application to pulp with very low residual lignin content leads inevitably to a serious cellulose degradation, as reflected in the distinct drop in viscosity by 250 ml/g. In ozone treatment cellulose chains are cleaved and carbonyl groups are formed, which are sensitive to alkali-induced further cleavage reactions [2].

If a Z stage is applied to delignify pulps to very low kappa numbers, the ozone treatment results in a remarkable brightening effect. In this case the brightness was improved by 20 points.

After ozone bleaching a second Q stage was carried out to stabilize the pulp as far as possible before final peroxide bleaching. In preliminary tests the P stage was only optimized with respect to the peroxide and sodium hydroxide charges. The conditions and results of the P stage conducted in bigger charge are presented in table 10.

The final bleaching results show that it is basically possible to bleach PH-ASA softwoods pulps in a TCF sequence. With regard to the final kappa number and brightness, the demands high-grade dissolving pulps can be fulfilled. Also the pulp purity is at a high level, as indicated by R₁₀ and R₁₈ values of 94.7 % and 96.5 %, respectively. While R₁₈ retains on the same level during bleaching, R₁₀ was slightly reduced which can be explained with cellulose degradation occurring particularly in the O and Z stages. The attack on cellulose in both stages is also mainly responsible for the reduction of the pulp viscosity by 50 % over the whole bleaching sequence, which restricts pulp use to applications that tolerate a low DP of cellulose.

The metal content is an important quality criterion for dissolving pulps because of its disturbing effects in many applications. Furthermore, transition metal ions, especially manganese, are harmful in TCF bleaching since they catalyze peroxide decomposition. Therefore, the metal profile over the bleaching process was monitored by AAS determination of the most important metal ions. Based on the results compiled in table 12, the following conclusions can be drawn:

- The transition metal content of unbleached ASA pulps is higher than in acid sulfite pulps. Under acid cooking conditions metal ions are dissolved and removed in brownstock washing.
- In the oxygen bleaching stage (and in the OP stage) the content of magnesium ions was dramatically increased due to the addition of magnesium sulfate. This must be accepted if a serious cellulose degradation is to be avoided in spite of extensive oxygen delignification necessary in TCF bleaching.
- The first Q stage was very effective in removal of manganese ions while keeping the magnesium ion content at

a continued high level. A very low manganese content and a high magnesium to manganese ratio are essential for selective OP (or P) bleaching under severe conditions.

- The acid treatment prior to ozone bleaching is an effective sink for calcium and magnesium ions.
- By measuring the metal ion content before and after pulp fluffing in a refiner it could be shown that the extreme increase of the iron content after acid pretreatment was presumably caused by mechanical abrasion.
- Iron is obviously very strongly fixed to the pulp fibers. It is therefore difficult to remove in Q or A stages, but it does not have that critical effect on peroxide decomposition that the more soluble manganese ions do.
- The second Q stage shows no remarkable effect with regard to removal of transition metal ions, but it is essential to avoid serious viscosity losses in the final P stage initiated by transition metal ions activated in the ozone stage.
- The final bleached pulp has a rather low metal content. If necessary, the content of the alkaline earth metals can be further reduced by a terminal acid treatment.

	Ca (ppm)	Mg (ppm)	Mn (ppm)	Fe (ppm)	Cu (ppm)
unbleached	1994	157	21	5	12
O	1970	1220	20	8	15
O-Q ₁	693	288	2	8	1
O-Q ₁ -OP	601	932	1	7	2
O-Q ₁ -OP-A	97	116	1	22*	2
O-Q ₁ -OP-A-Z	82	58	1	15	1
O-Q ₁ -OP-A-Z-Q ₂	86	52	1	14	2
O-Q ₁ -OP-A-Z-Q ₂ -P	64	45	1	13	2

* after pulp fluffing, 6 ppm before refiner fluffing

Table 12. Metal content of the pulp during bleaching

The composition of the carbohydrates was also tracked through the different production steps (Fig. 6). The hydrolysis stage resulted in an increase of the

cellulose content in the spruce chips to 50 %. Only a smaller part of the hemicelluloses was already dissolved in this stage, the major part was dissolved in the subsequent cooking stage. During cooking the cellulose content increased to 93 %. The further increase of pulp purity during oxygen delignification and bleaching is mainly the result of lignin removal. Those hemicelluloses surviving the ASA cooking stage are very resistant to removal during TCF bleaching and only a minor part could be dissolved.

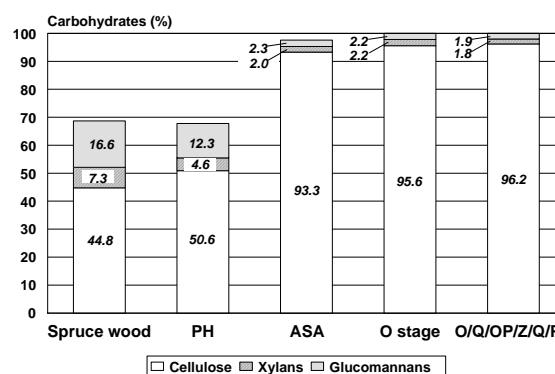


Figure 6. Carbohydrate composition in the different stages of the TCF bleached PH-ASA pulp

Conclusions

This investigation has shown that the high quality of ASAM dissolving pulp can also be achieved with the PH-ASA process. In ASAM reference cooks, an alkali ratio of 80:20 was applied. A high percentage of sodium sulfite in the total chemical charge provides a high selectivity but retards delignification. The latter effect can be tolerated because the added methanol supports delignification considerably, with the result that both high selectivity and effective delignification is achieved. In ASA pulping a higher percentage of sodium hydroxide is required in order to attain an adequate degree of delignification without addition of methanol. The loss in selectivity at the applied alkali ratio of 70:30 is compensated for by NaOH splitting with only 25 % of the total NaOH charge added at the beginning of the cook.

With the PH-ASA process, softwood pulps with low kappa number, high viscosity, and low content of hemicelluloses can be produced. These are excellent preconditions for TCF bleaching. The ASA pulp showed good bleachability. The applied TCF bleaching sequence, O/Q/OP/Z/Q/P, resulted in high brightness, low kappa number, and high α -cellulose content. However, due to the low selectivity of the chlorine free bleaching agents, the pulp viscosity was reduced to a level that impedes the use of such a pulp for many dissolving pulp products. The most critical bleaching stage in TCF bleaching of dissolving pulps is the ozone treatment necessary for removal of residual lignin. As ozone delignification is accompanied by serious cellulose damage, the ozone charge should be as low as possible. This can only be achieved by more intense delignification prior to this stage, preferably by a more efficient OP stage. If a pulp with significantly higher viscosity is needed, ASA cooking should be stopped at still high kappa number, and an ECF bleaching sequence must be applied. Certainly, a substantially higher viscosity can be attained just by applying small quantities of chlorine dioxide instead of ozone.

It would be interesting to see which pulp quality can be achieved with hardwoods, e.g. beech. It can be assumed that, even in the case of TCF bleaching, the pulp viscosity of corresponding pulps would be considerably increased.

References

- [1] Saake, B.; Puls, J.; Patt, R.; Papier 43 (1989) 12, 681-687
- [2] Gause, E.; Dissertation Universität Hamburg, FB Biologie (1994)
- [3] Patt, R.; Zimmermann, M.; Kordsachia, O.; Hinck, J.F.; Proc. Tappi Pulping Conf. (1994) 141-146
- [4] Zimmermann, M.; Fortschr. Berichte VDI-Reihe 3, Nr. 425; VDI-Verlag, Düsseldorf (1996)
- [5] Patt, R.; Kordsachia, O.; Rose, B.; Wbl. Papierfabrikation 131 (2003) 14-15, 892-897
- [6] Puls, J.; Lin, J.L.; Körner, H.U.; Proc. Intern. Dissolving Pulp Conf. Geneva (1989), 39-42
- [7] Janson, J.; Paperi ja Puu 52 (1970) 5, 323-328
- [8] Patt, R.; Wang, D.L-K.; Papier 41 (1987) 1, 7-12

MODELING OF THE ACID SULFITE PULPING PROCESS. – PROBLEM DEFINITION AND THEORETICAL APPROACH FOR A SOLUTION WITH THE MAIN FOCUS ON THE RECOVERY OF COOKING CHEMICALS

Martin G. Wolfinger¹, Herbert Sixta²

¹ Lenzing Technik GmbH&Co KG, Pulp Technologies, Lenzing,
+43 (0) 7672 701-2921, FAX: +43 (0) 7672 918-2921, m.wolfinger@lenzing.com

² Lenzing AG, Zellstoffforschung, Lenzing,
+43 (0) 7672 701-3415, FAX: +43 (0) 7672 918-3415, h.sixta@lenzing.com

This study investigates the requirements for modeling of acid sulfite pulping with regard to the recovery of cooking chemicals, especially SO₂. Such a model has to predict the temporal change of SO₂ distribution on solid, liquid and gaseous phase in the digester throughout the whole pulping process, dependent on the pulping parameters: total SO₂, free SO₂, liquor-to-wood ratio, temporal temperature course, maximum pressure and time. The approach is based on the mass balance of SO₂ to achieve data for determination of kinetics of relevant chemical reactions, such as

sulfonation of lignin, dissolution of lignosulfonate, or formation of sulfate, strong acids and carbon dioxide. Results from capillary electrophoresis measurements in laboratory experiments were used to determine the temporal change of inorganic sulfur components in cooking acid. Some experimental problems remain (pH- and gas measurements) for a comprehensive description acid sulfite pulping, considering the mass balance of sulfur dioxide.

Keywords: *modeling, pulping process, recovery, cooking chemicals*

Introduction

Contrary to kraft pulping, modeling of acid sulfite pulping process hasn't been a big issue in pertinent research efforts. Although the importance of acid sulfite pulping has decreased in recent years, it is still of interest because of the capabilities to gain chemical byproducts, such as xylose, acetic acid, furfural, etc. Lenzing AG (Austria) gains pulp from beech wood for production of viscose fibers by an acid magnesium sulfite pulping process. Results of laboratory pulping experiments suggest that the ratio of free SO₂ should be increased in order to achieve a higher yield of byproducts without an adverse effect on pulp quality. The simple solution of increasing the SO₂ charge is not desirable, because the loss of cooking chemicals would increase when no changes were done in the recovery process. This would certainly lead to an exceedance of the emission limit which is not permitted.

Developed Model

Therefore, a steady state model was developed to estimate the potential of emission reduction which covers the pulping and recovery process. The whole process can be subdivided into the pulping process itself and into three subprocesses of the recovery process which are:

- 1) Absorption of gaseous SO₂ of digester relief gases in raw acid at different pressure levels (primary recovery)
- 2) Countercurrent absorption of SO₂ with magnesium hydroxide regaining raw acid after combustion of thick liquor in the recovery boiler (secondary recovery)
- 3) Thermally splitting of excess magnesium monosulfite (ternary recovery)

The model is mainly based on process data and is evidently strongly simplified due to the complexity of the whole process. The use of the

process simulation software package Aspen Plus® has simplified the development.

Despite the simplifications, it has been successfully used for the pre-estimation of changes and improvements in the recovery process. In order to improve the reliability of the model predictions, it is necessary to replace the reproduction of a certain operation mode by a predictive model, which takes into account operation characteristics of the different process units. Thus, extrapolation should be possible, more precise and more reliable.

Required improvements

From the point of the recovery process, the pulping process is the „supplier“ and the „customer“ of cooking chemicals magnesium and sulfur dioxide. But they are treated in different ways: Magnesium is a component of the raw acid and remains after the pulping process in the liquid phase (spent liquor). In contrast, sulfur dioxide, or HSO_3^- respectively, reacts with wood components, mainly lignin. Gaseous SO_2 is integrated in the solid and liquid phase which changes the distribution of SO_2 in the solid, liquid and gaseous phases throughout the pulping process. Therefore, a model of the pulping process, with the main focus on the recovery of cooking chemicals, has to be capable to predict the SO_2 distribution on the solid, liquid and gaseous phase as well as the charge and discharge of SO_2 by the different process streams (spent liquor, pressure control relief gas, high-, medium- and low-pressure relief gas) dependent on the cooking parameters: time t , total SO_2 , free SO_2 , liquor-to-wood ratio, maximum pressure p_{\max} , temporal course of temperature $T(t)$.

Literature

A literature study on modeling of acid sulfite pulping showed that no proper model exists which considers the behavior of the cooking chemicals, especially SO_2 . The main focus of the published models is put on the properties and quality of the pulp. Most of the models are empirical and are able to predict the kappa-number or the lignin content of the pulp [[1], [2], [3], [8], [13]]. Furumoto [4] developed a knowledge-based model due to mathematical and statistical analysis of process data. Such a model is just specific for the plant and its operation mode. Such deduced relations don't need to

follow the mechanism of the process. Hagberg & Schön [[5]-[7]] and Kilian & De Vaal [9], respectively, has chosen a mechanistic approach which enables to follow temporal changes during the pulping process. Hagberg & Schön determine kinetic data for the delignification, the dissolution of hemicellulose and the formation of strong acids from experimental results in laboratory. Their model considers the electroneutrality, the protolysis equilibrium of sulfurous acid, the phase equilibrium of gaseous and dissolved SO_2 , and the assumption that the total pressure is the sum of SO_2 - and H_2O -partial pressure. Kilian & De Vaal used the same relations, but adjust the model parameters to experimental data measured at a plant digester. Additionally, they implement degradation kinetics of cellulose to predict and control the viscosity of pulp.

The assumption, that total pressure is the sum of SO_2 and H_2O partial pressure, is not transferable to beech wood pulping due to the fact that CO_2 is evolved during the pulping process. Additionally, the phase equilibrium of gaseous and dissolved SO_2 is influenced by other dissolved substances in the cooking liquor, which has an effect on the activity coefficient of the dissolved SO_2 and further on the phase equilibrium.

Another issue, which is not considered in any published model so far; is the pressure control relief. The main function of pressure control relief, beside compliance of maximum pressure, is the heat removal from the digester in order to control the temperature in the digester. Otherwise the generated heat, which is released by exothermal reactions during pulping, would result in exceeding the temperature limit.

All these neglected factors have an impact on gas composition and mass flow of digester relief gases which are especially important for primary recovery.

In order to eliminate these deficiencies of the models, the requirements were analyzed which are needed for establishing a sufficient model.

Analysis

Process Characteristics

The pulping process is very complex and can be characterized as follows:

Pulping is an unsteady reactive process. In a digester, three phases exist in parallel: solid, liquid and gaseous phase. The single phases are inhomogeneous in temperature and concentration and change their composition and their volume ratio during the pulping process. Therefore the three phases are under permanently mass and heat exchange, where the difference of real and equilibrium state is the driving force. The different chemical reactions can be subdivided in

- Reactions with involvement of sulfur components; e.g. formation of

lignosulfonates, α -hydroxysulfonates, sugar sulfonates, sulfates and thiosulfates.

- Reactions of the organic matter; e.g. acid hydrolysis of cellulose and hemicellulose, lignin condensation, formation of organic acids like formic and acetic acid and release of carbon dioxide CO_2 from carbonyl-groups

A simplified scheme of the most important chemical reactions, chemical and phase equilibria is shown in Figure 1.

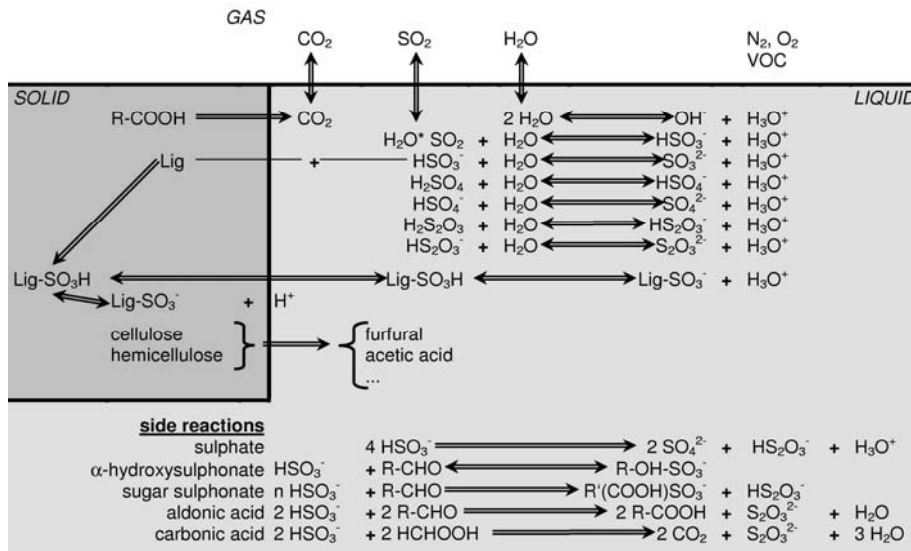


Figure 1. Scheme of phase equilibria and chemical reactions during acid sulfite pulping

Data basis

The basis of each model are relevant and reliable experimental data. The basis for an acid sulfite pulping model, considering recovery aspects, is the mass balance of the sulfur components during the pulping process. The different components and their distribution on the three phases:

- Solid phase (sol)
 - $[\text{Lig-SO}_3^-]_{\text{sol}}$ undissolved lignosulfonate
 - $[\text{R-SO}_3^-]_{\text{sol}}$ undissolved org. S-compound
 - Liquid phase (liq)
 - $[\text{Lig-SO}_3^-]_{\text{liq}}$ dissolved lignosulfonate
 - $[\text{R-SO}_3^-]_{\text{liq}}$ dissolved org.c S-compound
 - $[\text{H}_2\text{SO}_3], [\text{HSO}_3^-], [\text{SO}_3^{2-}]$ sulfite – S(IV)
 - $[\text{H}_2\text{SO}_4], [\text{HSO}_4^-], [\text{SO}_4^{2-}]$ sulfate – S(VI)
 - $[\text{H}_2\text{S}_2\text{O}_3], [\text{HS}_2\text{O}_3^-], [\text{S}_2\text{O}_3^{2-}]$ thiosulfate - S(II)
 - Gaseous phase (gas)
 - $[\text{SO}_2]_{\text{gas}}$ sulfur dioxide
- where:

$[i]_{\{j\}}$..concentration of substance i in phase j, mol/mol

LigLignin

Rcarbohydrate

Other essential parameters are:

- $[\text{H}_3\text{O}^+]$ -concentration in liquid phase: required for kinetics of chemical reactions and for dissociation equilibria
- $[\text{CO}_2]_{\text{gas}}$: increases total pressure and is required for determining the formation rate of CO_2
- $[\text{H}_2\text{O}]_{\text{gas}}$: is a monitoring parameter for gas concentration measurements
- \dot{V}_{gas} is required for mass balancing the pulping process and for estimating heat formation due to exothermal reactions

A conclusion of this analysis results in 21 unknown parameters:

3 phases, 17 concentrations and 1 gas flow.

An equivalent number of measurements, constraints, relations, assumptions and simplifications are needed for the determination of these 21 parameters; these are:

- Measurements
 - 1) capillary electrophoresis (CE)-measurement Σ sulfite S(IV)
 - 2) CE-measurement Σ sulfate S(VI)
 - 3) pH-measurement
 - 4) $[\text{SO}_2]_{\{\text{gas}\}}$ measurement
 - 5) $[\text{CO}_2]_{\{\text{gas}\}}$ measurement
 - 6) $[\text{H}_2\text{O}]_{\{\text{gas}\}}$ measurement
 - 7) flow measurement of total relief gas
 - 8) determination of total sulfur in liquid phase
- Constraints, relations
 - 9) $\text{pK}_a(\text{T})$ sulfurous acid 1. protolysis equil.
 - 10) $\text{pK}_a(\text{T})$ sulfurous acid 2. protolysis equil.
 - 11) $\text{pK}_a(\text{T})$ sulfuric acid 1. protolysis equil.
 - 12) $\text{pK}_a(\text{T})$ sulfuric acid 2. protolysis equil.
 - 13) $\text{pK}_a(\text{T})$ thiosulfuric acid 1. protolysis equil.
 - 14) $\text{pK}_a(\text{T})$ thiosulfuric acid 2. protolysis equil.
 - 15) volume balance
 - 16) mass balance sulfur
- Assumptions
 - 17) Σ thiosulfate = 0
 - 18) organic sulfur in solid phase is bound to lignin
 - 19) organic sulfur in liquid phase is bound to lignin
 - 20) gas volume = constant
 - 21) change of liquid volume proportional to dissolved organic sulfur

The assumption; that thiosulfate is not a component of the cooking liquor; is based on results of former CE-measurements.

For a model focusing on recovery of SO_2 it is not important to distinguish whether the sulfur is bound to lignin or to another organic compound. Therefore all sulfur bound to an organic compound is counted as a lignosulfonate. This assumption overestimates lignin sulfonation, but minimizes the experimental and analytical effort.

Unfortunately, volume measurements during cooking are not feasible because of undefined surfaces and interfaces of the different phases.

These experimental data can be used to determine the parameter for the chemical kinetics of

- Sulfonation of lignin in the solid phase

- Formation of strong organic acid anions
- Dissolution of solid lignosulfonate
- Formation of sulfate
- Formation of carbon dioxide

Especially the temporal courses of $[\text{HSO}_3^-]$ and $[\text{H}^+]$ can be determined, which are the basis for each sulfite pulping model considering chemical kinetics. ([5]-[7], [9]).

Also a relation can be deduced for the phase equilibrium of $\text{SO}_{2\{\text{gas}\}}$ and dissolved SO_2 from these data. A comparison with data from literature should allow an evaluation whether during gas relief thermodynamic equilibrium is reached or not.

Kinetic parameters valid for a broader range of pulping parameters can be obtained from a series of experiments, in which following parameters are varied:

- time
- total SO_2
- free SO_2
- temporal course of temperature
- temporal course of pressure
- liquor-to-wood ratio

These data establish a basis for the development of a comprehensive model of acid sulfite pulping focusing on recovery of sulfur dioxide.

Experimental and Evaluation Problems

Several questions arise for the determination of the essential data, summarized above:

CE-measurement

CE-measurement is a well established method to determine sulfite and sulfate concentration in the cooking liquor during the pulping process [[12]]. It was used several times at our lab digester and at our plant digester as well. The uncertainty in CE-measurement is about 5%.

pH measurement

Fundamental problems arise for the measurement of pH under conditions typically for acid sulfite pulping (up to 160°C, 10 bar, low pH), which are the long term resistance of the glass electrode, the precision and drift of pH measurement. The determination of pH is necessary for calculating $[\text{H}^+]$ and $[\text{HSO}_3^-]$ concentrations which are essential for chemical kinetics. An indirect determination of pH, by measuring concentration of strong acids in

liquid phase, does not consider solid lignosulfonate that also influences pH.

Measurement of gas concentration

The problems of gas concentration measurement are sampling during the cooking period without gas relief and the difficulties in measuring the composition of wet gas.

Determination of the exothermal effects during cooking

An exact determination of exothermal heat of reaction would need to solve the complete heat balance of the pulping process considering the heat loss to ambience, the heat capacity of digester and its content. Most of the generated heat is released by evaporation of water. Therefore the exothermal heat of reaction can be estimated by the amount of steam evolved during gas relief.

Evaluation of inorganic sulfur concentrations

Another issue is the combined evaluation of pH- and CE-measurements to calculate the temporal course of $[\text{H}_2\text{SO}_3]$, $[\text{HSO}_3^-]$ and $[\text{SO}_3^{2-}]$ concentrations or $[\text{H}_2\text{SO}_4]$, $[\text{HSO}_4^-]$ and $[\text{SO}_4^{2-}]$ concentrations, respectively. Therefore, the temperature dependency of the dissociation constants is needed that can be calculated according to equation (1) using the thermodynamic data of Table 1 [10].

Figure 2 shows the calculated pK values for H_2SO_3 and H_2SO_4 dependent on temperature. These curves are calculated with a constant value of $\Delta_r C_p$ and therefore they show only a slight dependency on temperature.

Figure 3 illustrates the good compliance of the calculated data with data from literature of pK_a for the first stage of protolysis of H_2SO_3 . The compliance can be improved when a quadratic temperature dependency of C_p is assumed, and the parameter fit to the data from literature (see Figure 3).

material data	$\Delta_f H_0$	$\Delta_f G_0$	C_{p0}
	[kJ/mol]	[kJ/mol]	[J/K mol]
$\text{H}_2\text{SO}_4(\text{aqu})$	-909,3	-744,5	-393
HSO_4^-	-887,3	-755,91	-84
SO_4^{2-}	-909,3	-744,53	-293
$\text{SO}_2(\text{aqu})$	-323,2	-300,5	195
H_2O	-285,8	-237,13	75,3
HSO_3^-	-626,8	-527,03	-1,9
SO_3^{2-}	-630,4	-486,09	-263,9
H^+	0	0	0

Reactions	$\Delta_r H_0$	$\Delta_r G_0$	$\Delta_r C_{p0}$
	[J/mol]	[J/mol]	[J/K mol]
$\text{H}_2\text{SO}_4(\text{aqu}) \rightleftharpoons \text{HSO}_4^- + \text{H}^+$	21960	-11410	309
$\text{HSO}_4^- \rightleftharpoons \text{SO}_4^{2-} + \text{H}^+$	21930	11380	-209
$\text{SO}_2(\text{aqu}) + \text{H}_2\text{O} \rightleftharpoons \text{HSO}_3^- + \text{H}^+$	-17800	10600	-272
$\text{HSO}_3^- \rightleftharpoons \text{SO}_3^{2-} + \text{H}^+$	-3650	40940	-262

Table 1. Thermodynamic data for the calculation of the temperature dependency of the thermodynamic equilibrium constant [[10]]

where

$\Delta_f G_0$ free enthalpy of formation at T_0 , kJ/mol

$\Delta_f H_0$ enthalpy of formation at T_0 , kJ/mol

C_{p0} heat capacity at T_0 , kJ/K mol

$\Delta_r G_0$ free enthalpy of reaction at T_0 , kJ/mol (see equation (2))

$\Delta_r H_0$ enthalpy of reaction at T_0 , kJ/mol (see equation (3))

$\Delta_r C_{p0}$ heat capacity of reaction at T_0 , kJ/K mol (see equations (4))

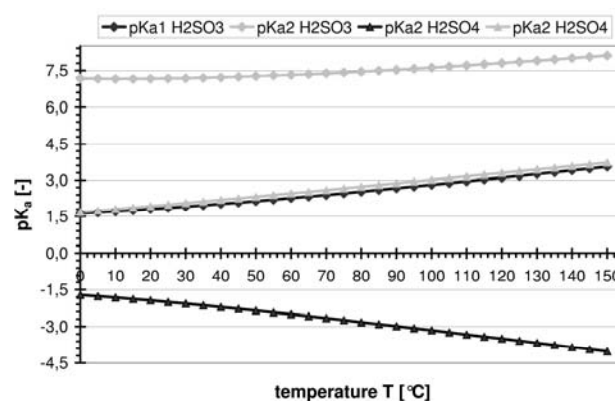
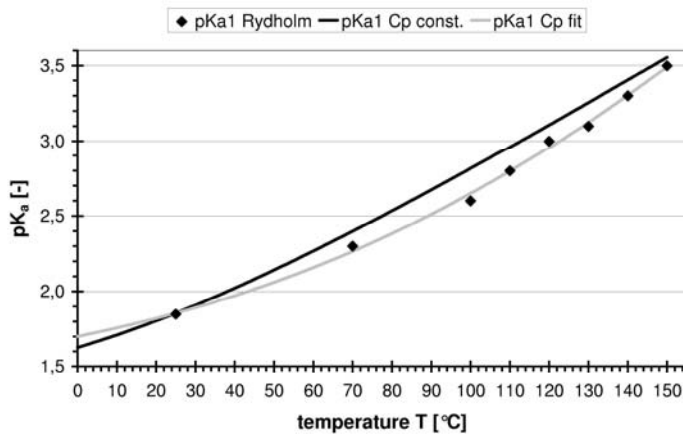


Figure 2. Calculated pK_a -values of sulfurous acid and sulfuric acid dependent on temperature



With experimental data of laboratory pulping experiments and an assumed temporal pH-course it is possible to calculate time-dependent concentrations of sulfurous and sulfuric acid anions using the equations (5) to (10), see Figure 4 and Figure 5).

Figure 3. Comparison of calculation and literature data of pK_{a1} of H_2SO_3 with different mathematical relations for C_p (black line: $C_p = C_{p0}$; gray line: $C_p = C_{p0} + A \cdot T + B \cdot T^2$ - A, B...fit parameters) [11]

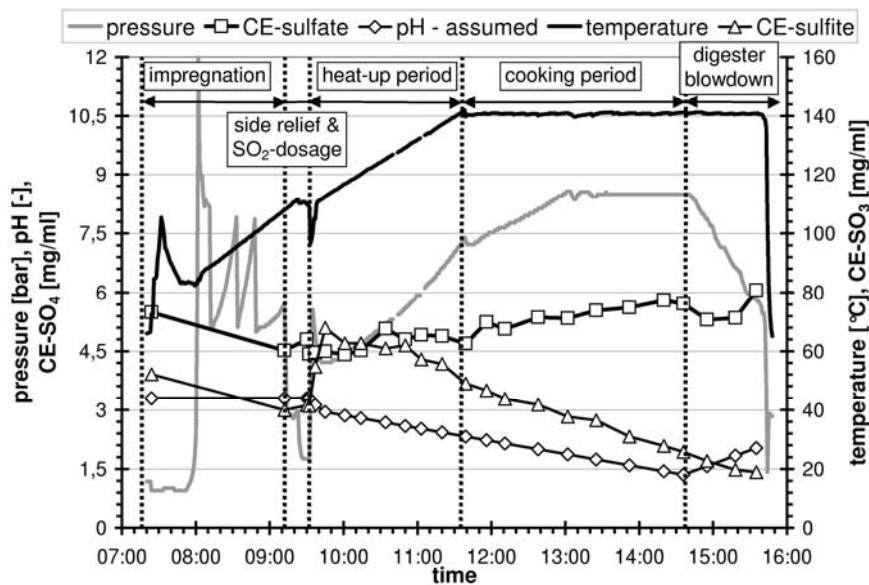


Figure 4. Experimental data and an assumed course of pH of a laboratory pulping experiment

The assumed pH in Figure 4 is based on:

- 1) In the period of impregnation and side relief the pH is assumed to be constant at the level of raw acid: On one hand the calculated pH based only on CE-measurement would estimate a slight increase of pH and on the other hand the dissolution of some acetic acid and other organic acids from the wood chips would decrease pH.
- 2) The decrease of pH in the cooking period was estimated with results of pH-measurements at a pilot digester. The experiments were carried out at different temperature, total SO_2 and free SO_2 than in the laboratory experiment. A linear

correlation with time was assumed and the measured data were extrapolated to the conditions of the laboratory experiment resulting in a pH decrease of about 0,3 per hour.

- 3) The linear increase of pH in the period of digester relief is based on pH-measurements carried out by Fischer [3].

The constraint of electroneutrality (equation (11)) determines the concentration of strong acid anions $[A^-]$ formed during pulping considering that the concentration of magnesium cation $[Mg^{2+}]$ is constant after side relief (see Figure 5).

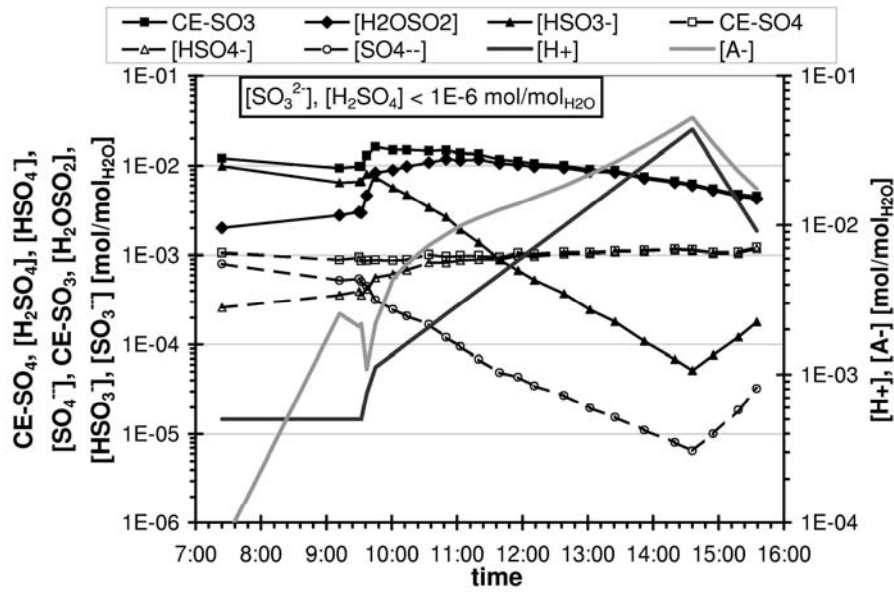


Figure 5: Calculated time-dependent concentrations of hydronium ion, strong acid, sulfurous acid and sulfuric acid anions in a laboratory pulping experiment

Not all experimental problems are solved up to now, especially some basics have to be clarified for the implementation of pH- and gas concentration measurement.

New Digester Model

For a better explanation of the model the digester is divided in two zones: a head space and a solid/liquid phase (see Figure 6). Both zones are described as ideal stirred tank and are corresponding by gas exchange.

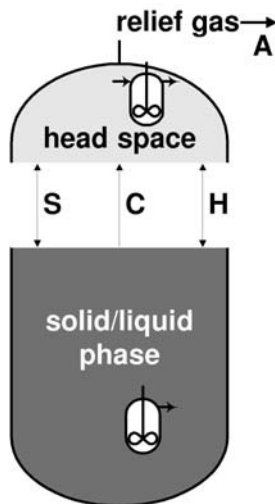


Figure 6: Scheme of digester model

Necessary inputs for both sections are

- Temporal temperature course
- Maximum pressure or the time-dependent pressure decrease during digester relief

- Initial values for load, liquor-to-wood-ratio, charge of SO₂ and ratio of free SO₂
-

Assumptions for modeling head space

Input streams:

- S ensuring gas exchange with
- C solid/liquid phase.
- H

Outlet stream A:

three periods have to be distinguished:

- Heat up and cooking period without gas relief
A=0,
 $p_{total}=f(T, \dot{r}_{CO_2}, \text{phase equilibrium gas/liquid})$
- Cooking period with gas relief
A= f(T, \dot{r}_{CO_2} , phase equilibrium gas/liquid, exothermal effect),
 $p_{total} = p_{max}$
- Digester relief –
A= f(T, \dot{r}_{CO_2} , phase equilibrium gas/liquid, exothermal effect),
 $p_{total}=f(t)$

where:

S, C, H, A (see Figure 6)

Ttemperature, K

t.....time, s

p_{total} ..total pressure, bar

p_{max} ..maximum allowable pressure, bar

\dot{r}_{CO_2} ..formation rate of carbon dioxide

Chemical reactions:

- none

Constraints:

- Head space and solid/liquid phase are in phase equilibrium

Further assumptions:

- Head space is homogeneous
- Volume of head space is constant.

A mathematical analysis of the head space results in 11 variables:

- ✓ 3 streams of known composition:
S ($x_{SO_2,S} = 1$), C ($x_{CO_2,S} = 1$), H ($x_{H_2O,S} = 1$)
- ✓ 1 relief gas stream of unknown composition:
A, $c_{SO_2,A}$, $c_{CO_2,A}$, $c_{H_2O,A}$
- ✓ 1 head space of unknown composition:
G, $c_{SO_2,G}$, $c_{CO_2,G}$, $c_{H_2O,G}$

The corresponding mathematical relations to calculate these variables are summarized in the appendix (see equations. (12) to (22)).

Assumptions for modeling the solid/liquid zone

Input streams:

- none

Output streams:

- S ensuring gas exchange with solid/liquid phase.
- C
- H

Chemical reactions:

- Sulfonation of lignin in solid phase
- Dissolution of lignosulfonates
- Formation of strong acids
- Formation of sulfate
- Formation of carbon dioxide

Constraints:

- Protolysis equilibrium of sulfurous acid
- Protolysis equilibrium of sulfuric acid
- Electroneutrality
- Mg^{2+} -concentration is constant

Further assumptions:

- Solid/liquid phase is homogeneous, its volume is constant
- Only lignin reacts with sulfur
- No thiosulfate in the cooking acid

A mathematical analysis of the solid/liquid zone results in 17 variables:

- ✓ 3 streams of known concentration:
S ($x_{SO_2,S} = 1$), C ($x_{CO_2,S} = 1$), H ($x_{H_2O,S} = 1$)
- ✓ 1 solid/liquid phase with 13 unknown concentrations:
Lig.....lignin
LS_{sol}.....lignosulfonate in solid phase
LS_{liq}.....lignosulfonate in liquid phase
[H₂SO₃], [HSO₃⁻], [SO₃²⁻].....sulfurous acid
[H₂SO₄], [HSO₄⁻], [SO₄²⁻].....sulfuric acid
[H⁺], [Mg²⁺].....cations

[A⁻].....anions of strong acids

[CO₂].....carbon dioxide

The corresponding mathematical relations to calculate these variables are summarized in the appendix (see equations (23) to (31)).

The total system is a differential-algebraic equation system which can be solved with commercial software packages or routines. It enables to calculate temporal course of [H⁺] and [HSO₃⁻] which are the main factors of chemical reactions of cellulose and hemicellulose. Therefore, the model can be extended for these reactions predicting pulp properties, too.

Conclusion and further developments

The essential parameters of acid sulfite pulping have been elaborated by a systematic analysis of the process considering published knowledge and relations. The temporal course and change of concentration of cooking chemicals on the solid, liquid and gaseous phase is required for a pulping model regarding recovery aspects. This leads to the problem to determine the sulfur components in each phase which is necessary for the sulfur mass balance. The temporal courses of [H₃O⁺] and [HSO₃⁻] are the basis for the determination of kinetic parameters of relevant chemical reactions, such as sulfonation, dissolution of lignosulfonate, formation of sulfate, strong acids and carbon dioxide.

The most important experimental problems, which have to be solved, are the measurement of pH under pulping conditions and the gas sampling during the cooking phase without gas relief. Afterwards an experimental program has to be conducted varying the pulping parameters: total SO₂, free SO₂, liquor-to-wood-ratio, temporal courses of temperature and pressure and time. In ideal case a universal set of kinetic parameters can be deduced for the essential chemical reactions, such as sulfonation of lignin in the solid phase, dissolution of solid lignosulfonate, formation of strong organic acid anions, sulfate and carbon dioxide. But these parameters are only valid for the lab digester and can't be used for modeling the pulping process at the plant. Therefore some additional measurements at the plant digester have to be done, but their number should be minimized due the experience from laboratory experiments.

Acknowledgement

The authors wish to thank the Austrian Kompetenzzentrum Holz GmbH, Linz, Austria and the Lenzing AG, Lenzing, Austria for financial support.

References

[1] Bylund, L., Thorsell, S., Häggglund, S. et al., J. Pulp Paper Sci. 11: 74(1983)
 [2] Fischer, K. Schmidt, I., Tappi J. 74(1): 181(1991)
 [3] Fischer, K., Schmidt, I., Rennert, S., Einfluß von Ablaugenkenngrößen auf die Parameter eines Sulfitzellstoffes. Report
 [4] Furumoto, H., Wissensbasierte Prozessführung oder wie fahre ich eine Produktionsanlage im Optimum, Report Siemens AG ANL A221, 1991
 [5] Hagberg, B., Schöön, N.-H., Svensk Papperstid. 76(15): 561(1973)

[6] Hagberg, B., Schöön, N.-H., Svensk Papperstid. 77(15): 557(1974)
 [7] Hagberg, B., Schöön, N.-H., Svensk Papperstid. 77(4): 127(1974)
 [8] Haywood, S. T., Pulp Paper Can. 90(6): 216(1989)
 [9] Kilian, A., De Vaal, P. L., TAPPI J. 83(11): 371(2000)
 [10] Luckas, M., Krissmann, J., Thermodynamik der Elektrolytlösungen – Eine einheitliche Darstellung der Berechnung komplexer Gleichgewichte, Springer-Verlag, Berlin Heidelberg, 2001
 [11] Rydholm, S. A., Pulping Processes, Reprint Edition, Robert E. Kreiger, Malabar, Florida: 1985
 [12] Schelosky, N., Baldinger, T., Lenzinger Berichte 79: 108(2000)
 [13] Yorston, F. H., Liebergott, N., Pulp Paper Mag. Can. 66: 272(1965)

Appendix

$$-\ln(K(T)) = \frac{\Delta_r G_0}{R_{gas} \cdot T_0} + \frac{\Delta_r H_0}{R_{gas} \cdot T_0} \cdot \left(\frac{T_0}{T} - 1 \right) + \frac{\Delta_r Cp_0}{R_{gas}} \cdot \left(1 - \frac{T_0}{T} - \ln \left(\frac{T}{T_0} \right) \right) \quad T_0 = 298,15K \quad (1)$$

$$\Delta_r G_0 = \sum_i \nu_i \cdot \Delta_f G_{i,0} \quad (2) \quad \Delta_r H_0 = \sum_i \nu_i \cdot \Delta_f H_{i,0} \quad (3) \quad \Delta_r Cp_0 = \sum_i \nu_i \cdot Cp_{i,0} \quad (4)$$

where

- K..... equilibrium constant
- T temperature, K
- R_{gas}..... universal gas constant, kJ/mol K
- Δ_rG₀ ... free enthalpy of reaction at T₀, kJ/mol
- Δ_rH₀ ... = enthalpy of reaction at T₀, kJ/mol
- Δ_rCp₀ . heat capacity of reaction at T₀, kJ/mol K
- Δ_fG_{i,0}.. free enthalpy of formation of substance i at T₀, kJ/mol
- Δ_fH_{i,0}.. enthalpy of formation of substance i at T₀, kJ/mol
- Cp_{i,0} ... heat capacity of substance i at T₀, kJ/mol K
- ν_i..... stoichiometric coefficient

$$SULFITE = \frac{MG_{SO_3}}{MG_{H_2SO_3}} \cdot [H_2SO_3] + \frac{MG_{SO_3}}{MG_{HSO_3}} \cdot [HSO_3^-] + [SO_3^{2-}] \quad (5)$$

$$K_{H_2SO_3}(T) = \frac{[HSO_3^-] \cdot [H^+]}{[H_2SO_3]} \quad (6) \quad K_{HSO_3}(T) = \frac{[SO_3^{2-}] \cdot [H^+]}{[HSO_3^-]} \quad (7)$$

$$SULFATE = \frac{MG_{SO_4}}{MG_{H_2SO_4}} \cdot [H_2SO_4] + \frac{MG_{SO_4}}{MG_{HSO_4}} \cdot [HSO_4^-] + [SO_4^{2-}] \quad (8)$$

$$K_{H_2SO_4}(T) = \frac{[HSO_4^-] \cdot [H^+]}{[H_2SO_4]} \quad (9) \quad K_{HSO_4}(T) = \frac{[SO_4^{2-}] \cdot [H^+]}{[HSO_4^-]} \quad (10)$$

where:

SULFITE..... total sulfite concentration (CE-measurement), mol/mol_{H2O}

SULFATE total sulfate concentration (CE-measurement), mol/mol_{H2O}

MG_i..... molecular weight of substance i, kg/kmol

K_i protolysis equilibrium constant of substance i

[] concentration, mol/mol_{H2O}

$$[A^-] = 2 \cdot [Mg^{2+}] + [H^+] - [HSO_3^-] - 2 \cdot [SO_3^{2-}] - [HSO_4^-] - 2 \cdot [SO_4^{2-}] \quad (11)$$

where:

[] concentration, mol/mol_{H2O}

Total mass balance: $G \cdot \frac{dc}{dt} = S + C + H - A$ (12)

SO₂-mass balance: $G \cdot \frac{dc_{SO_2,G}}{dt} = S - A \cdot c_{SO_2,A}$ (13)

H₂O-mass balance: $G \cdot \frac{dc_{H_2O,G}}{dt} = H - A \cdot c_{H_2O,A}$ (14)

Constraints of ideal stirred reactor: $c_{SO_2,G} = c_{SO_2,A}$ (15) $c_{CO_2,G} = c_{CO_2,A}$ (16) $c_{H_2O,G} = c_{H_2O,A}$ (17)

Constant gas volume: $G = konst. = G_0 = f(\text{load, } V_{\text{digester}}, \text{liquor - wood - ratio})$ (18)

Phase equilibrium of H₂O: $c_{H_2O,G} = c_{H_2O}^* = f(T)$ (19)

Phase equilibrium of SO₂: $c_{SO_2,G} = c_{SO_2}^* = f(T, [HSO_3^-], [H^+], ?)$ (20)

Total pressure: $P_{\text{total}} = P_{SO_2} + P_{CO_2} + P_{H_2O}$ (21)

Temporal course of total pressure or relief gas flow resp.: $A = 0 \Rightarrow P_{\text{total}} = f(\quad)$ (22)

$P_{\text{total}} = P_{\text{max}}$ bzw. $P_{\text{total}} = p(t) \Rightarrow A = (\quad)$

where:

t..... time, s

G..... volume of head space, m³

S, C, H, A in- and outlet streams, kg/s

c_{i,X}..... concentration of substance i in stream X or zone X resp. , mol/m³

c_i^{*} concentration of substance i in equilibrium, mol/m³

p_i partial pressure of substance i, Pa

V_{digester} total volume of digester, m³

Volume balance $LiqSol = V_{\text{digester}} - G_0$ (23)

Lignin mass balance $Lig(t) = Lig_0 - \frac{Lig}{LS} \cdot \int dLS_{sol}$ (24)

$\frac{Lig}{LS}$ "ratio of sulphonation"

Sulfonation of lignin $\frac{dLS_{sol}}{dt} = f([L], [HSO_3^-], [H^+])$ (25)

Dissolution of lignosulfonate $\frac{dLS_{liqu}}{dt} = f([LS_{sol}], [H^+])$ (26)

Formation of carbon dioxide $\frac{dCO_2}{dt} = f(?)$ (27)

Formation of sulfate / sulfate mass balance $\frac{dSULFATE}{dt} = f(?)$ and equ. (8) (28)

1. protolysis equilibrium $K_{H_2SO_4}(T) = \frac{[HSO_4^-] \cdot [H^+]}{[H_2SO_4]}$ (9)

2. protolysis equilibrium $K_{HSO_4}(T) = \frac{[SO_4^{2-}] \cdot [H^+]}{[HSO_4^-]}$ (10)

$$1. \text{ protolysis equilibrium } K_{H_2SO_3}(T) = \frac{[HSO_3^-] \cdot [H^+]}{[H_2SO_3]} \quad (6)$$

$$2. \text{ protolysis equilibrium } K_{HSO_3}(T) = \frac{[SO_3^{2-}] \cdot [H^+]}{[HSO_3^-]} \quad (7)$$

$$\text{Formation of strong acids } \frac{d[A^-]}{dt} = f([HSO_3^-], [H^+], ?) \quad (29)$$

$$\text{Constancy of Mg-ions } [Mg^{2+}] = [Mg^{2+}]_{t=0} = f(SO_{2,total,t=0}, \%SO_{2,free,t=0}) \quad (30)$$

$$\text{electroneutrality } 2 \cdot [Mg^{2+}] + [H^+] = [HSO_3^-] + 2 \cdot [SO_3^{2-}] + [HSO_4^-] + 2 \cdot [SO_4^{2-}] + [A^-] \quad (31)$$

Sulfur mass balance

Constraint of head space S, C, H

where:

LiqSol volume of solid and liquid phase, m³

Lig concentration of lignin in solid/liquid-phase, g/m³

LS concentration of lignosulfonate, g/m³

HEMICELLULOSE FOULING BEHAVIOUR DURING NANOFILTRATION OF PRESS LIQUOR*

Robert Schlesinger,¹ Thomas Röder,² Gerhard Götzinger,² Michael Harasek,³ Anton Friedl,³ Herbert Sixta,² Hedda Weber¹

¹ Competence Centre for Wood Composites and Wood Chemistry K-Plus, Area 6, Werkstrasse 1, A-4860 Lenzing, Austria; Phone: +43 7672 701 3110; Fax: +43 7672 918 3110; E-Mail: r.schlesinger@lenzing.com

² Lenzing AG, Department of Pulp Research, Werkstrasse 1, A-4860 Lenzing, Austria

³ Vienna University of Technology, Department of Chemical Engineering, Getreidemarkt 9/166, A-1060 Vienna, Austria

* A full article of this paper was submitted to *Desalination* for publication.

Nanofiltration of press liquor from viscose-type textile fibre production was investigated using a laboratory-scale cross-flow test apparatus. Feed solutions contained about 200 g/l sodium hydroxide and a high concentration of hemicellulose as a contaminant originating from the raw material wood. The effect of various pretreatments and the addition of reagents affecting the solution state of hemicellulose on flux, retention and irreversible fouling was studied. Turbidity measurements were used to track the evolution of hemicellulose aggregates. Aggregation generally coincided with distinct flux

decline during nanofiltration thus indicating that this phenomenon may result in the build-up of gel layers at the membrane surface. Partial neutralisation with sulfuric acid caused extremely severe fouling, whereas methanol addition had a minor effect. The impact of heat treatment and oxidative degradation of hemicellulose on nanofiltration performance was attributed to changes in molecular mass distribution.

Keywords: *viscose production, press liquor, nanofiltration, fouling, hemicellulose*

Introduction

Large volumes of caustic soda waste liquor (denominated as press liquor) are generated during the production of viscose-type cellulosic textile fibres. Press liquor contains high concentrations of sodium hydroxide and dissolved hemicellulose as an organic contaminant. Hemicellulose is a collective term for polysaccharides originating from the raw material wood and their degradation products, e.g. sugar acids and hydroxycarboxylic acids. In the process liquors studied here, the high molecular mass fraction mainly consists of 4-O-methylglucuronoxylan [1]. Hemicellulose is an undesired component in the viscose fibre production process because it deteriorates

both processability and fibre quality. To maintain a certain hemicellulose concentration in the process liquors part of the hemicellulose has to be removed from the process with simultaneous minimisation of caustic soda losses. The purification of these process liquors by nanofiltration is a challenge not only because of the high corrosiveness of caustic soda but also due to the high concentration of organic solutes (chemical oxygen demand above 40,000 mg/l). Fouling caused by hemicellulose is a critical issue that reduces flux and leads to the need for rigorous cleaning procedures. Carbohydrate chains in solution are able to interact with each other e.g. via hydrogen

bonds thus forming different conformations and types of aggregates. The observation that xylans have a strong tendency to self-associate was first reported by Blake and Richards [2]. Several researchers investigated size exclusion chromatography (SEC) as a technique to detect xylan aggregates in DMSO/water mixtures [3,4]. The mechanism of aggregation is not only influenced by the molar mass of the xylans but also by the nature and the occurrence of substituents such as acetyl groups and lignin residues. It was proposed that there is a relationship between xylan aggregation in aqueous solution and the formation of xylan structures on cellulose surfaces [4].

Massucco [5] modified the properties of ultrafiltration membranes by generating an irreversibly compressed hemicellulose gel layer under increased pressure. These gel layers adhered to the membrane surface even at high shear forces and reduced pressures and caused a permanent increase in retention at reduced flux. Aqueous suspensions of the acid-insoluble xylan fraction showed gelation at concentrations above 15-16 wt.% [6]. Gelation of the bulk phase has also been observed in solutions of hemicellulose in DMSO/water mixtures. It is therefore suggested that aggregation phenomena of hemicellulose in solution play an important role in the formation of gel layers during nano- and ultrafiltration.

Fouling phenomena during nanofiltration of polysaccharide solutions have been studied using both model substances [7-9] and real effluents from the pulp and paper industry [7,8]. It was observed that anionic substances were retained better and fouled less due to charge repulsion effects especially at high pH where most of the

membranes are negatively charged as well. Flux decline was more distinct when using more open membranes particularly if they were permeable to the model substance [7]. In nanofiltration of real effluents a gel or cake layer formed that was controlled by crossflow velocity. The fouling layer disappeared upon rinsing the system, irreversible fouling was therefore found to be low [8].

The aim of the present study was to relate hemicellulose composition and supramolecular structure to nanofiltration performance parameters such as permeate flux, retention of hemicellulose and decrease in pure water permeability. A series of experiments was carried out using a laboratory-scale crossflow membrane test equipment. The evolution of hemicellulose aggregates was studied by turbidity measurements. The formation of aggregates and gel layers was purposely provoked by partial neutralisation and by addition of methanol that affects the solution state of hemicellulose. Hemicellulose composition and molecular structure were influenced by heat treatment and oxidative degradation.

Experimental

Test equipment, operating procedures and membranes used. Nanofiltration (NF) was carried out in laboratory scale with a flat-sheet crossflow membrane test equipment (Figure 1) manufactured by KCS Osmota. The flow channel had a width of 40 mm, a length of 200 mm and a height of 1.1 mm, thus resulting in 80 cm² active membrane area. A 44 mil (1.1 mm) parallel spacer was inserted into the flow channel.

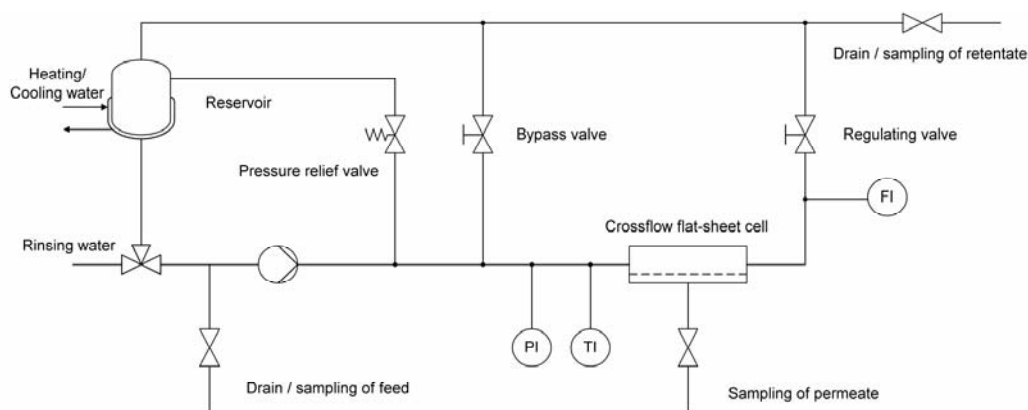


Figure 1. Schematic drawing of the crossflow test apparatus.

Alkaline resistant N30F membranes obtained from Microdyn-Nadir were used for all experiments (pH range 0 – 14). This polyethersulfone type of membrane is characterised by the manufacturer as follows. At the operating conditions of 40 bar, 20°C and 700 rpm in a stirred test cell, pure water permeability is between 40 and 70 l/m²h, sodium chloride (0.5%) retention ranges from 25 to 35% and lactose (4%) retention is between 70 and 90%.

The operating procedure started with cleaning the membrane using a 1% ultrasil 10 (Henkel-Ecolab) solution at 50°C for 60 min and thoroughly rinsing afterwards. This was followed by the determination of pure water flux at 20 bar, 20°C and a crossflow velocity of 0.75 m/s. After filling the apparatus with feed solution, all experiments were carried out at 25 bar, 30-40°C and 0.82 m/s. The retentate was always recycled back to the reservoir, whereas the permeate was either collected in a separate vessel (i.e. concentration mode) or recycled to the reservoir as well (i.e. total recycle mode). Flux was calculated by measuring the time needed to collect a certain volume of permeate.

After each experiment, the equipment was rinsed again, and the pure water flux was measured at the operating conditions described above. The decline of pure water flux was calculated from the fluxes before and after the experiment. This reduction is regarded as a measure for the extent of irreversible fouling [8,9].

Properties and composition of press liquor.

The process liquor studied here was taken from the pressing stage of the viscose production process, and it is accordingly designated as “press liquor”. It can be described as an orange-brown liquid containing about 200 g/l sodium hydroxide and a high concentration of organic solutes (Table 1). This causes appreciable viscosity and, in combination with high retention and low average molar mass, a high osmotic pressure difference between feed and permeate. The corrosiveness of this concentrated caustic soda solution is a challenge for materials selection, especially regarding the membrane material.

In the process liquors studied here, the high molar mass fraction which accounts for about one third of total hemicellulose mainly consists of 4-O-methylglucurono- β -1,4-D-xylan. Approx. 5% of the xylose units are substituted with 4-O-methylglucuronic acid residues [1]. The low molar mass fraction accounts for about two thirds of total hemicellulose. It predominantly consists of substances with a molar mass below 1,000 g/mol, but contains only 25% sugars in oligomeric form. Monomeric carbohydrates have not been detected in any of the fractions. The carboxylic acid groups of the hemicellulose molecules are deprotonated at the high pH leading to an anionic or polyanionic character of most organic molecules in the solution studied. Therefore it can be assumed that repulsive forces are acting

between the solutes and the negatively charged membrane surface.

Table 1. Composition and physical properties of press liquor.

Property	Value	Unit
Chemical oxygen demand (COD)	44,200	mg/l
Total organic carbon (TOC)	17,000	mg/l
Sodium hydroxide	202.96	g/l
Total alkali ¹⁾	207.18	g/l
Total inorganic carbon (TIC)	115	mg/l
Fe ²⁾	0.57	ppm
Mn ²⁾	0.01	ppm
Mg ²⁾	0.33	ppm
Si ²⁾	1.26	ppm
Ca ²⁾	3.73	ppm
density ³⁾	1.19	g/cm ³
dynamic viscosity ³⁾	3.33	mPas

¹⁾ expressed as sodium hydroxide equivalent

²⁾ analysed by ICP-OES

³⁾ at a temperature of 40°C

Methods of analysis.

Sodium hydroxide concentration was measured by titration with 0.5N sulfuric acid to pH 8.2 using a Metrohm 716 DMS titroprocessor equipped with a pH electrode. Total alkali concentration (including sodium carbonate and sodium carboxylates) was determined with the same method and titration to pH 3.7. Total organic carbon (TOC) and chemical oxygen demand (COD) measurements were used to calculate hemicellulose concentrations dividing by the ideal conversion factors for xylan of 1.212 and 0.454 for COD and TOC, respectively. COD was examined according to DIN 38409 – H41-1 using potassium dichromate in sulfuric acid solution as an oxidant and silver sulfate as a catalyst. TOC was measured according to DIN 38409 – H3-1 by catalytic oxidation of organic carbon and IR-spectrophotometric detection of the carbon dioxide generated.

The samples for SEC were diluted 1:20 with 0,5N NaOH prior to analysis. SEC was performed using 2 MCX columns with a pore size of 1000 Å, 300 mm length and 8 mm diameter, obtained from PSS. The mobile

phase was 0.5N NaOH at a flow rate of 1 ml/min; refractive index (RI) detection was employed. Calibration was carried out with a set of cello-oligomers, pullulan and dextran standards. The plot of log(Mw) vs. retention volume was approximately linear. Dynamic light scattering detection showed that the amount of aggregates under these analytical conditions does not significantly influence the determination of molar mass distribution by SEC measurements [10]. Turbidity measurements were used for routine analysis of aggregation behaviour though this method does not provide information about average size or size distribution of aggregates. Turbidity was determined with a Lovibond LAB-IR turbidimeter at a wavelength of 860 nm and a scattering angle of 90°. This device conforms to specifications set forth in ISO 7027. Calibration was carried out with three formazin standards having turbidities of 0.02, 10 and 1000 NTU, respectively. Viscosity was measured by means of a rolling ball viscometer by Höppler (manufactured by Haake) according to DIN 53015.

Results and Discussion

Heat treatment.

This treatment is a means to change chemical composition and molecular structure of hemicellulose. Press liquor was heat treated in the darkness, without access of oxygen, at 60°C for 400 h, and permeate from a NF pilot plant was heat treated under the same conditions for 200 h. Press liquor showed enhanced flux at lower retention after heat treatment, whereas the opposite effect on the pilot plant permeate was observed (Figure 2). These results were elucidated when the molar mass distributions before and after heat treatment (Figure 3) were taken into account. Press liquor was degraded during heat treatment, and the relative amount of the high molar mass fraction decreased while the concentration of the low molar mass fraction increased distinctly. Total hemicellulose

concentration remained constant, but the potential for the build-up of fouling layers was reduced as the fraction of high molar mass solutes diminished. Consequently, fouling was less severe after heat treatment of press liquor.

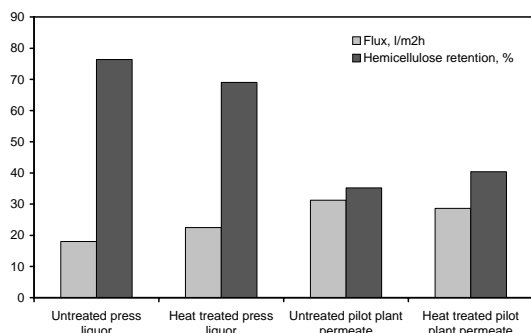


Figure 2. Flux and hemicellulose retention of untreated and heat treated press liquor and permeate from a nanofiltration pilot plant (volumetric recovery: 37%, 25 bar, 36°C, 0.82 m/s).

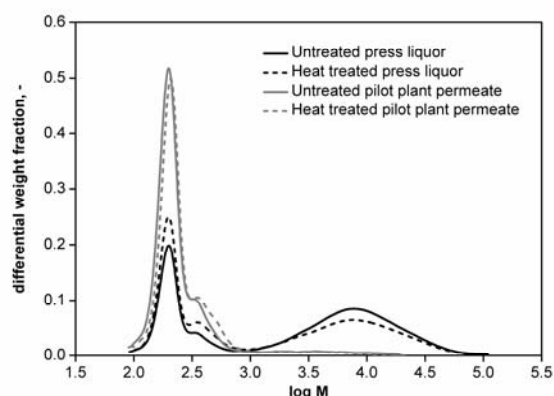


Figure 3. Molar mass distribution of press liquor and permeate from a nanofiltration pilot plant before and after heat treatment.

There was quite a different effect of heat treatment on pilot plant permeate. A re-condensation of oligosaccharidic components was observed, possibly of the aldol condensation type, resulting in a slightly increased average molar mass of hemicellulose after heat treatment. The change in molecular structure and chemical composition also increased the fouling propensity of pilot plant permeate. The reduction of pure water flux after the

experiment was noticeably higher for a treated pilot plant permeate than for untreated feed. The pure water fluxes during all experiments of this study were higher than specified by the manufacturer, probably due to the contact with strong caustic that increased membrane hydrophilicity.

Oxidative degradation.

Press liquor was oxidatively degraded by successive addition of a 30% hydrogen peroxide solution (20 ml per litre of press liquor) when boiling under reflux at atmospheric pressure for 24 h. Nanofiltration was carried out in concentration mode until 51% of the feed solution had been recovered as permeate. The permeate obtained thereafter was recycled to the reservoir to keep hemicellulose concentration constant.

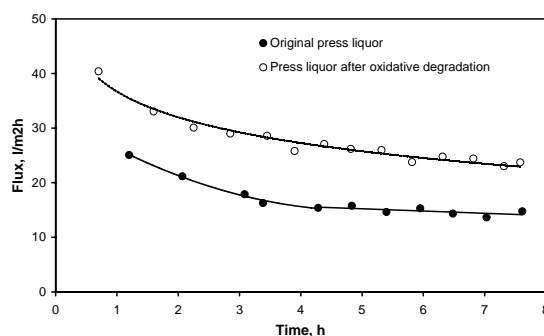
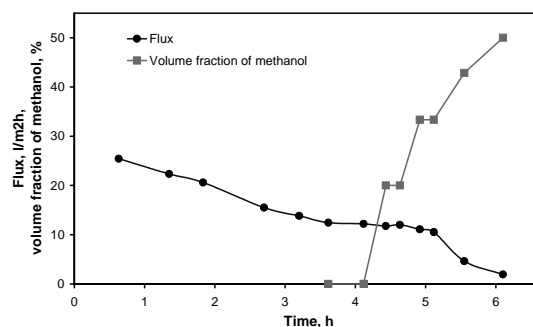


Figure 4. Flux during nanofiltration of original (filled circles) and oxidatively degraded process liquor (open circles) at 51% recovery, 25 bar, 41°C and 0.82 m/s.



Oxidative degradation resulted in a significantly higher flux compared to the original process liquor (Figure 4). Flux

continued to decrease at the end of the experiment in both cases, but flux decline was higher for the oxidatively degraded process liquor possibly because of a faster decrease of fouling layer porosity.

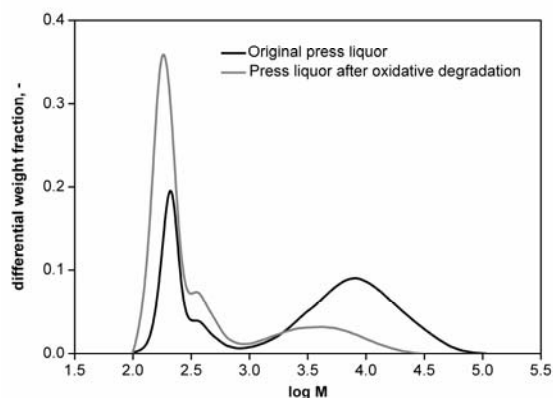


Figure 5. Effect of oxidative degradation on molar mass distribution of hemicellulose in press liquor.

SEC indicated a significant decrease of average molar mass as molecules were oxidatively degraded (Figure 5). The relative amount of the acid-insoluble high molar mass fraction dropped from 37 to 12% of total hemicellulose, and a high quantity of UV-active low molar mass molecules was created. Press liquor after oxidative degradation showed a slightly lower COD/TOC ratio indicating a higher level of oxidation of the organic substances in the liquor.

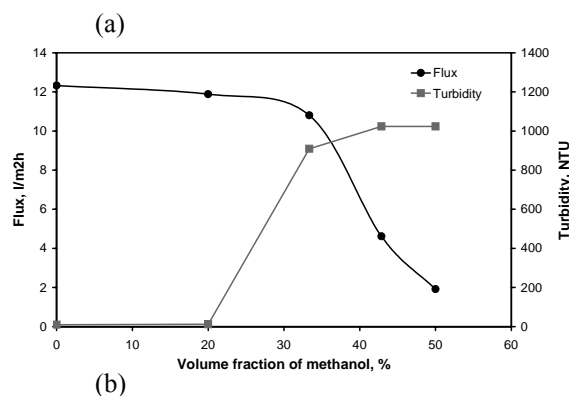
Hemicellulose retention was reduced from 81 to 59% after oxidative degradation, which was attributed to the lower average molar mass of hemicellulose. The reductions of pure water flux after the experiment were 12 and 9% for original and degraded press liquor, respectively. Thus, irreversible fouling slightly decreased upon oxidative degradation.

Methanol addition.

Lower alcohols are poor solvents for polysaccharides. For complete precipitation, alcohol has to be added in excess. In this study, comparatively low volumes of methanol were added to the press liquor to affect the solution state of hemicellulose and to provoke the formation of aggregates

without generating significant amounts of precipitate.

Figure 6. (a) Flux and volume fraction of methanol during incremental addition of methanol (48% recovery, 25 bar, 32°C, 0.82 m/s), (b) flux and turbidity as a function of methanol volume fraction.



When methanol was added incrementally during nanofiltration, an insignificant increase of turbidity was observed after the first addition (Figure 6). Appreciable amounts of aggregates were not formed, and flux remained approximately constant. The addition of another volume of methanol led to a marked increase in turbidity that can be attributed to a commencing formation of aggregates. Interestingly, flux did not yet respond to this observation and showed a minor decrease. A significant flux decline was encountered after the third addition of methanol. At that point turbidity exceeded the upper limit of detection. The fourth volume of methanol again decreased the flux significantly, but the instrument was not able to measure an additional increase of turbidity.

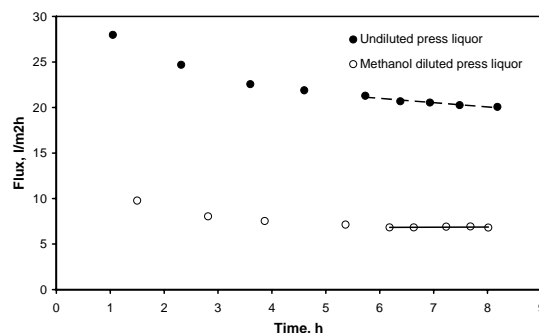


Figure 7. Time dependence of flux during NF of press liquor without (filled circles) and with (open circles) methanol addition (total recycle mode, 25 bar, 41°C, 0.82 m/s).

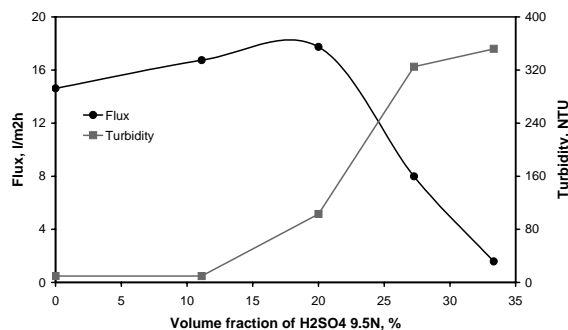
For a detailed nanofiltration experiment, a solution containing 62.5 vol.% of press liquor and 37.5 vol.% of methanol was prepared as feed, and a reference experiment was also done without methanol addition (Figure 7). Both runs were carried out in total recycle mode. Flux was distinctly lower with methanol added compared to the reference experiment which could not solely be attributed to a viscosity increase from 3.3 to 4.2 mPas.

The mixture was significantly turbid before the nanofiltration experiment indicating the formation of hemicellulose aggregates, but, surprisingly, the retentate became visually clear in the course of the experiment, and it got turbid again after discharge from the apparatus. Contrarily, a sample of retentate that was stored without stirring at the same temperature as the NF experiment remained highly turbid thus indicating that no significant redissolution of hemicellulose aggregates occurred. It can therefore be concluded that the decrease in turbidity during nanofiltration was probably due to reduction of average aggregate size caused by shear forces during flow through the apparatus. This is in agreement with the behaviour of hemicellulose suspensions reported previously [6]. The small hemicellulose aggregates may have formed a more compact gel or cake layer as compared to the reference experiment. Steady state flux at a low level was attained with methanol addition after six hours, whereas the flux of pure press liquor continued to decline within eight hours.

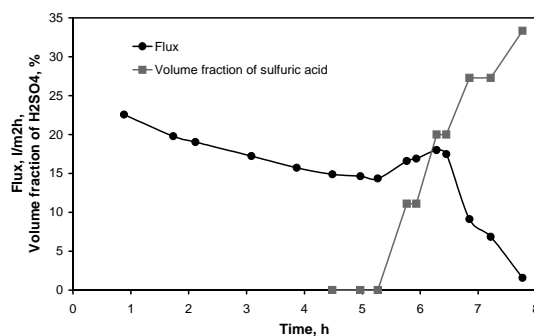
Partial neutralisation by addition of sulfuric acid.

Press liquor was partially neutralised by incremental addition of sulfuric acid thereby generating xylan aggregates and/or particles composed of high molar mass hemicellulose during nanofiltration. Each step of addition was carried out dropwise over a period of about eight minutes, then about 28 min of total recycle operation followed in which the system was allowed to equilibrate (Figure 8).

Figure 8. (a) Flux and volumetric fraction of sulfuric acid during incremental addition of 9.5N sulfuric acid (52% recovery, 25 bar, 42°C, 0.82 m/s), (b) flux and turbidity as a function of sulfuric acid volume fraction.



The behaviour of flux during incremental addition of sulfuric acid to the feed tank was characterised by a gradual increase of flux followed by an extremely steep decline. Increasing flux during the first steps of sulfuric acid addition was attributed to a significant decrease in solution viscosity caused by the reduction of sodium hydroxide and hemicellulose concentrations. Interestingly, there was a point at 20 % volume fraction of sulfuric acid where flux was higher than encountered without sulfuric acid addition although the solution already had noticeable turbidity. This point of operation corresponded to about 75 g/l of sodium hydroxide concentration remaining. In the region of the steep flux decline, formation of hemicellulose aggregates and particles as indicated by the evident increase in turbidity resulted in the build-up of a compact fouling layer.



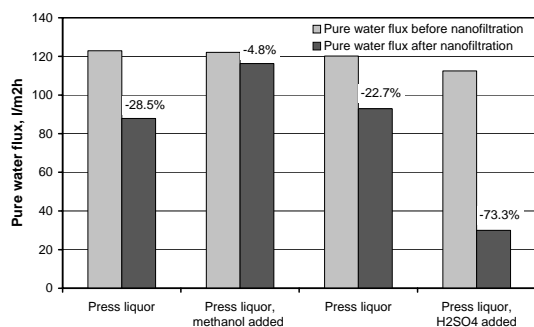


Figure 9. Pure water flux before and after the incremental addition of methanol and sulfuric acid, respectively.

A significant reduction of apparent hemicellulose retention from 81 to 77% was observed when the volume fraction of sulfuric acid was increased from 0 to 20%. This is probably due to increased concentration polarisation in the fouling layer resulting in higher hemicellulose surface concentration. Irreversible fouling was extremely severe after partial neutralisation in contrast to the corresponding methanol addition experiment (Figure 9).

Conclusions

Hemicellulose formed aggregates in strongly alkaline solutions. This process took place more slowly than in DMSO/water mixtures [3,4] due to repulsive forces between deprotonated carboxylic acid groups. Heat treatment of press liquor caused a degradation of hemicellulose and a decrease in average molar mass thus enhancing flux and reducing hemicellulose retention. Degradation by addition of hydrogen peroxide revealed similar effects. A slight reduction of flux at increased retention was observed after heat treatment of pilot plant permeate which was attributed to an increase in average molar mass resulting from re-condensation reactions. A decrease in relative amount of the high molar mass fraction resulted in lower irreversible

fouling, possibly due to a decreased ability of hemicellulose to generate gel layers at the membrane surface.

Precipitation agents in small to medium quantities were used to affect the solution state of hemicellulose thus purposely provoking aggregate formation and increasing the probability of gel or cake layer formation. The influence of several reagents having different effects on the mechanism of hemicellulose aggregation was studied. During nanofiltration of press liquor / methanol mixtures, a distinct flux decline was observed, however, irreversible membrane fouling was low. Sometimes shear forces were able to reduce average aggregate size during a nanofiltration experiment.

Flux was enhanced at the early stages of partial neutralisation by addition of sulfuric acid due to a decrease of solution viscosity that counteracted the build-up of a fouling layer. An extremely steep flux decline occurred when sulfuric acid volume fraction exceeded 20 vol.%. Sulfuric acid addition also reduced apparent hemicellulose retention possibly because of increased concentration polarisation when particulate matter blocked the back diffusion of dissolved molecules from the boundary layer to the bulk phase. This suggested that the formation of a compact gel layer at the membrane surface was considerably enhanced, which would explain the extremely severe irreversible fouling observed after the addition of sulfuric acid. Hemicellulose aggregation as measured by increasing solution turbidity usually coincided with distinct flux decline during nanofiltration. It was therefore suggested that the aggregation of hemicellulose results in the build-up of gel layers near the membrane surface.

Acknowledgement

Financial support was provided by the Austrian government, the provinces of Lower Austria, Upper Austria and Carinthia as well as by the Lenzing AG. We also

express our gratitude to the Johannes Kepler University, Linz, the University of Natural Resources and Applied Life Sciences, Vienna, and the Lenzing AG for their in kind contributions.

References

- [1] U. Mais and H. Sixta, Characterization of Alkali-Soluble Hemicelluloses of Hardwood Dissolving Pulps, In: P. Gatenholm and M. Tenkanen (Eds.), Hemicelluloses: Science and Technology, ACS Symposium Series No. 864, American Chemical Society, Washington 2004, pp. 94–107.
- [2] J.D. Blake and G.N. Richards, Evidence for molecular aggregation in hemicelluloses, *Carbohydr. Research* 18 (1971), 11–21.
- [3] B. Saake, T. Kruse and J. Puls, Investigation on molar mass, solubility and enzymatic fragmentation of xylans by multi-detected SEC chromatography, *Bioresource Technol.* 80 (2001), 195–204.
- [4] Å. Linder, J.P. Roubroeks and P. Gatenholm, Effect of Ozonation on Assembly of Xylans, *Holzforschung* 57 (2003), 496–502.
- [5] A.A. Massucco, Anisotropic ultrafiltration membrane having adhering coating and methods of forming and using this membrane, US Patent No. 3,556,992 (1971).
- [6] J. Lenz, J. Schurz and J. Bauer, Die Dickungs- und Geliereigenschaften von Hemicellulosen aus dem Viskoseprozeß, *Das Papier* 38 (1984), 45–54.
- [7] M. Nyström, L. Kaipia and S. Luque, Fouling and retention of nanofiltration membranes, *J. Membr. Sci.* 98 (1995), 249–262.
- [8] M. Mänttari and M. Nyström, Critical flux of high molar mass polysaccharides and effluents from the paper industry, *J. Membr. Sci.* 170 (2000), 257–273.
- [9] M. Mänttari, L. Puro, J. Nuortila-Jokinen and M. Nyström, Fouling effects of polysaccharides and humic acid in nanofiltration, *J. Membr. Sci.* 165 (2000), 1–17.
- [10] H. Sixta, N. Schelosky, W. Milacher, T. Baldinger and T. Röder, Proceedings of the 11th International Symposium on Wood and Pulping Chemistry, June 2001, Nice, France.

MONITORING OF THE PHASE TRANSITION OF MAGNESIUM SULPHITE HYDRATES BY ONLINE RAMAN SPECTROSCOPY⁺

Michael Steindl¹; Thomas Röder²; Reinhold Simharl²; Michael Harasek³; Anton Friedl³; Herbert Sixta²; Hedda Weber¹

¹ Competence Centre for Wood Composites and Wood Chemistry K-Plus, Area 6, Werkstrasse 1, 4860 Lenzing, Austria; Phone: +43 7672 701 3197; Fax: +43 7672 918 3197; E-Mail: m.steindl@lenzing.com

² Lenzing AG, Department of Pulp Research, Werkstrasse 1, 4860 Lenzing, Austria

³ Vienna University of Technology, Institute of Chemical Engineering, Getreidemarkt 9/166, 1060 Vienna, Austria

⁺A full article of this paper was accepted by *Chemical Engineering and Processing* for publication.

In the magnesium bisulphite wood pulping process, the phase transition of magnesium sulphite hexahydrate into its trihydrate is one important reaction during the absorptive SO₂ recovery from liquor burning waste gas. The kinetics of this phase transition was measured online by Raman spectroscopy. With increasing temperature the stability of the hexahydrate decreases. A decreasing

pH caused faster conversion. These results allow optimising the SO₂ recovery process and are used to improve the simulation model for the recovery process in magnesium bisulphite pulping.

Keywords: *Raman, magnesium, sulfite, recovery*

In the magnesium bisulphite wood pulping process [1], recovery of the spent process chemicals is of both economical and environmental importance. One part of the complex recovery system of the acid magnesium sulphite pulping process is the absorption unit, which is attached to the recovery burner (Figure 1).

There, the waste gas from the thick liquor burning is cleaned from SO₂ by reaction to magnesium bisulphite. The main part of the absorption system is a four-stage scrubber plant according to the venturi principle, working at 65°C and at pH-values from 7.8 to 4.7, where the flue gas, containing sulphur dioxide, is exposed to a Mg(OH)₂ washing solution.

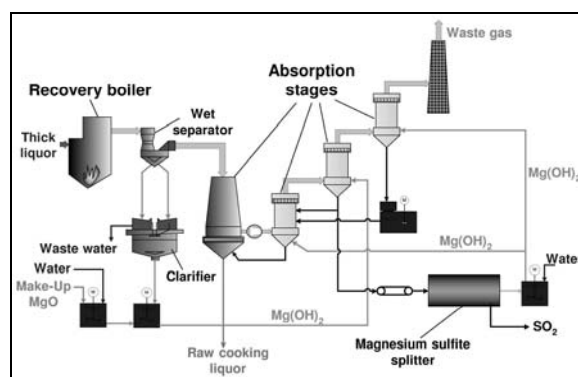


Figure 1. SO₂ absorption recovery system of Lenzing AG

In a two-step reaction, see Equation 3 and Equation 4, magnesium bisulphite is formed, which is re-introduced in the pulping process as cooking liquor.

$MgO + H_2O \rightleftharpoons Mg(OH)_2 \rightleftharpoons Mg^{++} + 2OH^-$	(1)
$SO_2 + 2OH^- \rightleftharpoons SO_3^{2-} + H_2O \rightleftharpoons HSO_3^- + OH^-$	(2)
$Mg^{++} + SO_3^{2-} + xH_2O \rightleftharpoons MgSO_3 \cdot xH_2O$	(3)
$Mg^{++} + 2HSO_3^- \rightleftharpoons Mg(HSO_3)_2$	(4)

One of the main problems during the absorption recovery process is the precipitation of solid magnesium sulphite hydrates $MgSO_3 \cdot xH_2O$. These solids cause several problems, such as mechanical abrasion, incrustations and higher loss of chemicals by discharging of solids. With Markant's [2] conclusions that only dissolved magnesium sulphite undergoes absorption reactions, there is a direct affect on the absorption by precepitation of solid hydrates and the kinetic of the precipitation becomes an important factor for operation and construction of the absorption recovery system.

Two different types of magnesium sulphite hydrates, magnesium sulphite hexahydrate ($MgSO_3 \cdot 6H_2O$) and magnesium sulphite trihydrate ($MgSO_3 \cdot 3H_2O$) are formed under working conditions. Below temperatures of $42^\circ C$ magnesium sulphite hexahydrate is the stable equilibrium solid phase, [3] [4], above this temperature the trihydrate $MgSO_3 \cdot 3H_2O$. However, the metastable hexahydrate often crystallizes first at temperatures higher than the transition temperature of $42^\circ C$. The solubility of the two hydrate types differs significantly, which was first reported by Hagusawa [3]

(Figure 2). Due to the smaller solubility of the trihydrate, process conditions should be used, which prohibit the transition of the hexahydrate.

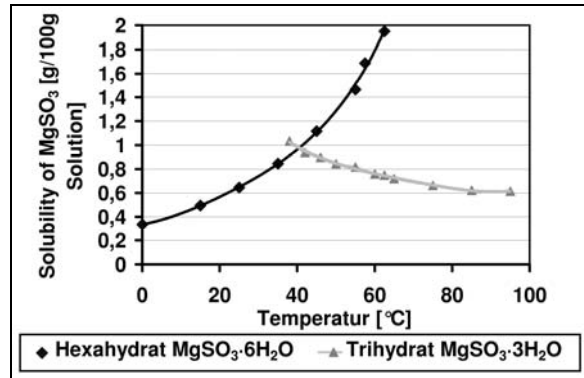


Figure 2. Solubility of magnesium sulphite hydrates

At the temperature in the absorption system ($65^\circ C$), formation of the hexahydrate proceeds first. Within this work, the precipitation of solid trihydrate during the phase transition was monitored.

Crystallographic and Raman data of magnesium sulphite hexa- and trihydrate were reported in the literature [5], [6], [7], [8].

The crystal structure of hexahydrate is rhombohedral, whereas the one of trihydrate is orthorhombic. Raman spectra of pure crystals of the two solid hydrates are shown in

Figure 3. Significant Raman shifts between magnesium sulphite hexa- and trihydrate bands were observed for instance in the range of $150-250\text{ cm}^{-1}$ and between 950 and 980 cm^{-1} .

The characteristic bands used for analysis are 172 cm^{-1} , 208 cm^{-1} , and 952 cm^{-1} for the hexahydrate, and 226 cm^{-1} and 962 cm^{-1} for the trihydrate.

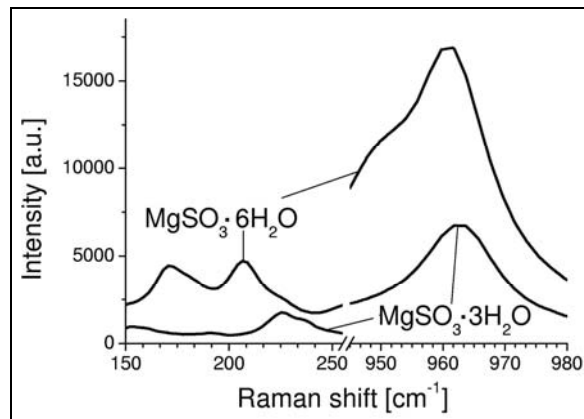


Figure 3. Raman bands of pure solid magnesium sulphite tri- and hexahydrate

Experimental

The experimental setup for the online measurements of the transition kinetics from magnesium hexahydrate to trihydrate is shown

Figure 4.

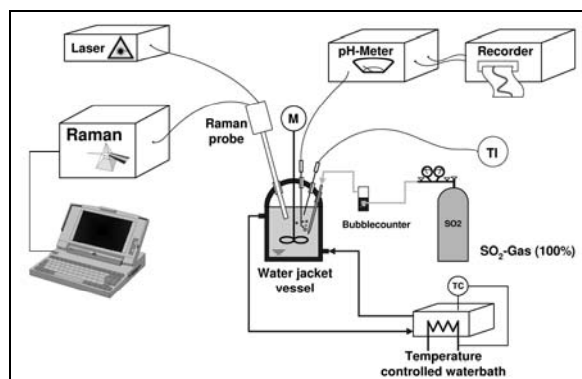


Figure 4. Experimental setup for online Raman spectroscopy of the phase transition of magnesium sulphite hydrate

Into a double-jacketed, temperature-controlled vessel, 350 mL of water and 40 g of MgO were agitated (Fluka 63091, different MgO-types were used in the recovery process). SO₂ gas was introduced into the vessel until the desired starting pH-value was reached after about 30 to 45 minutes. Then the gas flow was stopped and the solution was stirred at the defined temperature until the end of the transition. Formation of the different hydrate types was monitored online by Raman spectroscopy.

The Raman measurements were performed with a HoloLab Series 5000 Modular Raman Spectrometer (HL5R) from Kaiser Optical Systems Inc. (USA) equipped with f/1.8 optics, transmission grating, multichannel CCD array detector (optimized for NIR), and a 785 nm diode laser (400 mW) coupled via glass fibre to a holographic filtered probehead Mark II. A NIR immersion sampling optic (1/4") with short fixed focus on the sapphire window was connected to the probehead. Measurements were done with

approximately 120 mW on the sample. The pH was determined with a pH electrode linked to a Metrohm E588 pH meter.

Results and Discussion

Due to the different Raman signals of the hexahydrate and trihydrate it was possible to observe the transition of magnesium sulphite hexahydrate into the trihydrate in real time by Raman spectroscopy. The influence of various temperatures and of the starting pH value was determined.

Figure 5 shows the course of the transition recorded at 65°C at a starting pH of 6.8.

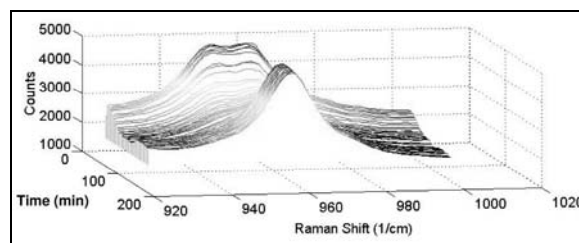


Figure 5. Online Raman spectra of the magnesium sulphite hydrate transition at 65°C and pH 6.8

After SO₂ addition, a bimodal peak, typical of solid magnesium hexahydrate in suspension, was detected. During the transition the bimodal peak faded and a single peak, which corresponds to the trihydrate, appeared. The amount of the hexahydrate was determined by the shoulder at 952 cm⁻¹ (area between 941.4 cm⁻¹ and 957.6 cm⁻¹). The peak at 962 cm⁻¹ was assigned to the trihydrate.

- Influence of temperature:

Söhnel et. al [9] reported the influence of temperature on the transition kinetics of magnesium sulphite hydrates.

Figure 6 shows conversion times of magnesium sulphite hexahydrate suspensions at the same starting pH of about 6.8 measured at temperatures between 55°C and 70°C. With increasing temperature the transition time decreased. These results were in good agreement with literature data [9], [10]. At temperatures of about 70°C the transition proceeds very fast

so that the accurate adjustment of the pH level became difficult.

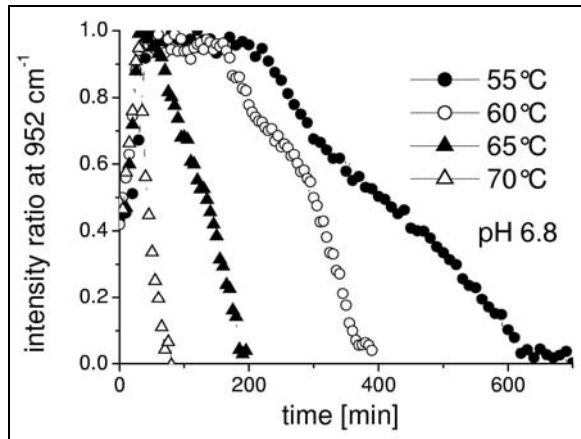


Figure 6. Transition time of magnesium sulphite hexahydrate (starting pH 6.8, temperature range 55°C to 70°C)

- Influence of the starting pH: During the recovery process several ranges of pH values are passed through. It is therefore important to know the influence of the pH on the transition kinetics. Figure 7 illustrates the conversion time of magnesium sulphite at 65°C and at a pH between 6.0 and 8.0. The results show an increasing conversion time with raising pH value.

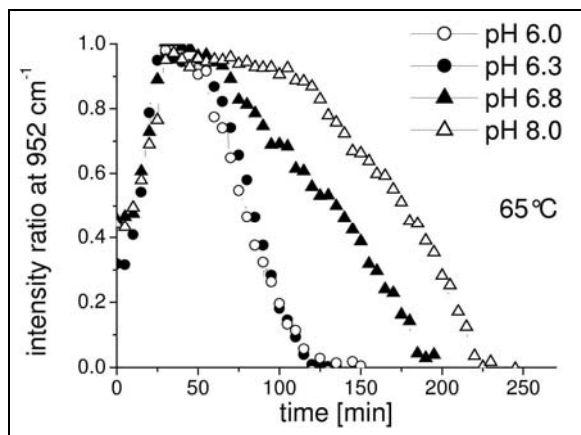


Figure 7. Transition time of magnesium sulphite hexahydrate at 65°C and a pH range between 6.0 and 8.0

During all experiments an increase of the pH-value during the phase transition was observed. $Mg(OH)_2$, which had not yet reacted and remained non-dissociated as a

consequence of the high MgO concentration of 40 g / 350 mL, is still present in the solution. During phase transition from the hexahydrate to the trihydrate the solubility of magnesium sulphite decreases and solid $MgSO_3$ is precipitated. To keep the solution equilibrium of Mg^{2+} constant, new Mg^{2+} ions are formed by $Mg(OH)_2$ dissociation Equation 1. Also OH^- ions are released due to an increase of pH value. The course of the pH relative to the conversion time is shown in Figure 8.

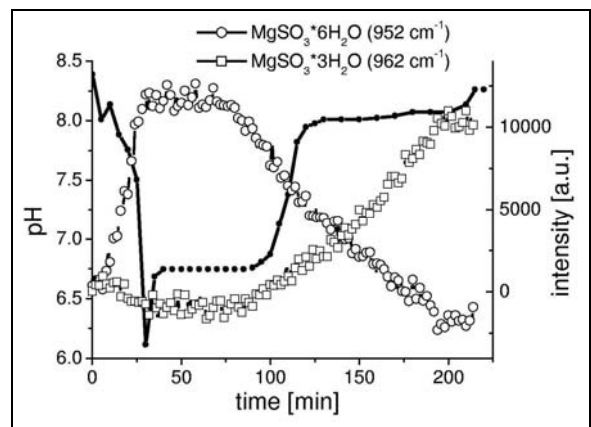


Figure 8. pH course during transition of magnesium sulphite hydrate at 65°C

Conclusions

It was possible to monitor the phase transition of magnesium sulphite hexahydrate into the trihydrate by online Raman spectroscopy. The results showed increasing conversion times with increasing starting pH and decreasing temperature. The increasing pH during conversion is caused by the decreased solubility of $MgSO_3 \cdot 3H_2O$ and progressive dissolution of undissolved $Mg(OH)_2$. Transition times measured with MgO material used in the recovery process showed no significant difference as compared to pure MgO.

Acknowledgement

Financial support was provided by the Austrian government, the provinces of Lower Austria, Upper Austria and Carinthia as well as by the Lenzing AG. We also express our gratitude to the Johannes Kepler University, Linz, the University of Natural Resources and Applied Life Sciences, Vienna, and the Lenzing AG for their in kind contributions.

References

- [1] O.V. Ingruber, 'Sulfite Science & Technology', Joint Textbook Committee of the Paper Industry, 3rd.edn, 1985, pp. 244-301.
- [2] H.P. Markant, R.A. McIlroy and R.E. Matty, Absorption Studies - MgO-SO₂ Systems, *Tappi*, 45(1962) 849 - 854.
- [3] H. Hagiwara, Studies of Magnesium Sulphite, *Bull. Inst. Phys. Chem. Res.*, 12(1933) 976 - 983.
- [4] J. Nývlt, Solubilities of Magnesium Sulfite, *J. Therm. Anal. Cal.*, 66(2001) 509 - 512.
- [5] H.D. Lutz, S.M. El-Suradi and B. Engelen, Zur Kenntnis der Sulfite und Sulfithydrate des Zinks, Mangans, Magnesiums und Cobalts - Röntgenographische, spektroskopische und thermoanalytische Untersuchungen, *Z. Naturforsch.*, 32b(1977) 1230 - 1238.
- [6] H.D. Lutz, W. Eckers, J. Henning, M. Jung and W. Buchmeier, High-Temperature Raman spectra in thermoanalytical studies on the hydrates of Magnesium and Zinc Sulfite, *Thermochim. Acta*, 74(1984) 323 - 330.
- [7] J.W. Bats, H. Fuess and Y. Ellerman, Deformation Density in Magnesium Sulfite Hexahydrate, *Acta. Cryst.*, B42(1986) 552 - 557.
- [8] L. Andersen and O. Lindquist, Neutron Diffraction Refinement of Magnesium Sulfite Hexahydrate, MgSO₃·6H₂O, *Acta. Cryst.*, C40(1984) 584 - 586.
- [9] O. Söhnel and A. Rieger, Phase Transition of Magnesium Sulphite Hydrates in Aqueous Suspension, *Cryst. Res. Technol.*, 28(1993) 487 - 493.
- [10] A.V. Gladkii, V.V. Govorov, A.I. Silantév and V.I. Budanov, Kinetics of the Recrystallization of Crystal Hydrates of Magnesium Sulfite, *Zhur. Prikl. Khim.*, 50(1977) 422 - 423.

MOLAR MASS DISTRIBUTIONS OF CELLULOSE BY ANALYTICAL ULTRACENTRIFUGATION

K. Bernhard¹ and W. Oppermann²

¹ University of Stuttgart, Institute of Textile and Fibre Chemistry,
Pfaffenwaldring 55, D-70550 Stuttgart, Germany
phone: +49 711 685 4486, fax: +49 711 685 4050, e-mail: kay.bernhard@itf.uni-stuttgart.de

² Technical University Clausthal, Institute of Physical Chemistry,
Arnold-Sommerfeld-Strasse 4, D-38678 Clausthal-Zellerfeld, Germany
phone: +49 5323 722205, fax: +49 5323 722863, e-mail: wilhelm.oppermann@tu.clausthal.de

The behaviour of cellulosic materials depends strongly on their molar masses and their molar mass distributions. With the exception of Size Exclusion Chromatography, no reliable technique for the determination of molar mass distributions of cellulose exists. Analytical Ultracentrifugation is known as an accurate and reliable technique for the determination of molar masses and molar mass distributions. For this reason a novel procedure for the

determination of molar mass distributions of cellulose by Analytical Ultracentrifugation was developed. A short review of this novel procedure will be given and the resulting distributions will be compared to those obtained by Size Exclusion Chromatography.

Keywords: *cellulose carbanilate, analytical ultracentrifugation, molar mass distribution*

Introduction

The behaviour of cellulosic materials depends strongly on molar mass and on molar mass distribution. These important properties can also be quantified via the degree of polymerisation (DP).

The determination of molar mass distributions is often quite complex and time-consuming. In former times it was common to fractionate the material and determine the molar mass of every fraction. This resulted in discontinuous distributions of low resolution. Modern analytical methods like Size Exclusion Chromatography (SEC) and Analytical Ultracentrifugation (AUC) are known to be reliable techniques for the determination of molar masses and their distributions.

Procedures for the determination of molar mass distributions of cellulose by SEC have been developed recently employing

the solvent system *N,N*-dimethylacetamide/lithium chloride (DMAc/LiCl) [1]. Since the behaviour of cellulose in DMAc/LiCl is reasonably understood, the results show high reproducibility [2].

Analytical ultracentrifugation is known to be another accurate method for the determination of molar masses and their distributions. Sedimentation velocity experiments can be analyzed to obtain sedimentation coefficient distributions, which are subsequently converted to molar mass distributions. In contrast to SEC no attempts were made within the last decades to use AUC for the determination of molar mass distributions of cellulose.

In this paper, we present a newly developed method for the determination of molar mass distributions of cellulosic materials by AUC [3].

Materials and Methods

For AUC measurements an Analytical Ultracentrifuge Optima XL-A 70 (Beckman-Coulter) with a titanium rotor An 60 Ti was used. The analytical ultracentrifuge is equipped with uv/vis-absorption optics to enable the sedimentation behaviour of the solute to be observed and recorded. The optical system is shown in figure 1.

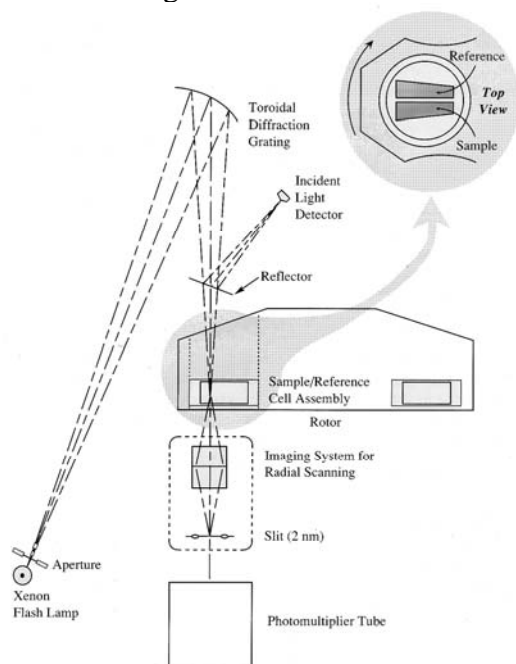


Figure 1. The scanning uv/vis absorbance optical system (taken from: Instruction Manual Optima XL-A 70)

A cavity in a cell centrepiece contains the solution to be centrifuged. The centrepiece is sandwiched between two transparent windows (quartz glass) and, together with various gaskets, held in a cell housing. The whole cell assembly is placed in a rotor in such a way that the cell crosses the light path of the optical system when the rotor is spinning. Thus absorbance and hence concentration can be obtained as a function of distance from the centre of rotation [4]. Since cellulose has no absorption peak within the operating range between 190 nm and 800 nm, the material has to be derivatised to introduce a suitable chromophore. Concurrently, the derivati-

sation enables or enhances the solubility of the material in common organic solvents.

Carbanilation by the following procedure proved to be a suitable method for the derivatisation: After activation by swelling in water, followed by solvent exchange via dry methanol to dry DMAc, the material was homogeneously dissolved in DMAc/LiCl. Treatment with 4-chlorophenylisocyanate yielded 4-chlorophenyl cellulose-tricarbanilate with a degree of substitution larger than 2.7. The product was soluble in different organic solvents such as acetone and tetrahydrofuran and showed a suitable absorption at 283 nm. It could be shown by size exclusion chromatography that the original molar mass distribution remains unchanged during this procedure. No degradation or fractionation occurs under the described conditions.

In order to obtain molar mass distributions, sedimentation coefficient distributions have to be determined first. The sedimentation coefficient s is defined as the rate of movement u of a solute per unit field:

$$s \equiv \frac{u}{\omega^2 r} = \frac{dr/dt}{\omega^2 r} \quad (1)$$

Therefore values for the sedimentation coefficient can be obtained by observing the velocity of molecules during a so-called sedimentation velocity experiment. Sedimentation coefficients can be converted to molar masses by empirical relationships such as

$$s = kM^\alpha \quad (2)$$

The values of the constants k and α have to be determined for each polymer-solvent system. For calibration, weight average molar masses can be obtained by sedimentation equilibrium experiments. Sedimentation results in the buildup of concentration differences within the solution. A concentration gradient will cause diffusion which tends to counteract this buildup. Sedimentation velocity experiments are performed at high rotor

speeds where diffusion effects can be neglected as long as the sedimenting particles are not too small. Such experiments are used to determine s .

At low rotor speed, an equilibrium between sedimentation and diffusion will eventually be attained. This is called a sedimentation equilibrium experiment. From the slope of the resulting concentration profile the weight average molar mass of the solute can be calculated. For the determination of weight average sedimentation constants, *Baldwin's Transport Method* was used [5]. This method gives weight average values and allows to determine the sedimentation coefficients of broadly distributed samples. Sedimentation coefficient distributions were determined by using *Stafford's Time Derivative Method* [6]. Using the time derivative of the raw data enhances the signal to noise ratio and thus the sensitivity of the method. A second advantage of this method is that it makes no assumptions about the characteristics of the macromolecules. Thus this method is appropriate for broadly distributed samples.

Weight average molar masses were obtained by the *M-Star* procedure [7]. Data of broadly distributed samples such as cellulose cause specific problems, when analysed by standard methods. The *M-Star* method includes an extrapolation procedure eliminating these problems reliably.

Results and Discussion

Weight average sedimentation coefficients, sedimentation coefficient distributions, and weight average molar masses were determined at different rotor speeds and initial concentrations in THF for the carbanilates of three different samples of cellulose. The sedimentation coefficients and molar masses are compiled in Table 1.

Table 1. Sedimentation coefficients and molar masses for three different carbanilated cellulose samples.

sample	sed. coefficient [sved]	molar mass [kg/mol]
I	10.8	430
II	14.4	711
III	19.5	1 225

By plotting $\log s$ against $\log M$ according to Eq. (2) it was possible to determine k and α . Thus a molar mass - sedimentation coefficient relationship could be obtained, which served as a calibration to convert sedimentation coefficient distributions into molar mass distributions [8]:

$$s = 0,0072 \cdot M^{0.56} \quad (3)$$

The molar mass distributions for a sample of carbanilated eucalyptus pulp (sample II) obtained from measurements at different rotor speeds [9] are shown in figure 2.

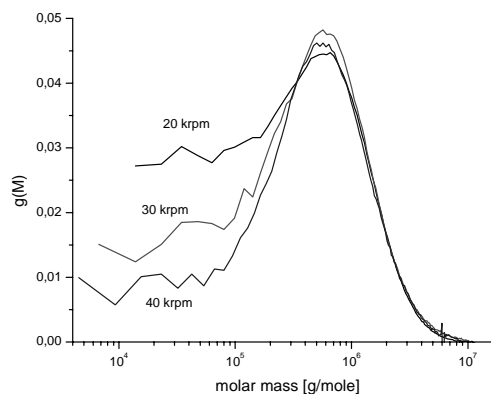


Figure 2. Molar mass distributions of carbanilated eucalyptus pulp determined at different rotor speeds.

The distribution curves show good agreement except for low molar mass values (as a result of diffusion effects).

The molar mass distribution of the same but non-derivatized eucalyptus pulp was determined by SEC in DMAc/LiCl at Lenzing AG. Figure 3 shows a normalised overlay of the DMAc/LiCl - SEC distribution and the distribution determined by AUC at 30 000 rpm, where

molar mass data were converted to refer to unsubstituted cellulose.

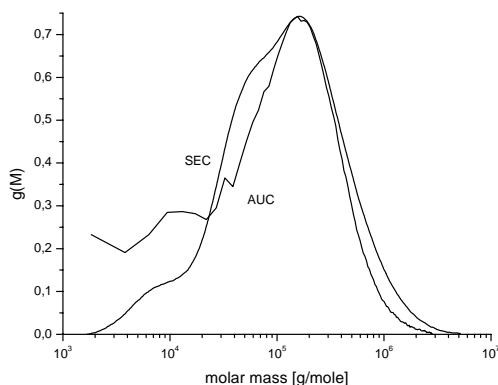


Figure 3. The molar mass distributions of eucalyptus pulp determined by DMAc/LiCl-SEC and AUC.

The agreement between the two methods is surprisingly good. The DP-values at the maximum are about 1000 for the ultracentrifugal distribution and 1015 for SEC. The weight average DPs are 1350 and 1380, respectively.

Conclusions

A novel method for the determination of molar mass distributions of cellulosic materials by analytical ultracentrifugation was developed. This comprises a derivatisation procedure, which could be shown to preserve the original distribution. Sedimentation coefficient distributions determined from sedimentation velocity runs can be converted to molar mass distributions by a relationship obtained from sedimentation equilibrium experiments. The results showed an excellent agreement with those obtained by SEC in DMAc/LiCl.

Acknowledgement

The authors would like to thank the R&D group at Lenzing AG for the DMAc/LiCl – SEC measurements.

References

- [1] Schelosky, N.; Röder, T.; Baldinger, T.: *Das Papier*, 1999, 53, 728-738.
- [2] Röder, T., Potthast, A., Rosenau, T., Kosma, P., Baldinger, T., Morgenstern, B., and Glatter, O.: *Macromol. Symp.*, 2002, 190, 151–159.
- [3] *for details see:* Bernhard, K.: 'Die Bestimmung der Molmassenverteilungen von Cellulose mittels Analytischer Ultrazentrifugation', PhD Thesis, University of Stuttgart, 2004 (in prep.)
- [4] *for an introduction to ultracentrifugal theory see:* Mark, H.; Gaylord, N.; Bikales, N. (Eds.): *Encyclopedia of Polymer Science and Technology*, Vol. 14, Interscience Publishers, New York, 1971, pp. 97-116 and Budd, P.: *Sedimentation and Diffusion* in: Allen, G.; Bevington, J.; Booth, C.; Price, C. (Eds.): *Comprehensive Polymer Science*, Vol. 1, Pergamon, Oxford, 1989, pp. 199-214.
- [5] Schachman, H.: *Ultracentrifugation in Biochemistry*, Academic Press, New York, 1959, pp. 85-90.
- [6] Stafford, W. F.: *Anal. Biochem.*, 1992, 203, 295-301.
- [7] Cölfen, H.; Harding, S. E.: *European Biophysics Journal*, 1997, 25, 333-346 and Creeth, J. M.; Harding, S. E.: *Journal of Biochemical and Biophysical Methods*, 1982, 7, 25-34.
- [8] s = sedimentation coefficient in Svedberg (1 sved = 10^{-13} sec), M in g/mole.
- [9] krpm = kilo rotation per minute.

APPLICATIONS OF FT RAMAN SPECTROSCOPY FOR THE CHARACTERIZATION OF CELLULOSE

Karla Schenzel and Steffen Fischer

Agricultural Department, Martin Luther University Halle-Wittenberg, Ludwig-Wucherer-Str. 2, 06108 Halle, Germany; E-mail: schenzel@landw.uni-halle.de

Fraunhofer Institute of Applied Polymer Research, Geiselbergstraße 69, 14476 Potsdam, Germany; E-mail: steffen.fischer@iap.fhg.de

FT Raman spectroscopy was used for the investigation of cellulose and cellulose derivatives. Lattice structures of cellulose, polymorphic modifications I and II, as well as amorphous structure were clearly identified by means of FT Raman vibrational spectra. Chemometric models were developed utilizing univariate calibration as well as

methods of multivariate data analyses of the FT Raman spectral data. Cellulose properties like the degree of crystallinity XcRaman and the degree of substitution DSCMC as well as DSAC were determined.

Keywords: *FT Raman spectroscopy, cellulose; cellulose derivatives*

Introduction

Vibrational spectroscopy, especially Raman spectroscopy, has played an important role in the investigation of cellulose structures. The fundamental studies of Atalla and co-workers confirmed the advantage of this analytical method over IR and NMR spectroscopy, for determining the molecular conformations and hydrogen bonding patterns of cellulose and cellulosic biomaterials.^[1-9]

The main reason for the trend to Raman spectroscopy was the development of effective FT Raman spectrometers using NIR or red excitation lasers which avoid the fluorescence of the samples which normally blank the Raman signals. The development of high sensitive detectors in conjunction with the coupling of optical fibres and microscopes enhanced the capacity of Raman spectroscopy for analytical analysis and online process control. FT Raman microscopes equipped with mapping units became very powerful tools especially for *in situ* investigations of biomaterials.^[10-12]

We began a still ongoing examination of cellulose structures using methods of deconvolution of the FT Raman spectra, utilizing all the advantages of new spectrometers, computational technologies as well as methods for analysing the Raman vibrational spectra. We developed methods for quantification and fast prediction of cellulose properties using methods of spectra fine resolution in combination with multivariate analyses of the spectral data.

In this paper we report on new results and give a summary of past results of our FT Raman spectroscopic investigations on cellulose, which clearly demonstrate the capability and convenience of this analytical method.

Investigations on cellulose structures

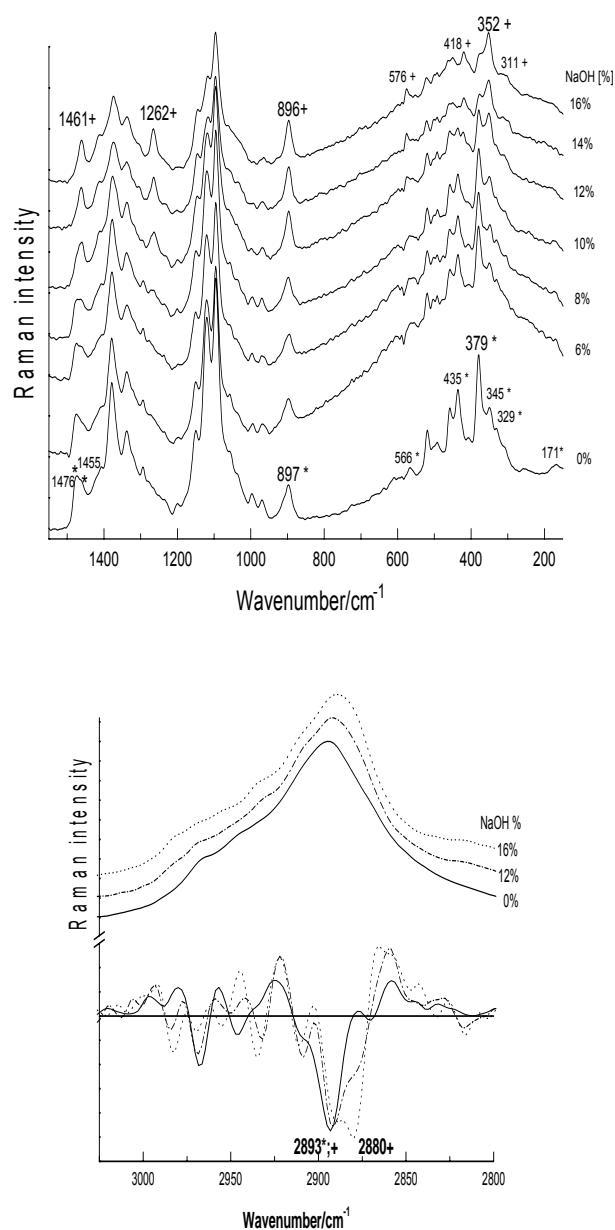
Cellulose modifications I and II

FT Raman spectra of the polymorphic modifications cellulose I and II reflect the conformational differences of both lattice types most clearly in the low frequency

range of the spectra, see Figure 1 (on top). Obviously, cellulose modification I and II differ in the conformational arrangements of the side chains of the anhydroglucopyranose residues. Our findings by FT Raman experiments which were reported earlier^[13], confirmed findings by Wiley & Atalla^[5, 6] using “classical” Raman spectroscopy with visible laser excitation. The FT Raman spectra of cellulose modification I indicated the simultaneous presence of two stereo chemically non-equivalent CH₂OH groups resulting from the rotation of the side chains about the C(5)–C(6) atoms. In cellulose II, only one type of the CH₂OH groups was present. This causes the two scissoring vibrations of the methylene groups to merge into one single signal.

In contrast to the investigations of Atalla & co-workers, we recorded the Raman vibrational spectra by means of NIR laser excitation. Thus, fluorescence-free Raman spectra of cellulose, pulps and plant material were measured without special sample preparations.

Furthermore, using methods of derivative spectrometry already small differences in the vibrational behaviour of cellulose modifications or cellulose forms were identified at their FT Raman spectra. For instance, the alkaline treatments of cellulose indicated a frequency shift $\Delta\nu$ of 13 cm^{-1} of the most intensive Raman line (2893 cm^{-1}), as can be seen from the second derivatives, see Figure 1 (below). After the treatments ($c_{\text{NaOH}} = 16\%$) the intensity maximum appeared at 2880 cm^{-1} , which is a characteristic of cellulose modification II.^[14]



(*) cellulose modification I; (+) cellulose modification II

Figure 1. FT Raman spectra following the polymorphic transformation cellulose I into cellulose II due to cellulose treatments with different alkaline concentrations; (on top): low frequency range; (below): CH stretching region of the spectra and their second derivatives.

The polymorphic transformation of cellulose I into cellulose II is caused also by dissolving cellulose in different molten inorganic salt hydrates. Previously, it was reported that several molten inorganic salt

hydrates may serve as solutes for cellulose.^[15-17] Interestingly, from cellulose, regenerated from the melts of $\text{ZnCl}_2 \cdot 4\text{H}_2\text{O}$, $\text{LiSCN} \cdot 2,5\text{H}_2\text{O}$ and $\text{LiCl} \cdot 2\text{ZnCl}_2 \cdot 6\text{H}_2\text{O}$, can be proven that dissolution leads to the transformation of cellulose I to cellulose II. This was confirmed by FT Raman spectra and WAXS investigations.^[13]

Amorphous cellulose

The three molten salts $\text{ZnCl}_2 + 4\text{H}_2\text{O}$, $\text{LiSCN} \cdot 2,5\text{H}_2\text{O}$ and $\text{LiCl} + 2\text{ZnCl}_2 + 6\text{H}_2\text{O}$ served as solvents for the cellulose for the dissolution experiments. Solutions of cellulose (5 % w/w) were prepared using the melts. Whereas solutions of cellulose in $\text{ZnCl}_2 + 4\text{H}_2\text{O}$ appeared liquid after rapid cooling to room temperature, solutions in $\text{LiSCN} \cdot 2,5\text{H}_2\text{O}$ and $\text{LiCl} + 2\text{ZnCl}_2 + 6\text{H}_2\text{O}$ formed a glassy state. In all cases no precipitation of cellulose fibres was observed. It can be concluded, that the specific interactions between cellulose and molten salts within the solution are maintained also in the solid state after cooling.

The dissolving process could be controlled easily by online FT Raman spectroscopic investigations, because the pure molten salts do not show any vibrational mode at the observed frequency range of the FT Raman spectra. It turned out that the Raman lines of the dissolved cellulose are broader in the melt systems than for the pure polymers. Nevertheless, a Raman shift of the $\nu(\text{C-O-C})$ modes of cellulose ($\Delta\nu$ of $\sim 10 \text{ cm}^{-1}$) to lower wave numbers was observed indicating different vibrational coupling between the anhydroglucopyranose units when compared with the crystalline cellulose.

A comparison of the FT Raman spectra of amorphous cellulose with the spectra of cellulose dissolved in the hydrated melts is shown in Figure 2. It can easily be seen that the vibrational frequency of the $\nu(\text{C-O-C})$ mode of cellulose in the melts and

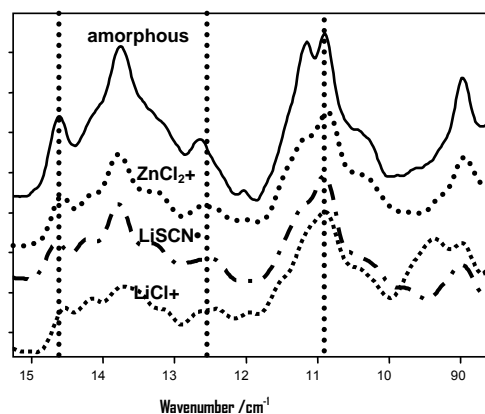


Figure 2. FT Raman spectra of amorphous cellulose in comparison to FT Raman spectra of cellulose dissolved in $\text{ZnCl}_2 + 4\text{H}_2\text{O}$, $\text{LiSCN} \cdot 2\text{H}_2\text{O}$ and $\text{LiCl} + 2\text{ZnCl}_2 + 6\text{H}_2\text{O}$ recorded directly within the molten salts.

that of amorphous cellulose are nearly the same. Additionally, typical vibrations of amorphous cellulose were observed at 1260 cm^{-1} and 1460 cm^{-1} . This was also the case for the cellulose in the hydrated melts. Therefore it was deduced, that cellulose dissolved in molten salts undergoes a transition into an amorphous state. This was also confirmed by ^{13}C NMR measurements.^[16] No indication for the formation of additional compounds have been observed.

Crystalline and amorphous cellulose - Determination of $X_{\text{CRaman}}/\%$

In view of those results, it became interesting to examine the vibrational behaviour of crystalline cellulose I, and compare it with the amorphous forms, which were produced by grinding of the crystalline ones.

Two model systems of cellulose I, a bacterial cellulose as well as an Eucalyptus sulphite pulp system were investigated. These also served as calibration models which represented entire ranges of cellulose I crystallinity of 0-69% and 0-40%.

Once more, using methods of fine resolution of the convoluted FT Raman spectra of cellulose, significant differences

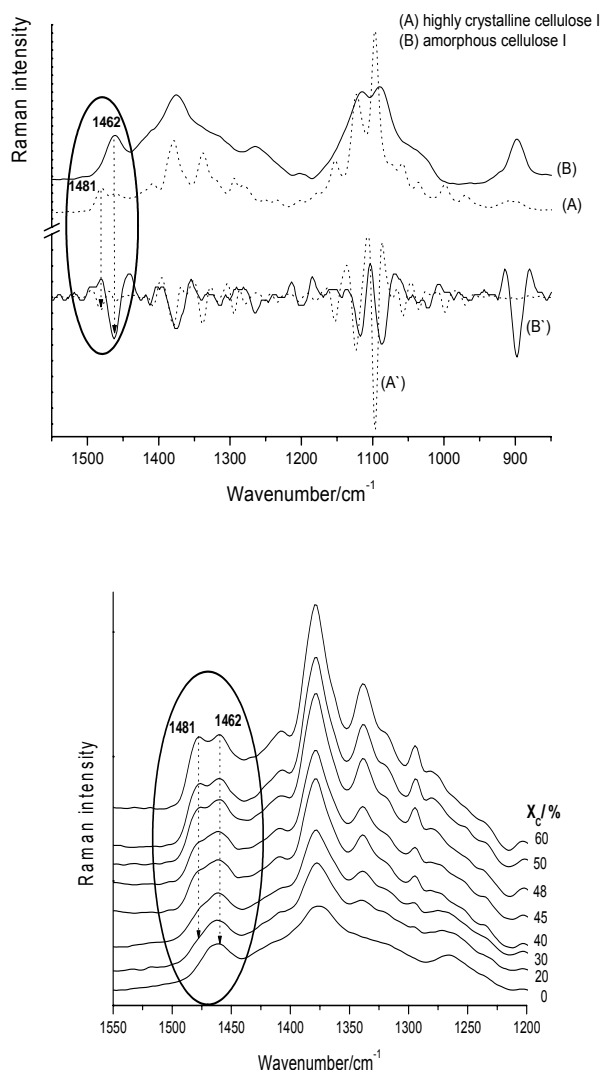


Figure 3. FT Raman spectra and second derivatives of cellulose I model compounds, (top). FT Raman spectra of generated mixtures of cellulose I with different adjusted degrees of crystallinity, X_c / %, (bottom).

between crystalline cellulose I and its amorphous form were observed in the range of δ -CH₂ of the CH₂OH side chains of the cellulose skeletons. Vibrational modes of methylene bendings δ CH₂, characteristic of each form, crystalline (1481 cm⁻¹) and amorphous (1462 cm⁻¹), were determined, see Figure 3 (on top). A strong intensity dependence of these two peaks was observed due to the transition from crystalline to amorphous state, as it is presented in Figure 3 (below) by physical mixtures of cellulose I with different

degrees of adjusted crystallinity, X_c / %: 0%; 10%; ...60%.

As a result, the intensity ratio of the two characteristic lines is strongly influenced by the degree of crystallinity of cellulose I, and therefore also suitable for its quantification. Taking this into account, a Raman crystallinity index, $X_{C_{Raman}} / \% = (I_c / I_c + I_a) \times 10^2$, was defined to determine the percentage crystallinity - $X_{C_{Raman}}$ - of cellulose I.

Intensities of the Raman modes of crystalline (I_c) and amorphous (I_a) content were obtained by peak fitting using Gaussian bands and linear baselines. Linear calibration curves illustrating the relationship between experimentally determined percentage crystallinities, $X_{C_{Raman}}$ and adjusted crystallinities, X_c , were obtained by least square analyses of the data for both model systems.

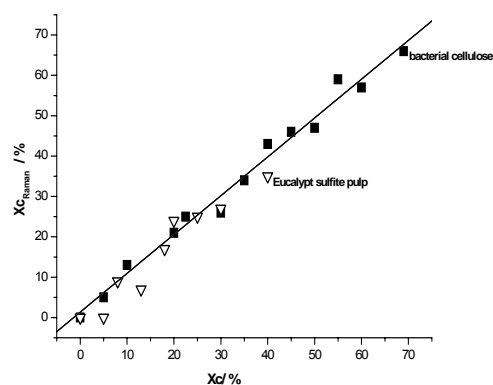


Figure 4. Eucalypt sulfite pulp model (∇) included into the bacterial cellulose calibration set (\blacksquare), described by $X_{C_{Raman}} = 0.962 X_c + 1.34$.

In Figure 4, the Eucalyptus sulphite pulp system was included into the bacterial cellulose calibration set. KBr was used for homogenisation of the powder blends to keep effects of light diffraction due to different refractive indices at a minimum. Thus, it became possible to describe the two cellulosic systems by one calibration model.

Microcrystalline cellulose with known $X_{C_{NMR}}$ values was examined for validation of this univariate calibration model.

Generally, $X_{C_{Raman}}$ values and $X_{C_{NMR}}$ values agree to within $\pm 5\%$. These investigations using methods of univariate spectra analysis led to the development of a new method for quantification of cellulose I crystallinity. This method is described in full somewhere else.^[18]

Quantification and prediction of cellulose properties

In accordance with the new spectroscopic approaches, it is necessary to establish reliable and rapid methods to perform FT Raman analyses for quantification or for prediction of physical and chemical properties also of such complex molecules like cellulose and high variable systems like biological materials. For these purposes, methods of multivariate calibration, classification and clustering of the analytical data may be used.

Determination of $X_{C_{Raman}}$ - a multivariate calibration model

The cellulose I model systems with known percentual crystallinity values $X_{C_{Raman}}/\%$ that were obtained by means of the univariate calibration model as described above were examined using the Bruker OPUS/Quant 2 software. A partial least square algorithm (PLS) was utilized in order to find the best correlation function between spectral and concentration matrix. A very fast multivariate chemometric calibration model for predicting the percentage of cellulose crystallinity, $X_{C_{Raman}}/\%$ was developed by applying cross-validation.^[19] In Table 1 the $X_{C_{Raman}}/\%$ values of different cellulose determined by means of the univariate as well as the multivariate calibration model are presented and compared with the corresponding $X_{C_{NMR}}$ values.

It is necessary that the number of calibration spectra exceeds the number of components in the mixture in order to obtain statistically significant results for PLS software. 22 FT Raman spectra, one

for each generated cellulose I mixture with known degree of crystallinity $X_{C_{Raman}}/\%$ as predicted by the univariate chemometric model, were used for generating the multivariate calibration model. FT Raman spectra were vector normalized and the first derivatives of the spectra were calculated for all pre-calibrations. Not the total spectral range from 3500- 150 cm^{-1} was used to perform the PLS studies. We preferred to select the small spectral region 1510-1210 cm^{-1} because of its strong crystallinity dependence, which turned out to improve the prediction of results. The accuracy of the established calibration model it was validated by using a cross-validation method. The validation statistics described the resultant calibration model with good fits ($R^2 = 0.9805$) and with low error between modelled and reference values (RMSECV= 2.04).

Cellulose	$X_{C_{NMR}}/\%$	$X_{C_{Raman}}/\%$	$X_{C_{Raman}}/\%$ multivariat
ElcemaF100	26 %	23 %	28 %
ElcemaF150	32 %	18 %	30 %
Vitacell A300	29 %	21 %	30 %
Vivapur 102	60 %	59 %	55 %
Avicel PH200	59 %	59 %	58 %
Avicel PH301	62 %	52 %	57 %
Bacterial cell.	72 %	69 %	69 %
BuckeyLinters	60 %	56 %	58 %
Cotton Linters	67 %	50 %	61 %
Borregard	55 %	51 %	54 %

Table 1: Degree of crystallinity $X_c/\%$ of different cellulose materials determined by ^{13}C NMR and FT Raman spectroscopy utilizing univariate and multivariate methods for the analysis of FT Raman spectral data.

Determination of the degree of substitution (DS) of cellulose derivatives - multivariate calibration models

FT Raman spectra of cellulose derivatives like carboxymethylcellulose (CMC) and cellulose acetate (CA) were also recorded. The degrees of substitution of CMC^[20] and CA^[21] were determined through NMR measurements. Multivariate chemometric models for the determination of DS_{CMC} and DS_{CA} were obtained by applying the PLS algorithm of the BRUKER software OPUS/Quant 2 to the FT Raman spectral data of the calibration samples. In both cases cross-validation was used for the verification of the predictions of the calibration model.^[19]

In Figure 5 (top) an example of a FT Raman spectrum of a carboxymethylcellulose is presented. Typical Raman signals which characterise the pattern of substitution were observed at the frequency ranges of $\nu(\text{COO}^-)$, $\nu(\text{C-O})$ and $\nu(\text{C-C})$ modes. Consequently, the wave number range 1730-800 cm^{-1} of the spectra was utilized for the development of the multivariate calibration model. A PLS regression algorithm was applied for finding the best correlation function between the vector normalized FT Raman data and the corresponding DS values of the carboxymethylcellulose.

The calibration model was evaluated by cross-validation.

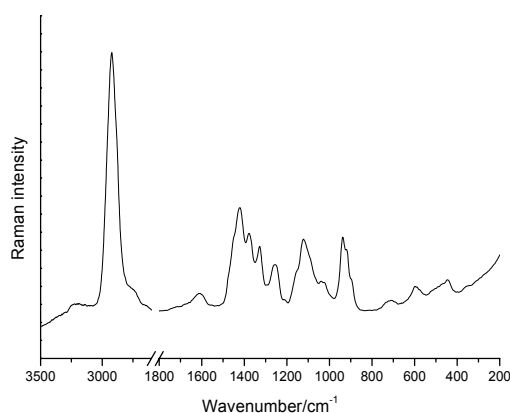


Figure 5. Exemplarily FT Raman spectra of a carboxymethylcellulose.

As a result, a multivariate calibration model for predicting DS_{CMC} values in the range of 0.39–2.00 with high accuracy ($R^2=0.9779$) and low error between modelled and reference values (RMSECV= 0.0815) could be developed.

A similar calibration model for determining the degree of substitution of cellulose acetate DS_{CA} in the range of 1.25–2.90 was generated. For this purpose, the FT Raman spectral data were pre-calibrated by calculating their second derivatives. Here, the frequency range of 1860-1275 cm^{-1} of $\nu(\text{C=O})$ is most suitable for the calibration procedure. The final cross-validation statistics certified a calibration model of high accuracy ($R^2=0.959$) and with low error between the modelled and reference values (RMSECV=0.119) for the fast prediction of DS_{CA} values.

Conclusion

The results reported in this work clearly demonstrate that FT Raman spectroscopy is an effective method for the characterization of native cellulose, pulps, as well as cellulose derivatives.

The important advantages of FT Raman spectroscopy are the ease of sample preparation and the short time required for the measurements. The effective combination of macroscopic and microscopic tools as well as the possibility for on line process control will establish this analytical method for production and quality control of all processes in which changes of conformational arrangements and molecular compositions of cellulose occur.

For the first time univariate and multivariate calibration models were developed utilizing FT Raman spectral data for determining the degree of cellulose I crystallinity, $X_{\text{C-Raman}}$ and the degrees of substitution DS_{CMC} as well as DS_{CA} for native cellulose and cellulose derivatives.

References

- [1] J. Blackwell, P. D. Vasko, J. L. Koenig, *J. Appl. Phys.* 1970, 41, 4375.
- [2] R. H. Atalla, *App. Polym. Symp.* 1976, 28, 659.
- [3] R. H. Atalla, *J. Appl. Polym. Sci., Appl. Polym. Symp.* 1983, 37, 295.
- [4] R. H. Atalla, J. Ranua, E.W. Malcolm, *Tappi J.* 1984, 67, 96.
- [5] J. H. Wiley, R.H. Atalla, *Carbohydr. Res.* 1987, 160, 113.
- [6] J. H. Wiley, R.H. Atalla, *ACS Symp. Ser.* 1987, 340, 151.
- [7] R. H. Atalla, in: „Cellulose“, J. F. Kennedy, G.O. Phillips, P.A. Williams, Eds., Ellis Horwood, Chichester 1989, 61 pp.
- [8] U.P. Agarwal, R.H. Atalla, *Planta* 1986, 169, 325.
- [9] R.H. Atalla, R.E. Whitmore, C.J. Heimbach, *Macromolecules* 1980, 13, 1717.
- [10] B. Schrader, in: „Infrared and Raman Spectroscopy - Methods and Applications“, B. Schrader, Ed. VCH Weinheim, New York, Basel, Cambridge, Tokyo, 1995, III/ pp155.
- [11] H.G.M. Edwards, D.W. Farwell, D. Webster, *Spectrochim. Acta* 1997, 53A, 2383.
- [12] E. Urlaub, J. Popp, W. Kiefer, G. Bringmann, D. Koppler, H. Schneider, U. Zimmermann, B. Schrader, *Biospectroscopy* 1998, 4, 113.
- [13] K. Schenzel, S. Fischer, *Cellulose* 2001, 8, 49.
- [14] A. Jähn, M. Fütting, K. Schenzel, W. Diepenbrock, *Spectrochim. Acta* 2002, 58A, 2271.
- [15] S. Fischer, W. Voigt, K. Fischer, *Cellulose*, 1999, 1, 3.
- [16] S. Fischer, H. Leipner, K. Thümmeler, E. Brendler, J. Peters, *Cellulose*, 2003, 10, 227.
- [17] S. Fischer, H. Leipner, E. Brendler, W. Voigt, K. Fischer, *ACS Symp. Ser.* 1999, 10, 737.
- [18] K. Schenzel, S. Fischer, E. Brendler, *Cellulose* 2005, in print.
- [19] K. Schenzel, S. Fischer, K. Fischer, CSIRO Publishing, *XIXth International Conference on Raman Spectroscopy*, 2004, Australia, Proceedings p. 415.
- [20] A. Baar, W.-M. Kulicke, K. Szablikowski, R. Kieseewetter, *Macromol. Chem. Phys.* 1994, 195, 1483.
- [21] J. Kunze, A. Ebert, H.-P. Fink, *Cell. Chem. Technol.* 2000, 34, 21.

UNCONVENTIONAL DISSOLUTION AND DERIVATIZATION OF CELLULOSE

Steffen Fischer

Fraunhofer Institute of Applied Polymer Research, Geiselbergstraße 69, 14476 Potsdam, Germany; E-mail: steffen.fischer@iap.fhg.de

The preparation of cellulose solutions is important for derivatization and blend formation of the natural polymer. Besides solvents like CS₂/NaOH and NMMNO•H₂O unconventional solvent systems can be applied for dissolution of cellulose. This group of solvents includes inorganic molten salts and ionic liquids. Inorganic molten salts can be used as efficient solvents for cellulose in a wide range of degree of polymerization. Furthermore molten salts can be applied as reaction medium for the derivatization of cellulose.

For both dissolution and derivatization of cellulose the knowledge of the solution state as well as information about chemical interactions with the

solvent system is essential. Using the melts of LiClO₄•3H₂O, NaSCN/KSCN/LiSCN•2H₂O and LiCl/ZnCl₂/H₂O as cellulose solvents factors which determine the dissolving ability will be discussed. Besides the specific structure of the molten salt hydrate, the cation and the water content of the melt are the most important factors for the dissolving capability of a molten salt hydrate system.

The application of inorganic molten salts as a medium for cellulose functionalization is demonstrated for cellulose carboxymethylation and acetylation.

Keywords: *cellulose dissolution, molten inorganic salts, derivatization*

Introduction

The search for new cellulose solvents is still a focus of research. Alternative systems are of special interest for cellulose fiber production and functionalization. Concentrated salt solutions have been known for long time as solvents for cellulose. Intensive investigations have been carried out on swelling and dissolution of cellulose in aqueous zinc chloride.

A review about the swelling ability of inorganic salt solutions was published by Warwicker et al. [1]. He stated that a lot of salt systems should be able to swell or dissolve cellulose. But in later publications only three water/salt-systems were described as effective cellulose solvents in

more detail: Ca(SCN)₂/H₂O, LiSCN/H₂O und ZnCl₂/H₂O.

Lukanoff et al. [2] investigated the dissolving ability of the eutectic melt NaSCN/KSCN and of mixtures of this melt with Ca(SCN)₂•3H₂O. Only the mixture of NaSCN/KSCN with Ca(SCN)₂•3H₂O or dimethyl sulfoxide was able to dissolve cellulose. In addition the authors described molten LiSCN•2.5H₂O as cellulose solvent.

The solubility of cellulose with different degrees of polymerization (DP) in Ca(SCN)₂•3H₂O was discussed by Kuga [3]. In the temperature range from 120 °C to 140 °C he observed the solution of the polymer within 40 minutes accompanied by a decrease of DP.

There are several papers discussing the formation of addition compounds between cellulose and the dissolving salts. Xu and Chen [4] worked on the dissolution and fiber formation of cellulose in zinc chloride solutions. The regeneration occurred by precipitation of a zinc-cellulose-complex by alcohol. By treatment with water this complex released cellulose II. The formation of the proposed complex was explained using ^{13}C NMR measurements on cellobiose solutions in zinc chloride.

Systematic investigations regarding the solubility of cellulose in $\text{Ca}(\text{SCN})_2 \cdot 3\text{H}_2\text{O}$ solutions were carried out by Hattori et al. [5]. They discussed complex formation between cellulose and $\text{Ca}(\text{SCN})_2$ using IR measurements and reported coordination of the Ca^{2+} ions at O(6) and O(5) of the

cellulose. These results were also confirmed by ^{13}C and ^1H NMR measurements [6]

Solubility of cellulose in molten salt hydrates

A multitude of pure molten salt hydrates as well as salt mixtures were investigated with respect to their interaction with cellulose. As a result it turned out to be reasonable to divide the salt hydrates into groups according to their optical visible effect on cellulose. The classification was done as follows: molten salts which a) dissolve, b) swell, c) decompose cellulose, or which d) have no effect on cellulose. Table 1 gives this classification for the molten salt hydrates investigated.

Table 1. Molten salt hydrates and their interaction to cellulose

group	pure melt	melt mixtures
dissolution	$\text{ZnCl}_2 \cdot 3 \cdot 4\text{H}_2\text{O}$ $\text{LiClO}_4 \cdot 3\text{H}_2\text{O}$ $\text{FeCl}_3 \cdot 6\text{H}_2\text{O}$	$\text{LiClO}_4 \cdot 3\text{H}_2\text{O} - \leq 25\% \text{Mg}(\text{ClO}_4)_2/\text{H}_2\text{O}$ $\text{LiClO}_4 \cdot 3\text{H}_2\text{O} - \leq 10\% \text{NaClO}_4/\text{H}_2\text{O}$ $\text{LiClO}_4 \cdot 3\text{H}_2\text{O} - \text{MgCl}_2 \cdot 6\text{H}_2\text{O}$ NaSCN/KSCN (eutectic) – $\text{LiSCN} \cdot 2\text{H}_2\text{O}$ $\text{LiCl}/2\text{ZnCl}_2/\text{H}_2\text{O}$
swelling	$\text{LiCl} \cdot 2 \cdot 5\text{H}_2\text{O}$ $\text{LiNO}_3 \cdot 3\text{H}_2\text{O}$ $\text{Na}_2\text{S} \cdot 9\text{H}_2\text{O}$	$\text{LiClO}_4 \cdot 3\text{H}_2\text{O} - > 25\% \text{Mg}(\text{ClO}_4)_2/\text{H}_2\text{O}$ $\text{LiClO}_4 \cdot 3\text{H}_2\text{O} - > 10\% \text{NaClO}_4/\text{H}_2\text{O}$
decomposition	$\text{Mg}(\text{ClO}_4)_2 \cdot 6\text{H}_2\text{O}$ $\text{MgCl}_2 \cdot 6\text{H}_2\text{O}$	$\text{ZnCl}_2/\text{MgCl}_2/\text{H}_2\text{O}$
no effect	$\text{NaOOCCH}_3 \cdot 3\text{H}_2\text{O}$	$\text{CaCl}_2 \cdot 6\text{H}_2\text{O}$

Designation of salt-water-systems:

- e.g. $\text{LiClO}_4 \cdot 3\text{H}_2\text{O}$: the hydrate is solid at room temperature marked by the symbol “•”
- e.g. $\text{ZnCl}_2 \cdot 4\text{H}_2\text{O}$: the hydrate is liquid at room temperature marked by the symbol “+”
- e.g. $\text{ZnCl}_2/\text{MgCl}_2/\text{H}_2\text{O}$: systems of variable compositions marked by the symbol “/”

The melts which were able to dissolve cellulose are very different in composition. They vary in cation and anion and in their water content. This results in the question, which factors determine the dissolving ability of the molten salt hydrates. Until now only one rule for salt-water-systems was published. It says that salts combining small hard cations with soft polarizable anions have the best dissolving power for cellulose. But the good dissolving ability of lithium perchlorate melts observed by us is inconsistent with this statement, and

several other hydrated melts containing lithium with different anions do not show any dissolving ability to cellulose [7].

After a detailed investigation of the melts the following characteristics that mainly determine the dissolution power towards cellulose were recognized:

- the acidity ,
- the water content of the melts,
- and the properties of the coordination sphere of the cations. [8,9], respectively.

Often these properties influence each other as could be shown by acidity measurements in the system $\text{ZnCl}_2/x\text{H}_2\text{O}$ depending on the amount of water x [10]. A change in the water amount correlates with the acidity, which increases with decreasing x . The acidity parameters of the melting systems $\text{ZnCl}_2/\text{H}_2\text{O}$ and $\text{LiClO}_4/\text{H}_2\text{O}$ were investigated using solvatochromic probe molecules. They are comparable to those described for mineral acids. If a hydrated melt should be an effective dissolving agent for cellulose it must have a relative high acidity [7].

The dependence of the dissolving power on the water content in different melt systems could be shown for several systems. Molten $\text{LiClO}_4 \cdot 3\text{H}_2\text{O}$ for instance is an excellent cellulose solvent. An increase of the water amount up to a composition of $\text{LiClO}_4 \cdot 4\text{H}_2\text{O}$ results in a melt which is not able to dissolve the polymer. A significant increase of the swelling grade can be observed by decreasing the water amount of the system $\text{LiCl} + x\text{H}_2\text{O}$ from $x=5$ to $x=2$. The swelling

of cellulose in $\text{LiCl} + 2\text{H}_2\text{O}$ is strong enough to cause a transformation of the cellulose modification I into modification II.

The influence of the structural conditions of the co-ordination sphere of the cations could be explained in Figure 1 by a comparison of the two trihydrates $\text{LiClO}_4 \cdot 3\text{H}_2\text{O}$ (solvent) and $\text{LiNO}_3 \cdot 3\text{H}_2\text{O}$ (no solvent) [7]. Although the salts have the same water content, there are differences in their structures. In the case of the perchlorate the water is completely bridged and bound to the cations. The anions do not affect the co-ordination sphere of the lithium ions. The cleavage of the water bridges results in "free" co-ordination sites. The replacement of water molecules by hydroxyl groups of the cellulose is possible, too.

The structure of the nitrate is characterized by water molecules not only bridged between the cations but also at interstitial positions. Because of the bound anions at the cations there is a water deficit at the lithium cations.

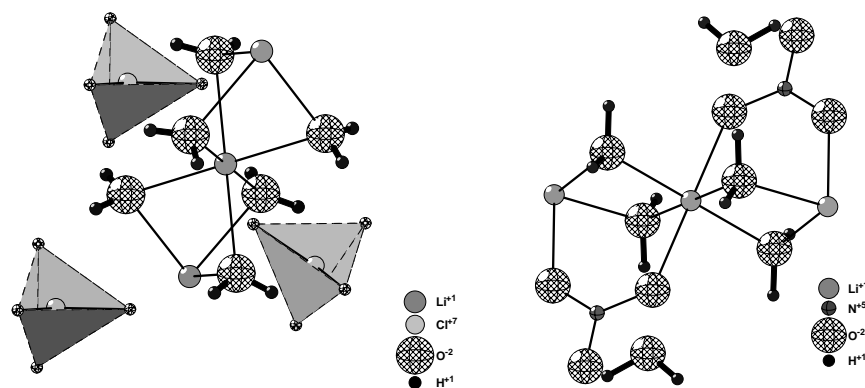


Figure 1. Crystal structure of $\text{LiClO}_4 \cdot 3\text{H}_2\text{O}$ (left) and $\text{LiNO}_3 \cdot 3\text{H}_2\text{O}$ (right)

The nitrate ions can not be replaced by hydroxyl groups because the water from the interstitial positions will prefer to saturate the co-ordination sphere of the cations.

The different interactions between cellulose and the solvent are reflected in the properties of cellulose samples

regenerated from the molten salts. The regenerated products were characterized by WAXS, ^{13}C CP/MAS NMR spectroscopy, surface-area determinations, SEC measurements, solvatochromic, and SEM investigations in comparison with the raw material.

Using WAXS the transformation of cellulose I into cellulose II could be observed which indicates a strong swelling or dissolution of the polymer. The crystallinity was investigated using solid state NMR spectroscopy [7,8]. Raman spectroscopy has been established too as an effective method to discuss the transformation of cellulose regenerated from molten inorganic salts [11]

The molar mass distributions determined according a method of Fischer et al. [12] of cellulose regenerated from different molten hydrates are compared with the raw cellulose in Figure 2.

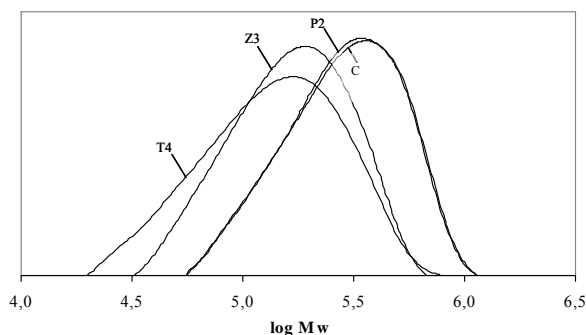


Figure 2. Molar mass distribution of the nitrates of the cellulose samples regenerated from P2: $\text{LiClO}_4 \cdot 3\text{H}_2\text{O}$, Z3: $\text{ZnCl}_2 + 4\text{H}_2\text{O}$, T4: $\text{NaSCN/KSCN/LiSCN/H}_2\text{O}$, C: raw cellulose

It is to be seen that the cellulose regenerated from $\text{LiClO}_4 \cdot 3\text{H}_2\text{O}$ exhibits no decrease in the molar mass compared with the raw cellulose, the other samples show a slight shortening of the chain length. The decrease of the molar mass observed here was in the range known for the pre-treatment of cellulose with NaOH-water. Therefore it could be proved that dissolving of cellulose in molten salt hydrates does not lead to a drastically reduction of the chain length.

Dissolution of cellulose in different melts results in varying morphological properties of the regenerated products. This is indicated by differences in the specific surface-area and the pore size and is clearly recognizable in the SEM structures. Fiber-like samples similar to the raw cellulose were obtained from the thiocyanate melts, but also lamellar samples (from $\text{LiClO}_4 \cdot 3\text{H}_2\text{O}$) and layered structures (from chlorides) were regenerated [9]. Examples for the different morphologies obtained are given in Figure 3.

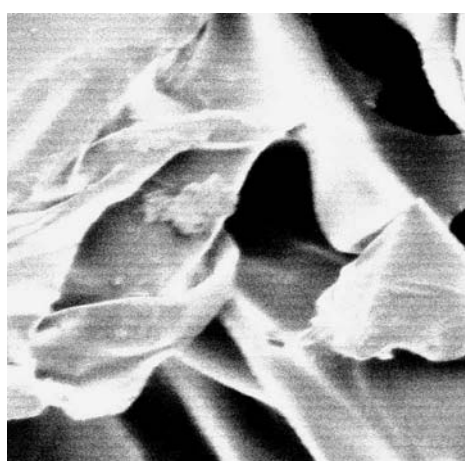
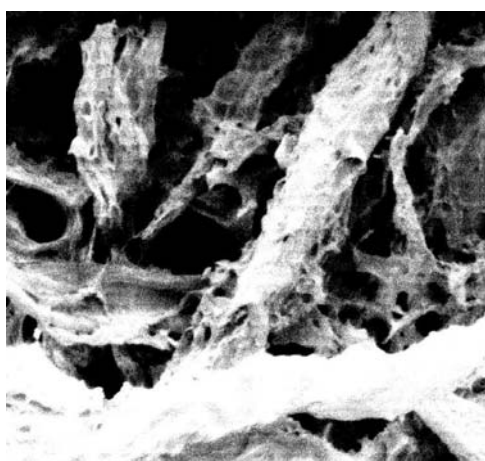


Figure 3. SEM pictures of celluloses regenerated from $\text{NaSCN/KSCN/LiSCN/H}_2\text{O}$ (left) and $\text{LiClO}_4 \cdot 3\text{H}_2\text{O}$ (right)

Interactions between cellulose and the molten salt hydrate

As a very sensitive tool to characterize the state of cellulose in molten salt hydrates

NMR spectroscopy can be used. Figure 4 shows the ^{13}C NMR spectra of cellulose dissolved in molten $\text{ZnCl}_2 + 4\text{H}_2\text{O}$, $\text{LiClO}_4 \cdot 3\text{H}_2\text{O}$, and $\text{LiSCN} \cdot 2.5\text{H}_2\text{O}$. The

signals of the carbon atoms $C_1 - C_6$ are well resolved and the spectrum is very similar to that of cellulose dissolved in conventional solvents like sodium hydroxide solution [13]. A derivatization by the solvent was not observed. Therefore molten salt hydrates can be attributed to the group of non-derivatizing solvent systems.

Due to the different magnetic susceptibilities and melting points of the molten salt hydrates it is difficult to compare the chemical shifts of the carbon nuclei in the different solvents.

Nevertheless it can be pointed out that the relative positions of the carbon signals differ for the investigated solvents. Whereas the chemical shifts of the cellulose carbon nuclei are nearly identical in the molten lithium salts the values for especially C_1 to C_5 are significantly smaller in the $ZnCl_2+4H_2O$ melt. We interpret this as an indication for cellulose – solvent interactions of different strength.

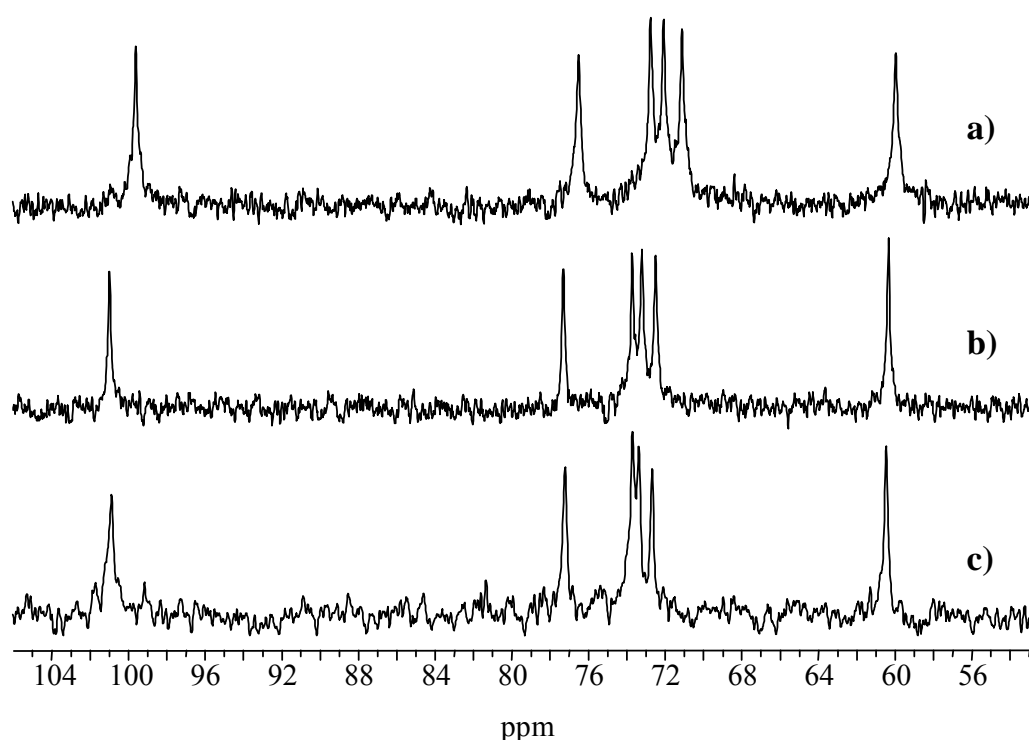


Figure 4. ^{13}C NMR spectra of cellulose dissolved in molten
a) $ZnCl_2+4H_2O$ at 65 °C, b) $LiClO_4\cdot 3H_2O$ at 110 °C, c) $LiSCN\cdot 2H_2O$ at 130

Further information about the interaction between cellulose and molten inorganic salts can be acquired by 7Li NMR investigations [14] and Raman measurements [15].

Derivatization in molten inorganic salt hydrates

Molten inorganic salt hydrates as so-called non-derivatizing solvents were not only established as very efficient solvents for

cellulose, they can also be applied as a medium for the chemical functionalization of the polymer. Using molten inorganic salt hydrates as new reaction media etherification (e.g. carboxymethylation) and esterification (e.g. acetylation) of cellulose are possible and will be discussed here.

a) Carboxymethylation

Because of the fact that the solvent $\text{LiClO}_4 \cdot 3\text{H}_2\text{O}$ was extensively studied [9] preliminary experiments concerning its use as reaction medium were carried out [16]. The results were very promising and therefore systematic studies regarding carboxymethylation of cellulose in different inorganic molten salts were started. The method and the preparation procedure were described in [17].

The homogeneous carboxymethylation of cellulose in molten $\text{LiClO}_4 \cdot 3\text{H}_2\text{O}$ is possible using sodium monochloroacetate in the presence of NaOH.

A remarkable finding is that polymers with DS values as high as 2 can be prepared within a short reaction time (4 hours) applying a one-step synthesis. Up to now this was only possible by conversion of cellulose in DMA/LiCl or using the so-called induced phase separation [18] which starts from organo-soluble hydrolytically unstable intermediates. In the case of homogeneous carboxymethylation or reaction in slurry the highest DS reachable in a one step procedure is about 1.3.

Selected samples were characterized by means of $^1\text{H-NMR}$ spectroscopy after chain degradation with a mixture of $\text{D}_2\text{SO}_4/\text{D}_2\text{O}$ [19, 20]. A distribution of substituents on the level of the AGU in the order $\text{C-6} > \text{C-2} \approx \text{C-3}$ was discovered and the investigations showed that a complete substitution at position *O-6* is possible.

Further investigations showed that carboxymethylation is also possible in the system $\text{LiCl-H}_2\text{O}$ starting from swollen cellulose. The DS of CMC prepared in molten $\text{LiCl} \cdot x\text{H}_2\text{O}$, i.e. in a heterogeneous reaction, is generally lower than the DS of the samples obtained from dissolved cellulose in molten $\text{LiClO}_4 \cdot 3\text{H}_2\text{O}$. The DS also depends on the molar ratio AGU : sodium monochloroacetate : NaOH and the DS decreases with increasing water content of the molten salt hydrate.

The samples have a similar distribution of carboxymethyl groups like CMCs prepared under homogeneous conditions. The results show a distribution of substituents on the level of the AGU in the order $\text{C-6} > \text{C-3} \approx \text{C-2}$. That means, there is also a difference between carboxymethylation in this swelling medium and conventionally produced CMCs.

Comprehensively it can be said that an etherification like carboxymethylation of cellulose in hydrated melts yields products of a high degree of substitution of up to 1.96 in an one step synthesis within a short reaction time. Consequently, molten $\text{LiClO}_4 \cdot 3\text{H}_2\text{O}$ is an efficient solvent for carboxymethylation of cellulose yielding highly functionalized polymers. Moreover, a specific influence on the distribution of functional groups on the level of the AGU is accessible.

b) Acetylation

Several molten inorganic salt hydrates were applied as media for the acetylation of cellulose. The formation of cellulose acetate depends on the used molten salt hydrate itself as well as on the water content of the melt.

However, the only melt in which the acetylation was successful is the eutectic mixture of NaSCN and KSCN with addition of 10% $\text{LiSCN} \cdot 2\text{H}_2\text{O}$. The most important condition for the success of the reaction was the minimization of the water content of the melt. The acetylation was carried out at a temperature of 130°C with a high excess of acetic anhydride (50-100%). During a short reaction time (0.5 – 3h) cellulose acetate with a DS in a range between 1 and 2.5 was obtained. The samples were characterized by IR-spectroscopy. For a detailed characterization X-ray and NMR-measurements were carried out. By these investigations it could be shown that the acetylation in molten thiocyanate leads to the formation of amorphous cellulose acetate [21]. The DS obtained for the

cellulose acetates depends on the reaction time and on the molar ratio between AGU and acetanhydride.

For future work we will extend the use of molten salt hydrates to other applications. So it is possible to use the acidic properties of the molten inorganic hydrates for the cleavage of functional groups. For instance cellulose triacetate deacetylation can be carried out in molten $\text{ZnCl}_2+4\text{H}_2\text{O}$. After a reaction time of 21h a DS of 1.81 and PDS (C6) of 0.53 were obtained [10]. Furthermore molten $\text{ZnCl}_2+4\text{H}_2\text{O}$ or $\text{LiClO}_4\cdot 3\text{H}_2\text{O}$ can be applied as medium for deprotection of triphenylmethyl cellulose. A complete deprotection occurred in the comparatively short reaction time of 3 to 5 hours [22].

Conclusion

Molten salt hydrates are effective and efficient media for cellulose dissolution. During the investigations regarding the solubility of cellulose in molten salts new solvents were found ($\text{LiClO}_4\cdot 3\text{H}_2\text{O}$). First time factors which determining dissolution ability of cellulose in molten inorganic salt hydrates were found. This knowledge is a basis for discovering further molten hydrates as solvents for cellulose.

The structural change of cellulose after dissolution depends on the respective hydrated molten salt. Therefore it should be possible to adjust specific cellulose structures by choosing a certain salt melt for cellulose dissolution and regeneration. For cellulose carboxymethylation and acetylation it was shown exemplary, that molten salt hydrates are efficient solvents for cellulose derivatization yielding highly functionalized polymers.

The results are a basis for further investigations using molten inorganic salts as a reaction medium for cellulose, which will be extended to other polysaccharides.

References

- [1] Warwicker J. O., Jeffries R., Colbran I. and Robinson R. N. 1966. Shirley Institute Pamphlet. No. 93, Manchester
- [2] B. Lukanoff, H. Schleicher, B. Philipp, 1983 Cell. Chem. Technol. 17, 593-599.
- [3] S. Kuga, 1980 J. of Colloid und Interface Sci. 77, 413-418.
- [4] Q Xu. , L. F. Chen, 1996 Textile Techn. International 40, 19-21
- [5] M. Hattori, Y. Shimaya, M. Saito 1998. Polymer Journal 30, 43-48
- [6] M. Hattori, Y. Shimaya, M. Saito 1998. Polymer Journal 30, 49-55
- [7] S. Fischer , W. Voigt, K. Fischer K. 1999 Cellulose 6, 213-219
- [8] S. Fischer, H. Leipner, E. Brendler, W. Voigt, K. Fischer 1999 ACS Symposium Series 737, 143-150.
- [9] H. Leipner, S. Fischer, E. Brendler, W. Voigt 2000. Macromol. Chem. Phys. 201, 2041-2049.
- [10] H. Leipner, 2002. Dissertation A, Freiberg
- [11] K. Schenzel, Fischer S. 2001. Cellulose 8, 49-57
- [12] K. Fischer, I. Schmidt, H. Hintze, 1994 Papier 48, 769-774
- [13] I. Nehls, W. Wagenknecht, B. Philipp, D. Stscherbina, 1994 Prog. Polym. Sci. 78, 1929-1979
- [14] E. Brendler, S. Fischer, H. Leipner, 2002. Cellulose 8, 283-288
- [15] S. Fischer, H. Leipner, K. Thümmel, E. Brendler, J. Peters, 2003, Cellulose 10, 227-236
- [16] T. Heinze, T. Liebert, P. Klüfers, F. Meister 1999, Cellulose 6, 153-165
- [17] S. Fischer, K. Thümmel, K. Pfeiffer, T. Liebert, T. Heinze, 2002 Cellulose 9, 293-300
- [18] T. Liebert, T. Heinze, 1998. ACS Symposium Series 688, 61-72.
- [19] W. Gronski, G. Hellmann 1987. Papier 41, 668-672.
- [20] A. Baar, W-M. Kulicke, K. Szablikowski, R. Kiesewetter, 1994.

Macromol. Chem. Phys. 195, 1483-1492

- [21] S. Fischer, 2004. Habilitationsschrift, TU Bergakademie Freiberg
- [22] S. Fischer, H. Leipner, T. Liebert, T. Heinze, 2001. Polymer Bulletin 45, 517-521

THERMAL TREATMENT OF CELLULOSE PULPS AND ITS INFLUENCE TO CELLULOSE REACTIVITY

Thomas Röder and Herbert Sixta

Department Zellstoff-Forschung, Lenzing AG, Werksstrasse 1, A-4860 Lenzing, Austria
Phone: (+43) 07672-701-3082; Fax: (+43) 07672-918-3082; E-mail: t.roeder@lenzing.com

The loss of paper strength made from dried pulp as compared to never dried pulp is well known. Due to modified surface properties the fibre-fibre bonds of the dried pulps are weaker than for the never dried pulps. During the drying process of pulps the cellulose fibrils can aggregate by hydrogen bonds and build fixed domains, which cannot be accessed easily by water.

Analytical methods, such as small angle X-ray scattering (SAXS), IR spectroscopy, inverse size exclusion

chromatography (ISEC), and water retention volume (WRV), were applied to compare the behavior of pulps during drying. It was shown that in a beech magnesium bisulfite pulp the amount of carbonyl groups increased while the carboxyl group content slightly decreased. Two overlapping effects were observed: hornification and thermal degradation.

Keywords: *pulp, hornification, cellulose, SAXS*

Introduction

Chemical and physical properties of cellulose are determined by its strong hydrogen bond system. The first drying of cellulose after wood pulping leads to a tight cohesion of fibrillar elements, the so-called hornification [1], [2]. Pore size and pore volume decrease and will not be restored completely. This effect can be prevented by freeze drying, solvent exchange [3], or derivatization [4] of wet pulp. The partial pore collapse can easily be proved by measurements of the water retention volume (WRV) [5].

Pore size and pore volume can be determined by inverse size exclusion chromatography (ISEC) [6] as well as by mercury porosimetry and small angle X-ray scattering (SAXS). The values obtained according to these different methods differ considerably. This is due to the detectable range of pore size. In contrast to SAXS and mercury porosimetry, ISEC data are evaluated in a fluid medium. SAXS data including the range between 2 and 80 nm,

mercury porosimetry between 15 and 1000 nm (Klemm et al., [3]), and ISEC data between 2 and 100 nm.

The mechanism of pore collapse is discussed controversially in the literature. One of the theories [7] explains the cohesion of micro fibrils by building up hydrogen bonds resulting in a saturation of hydroxyl groups and in an irreversible closure of pores. Micro fibrils in the plant cell wall are separated by amorphous substances (e.g. lignin, hemicellulose). During pulping these substances will be dissolved. The free hydroxyl groups will be bounded by water molecules. Removal of water leads to the formation of hydrogen bonds between nearby lying hydroxyl groups. The model of Newman and Hemmingson [8] describes a co-crystallization in microcrystalline areas as the main reason for hornification.

Back [9] postulated an internal cross-linking of micro fibrils by covalent C-C bonds due to radicals generated by degradation during

drying. In contrast, Carlsson et al. [10] observed hornification already during dry pressing without changes of temperature. De Ruvo and Htun [11] pointed out the thermal degradation of cellulose, but found no indication of cross-linking.

The content of carboxyl groups influence the accessibility of cellulose [12]. Ionized carboxyl groups with Na^+ as counter-ion form only weak hydrogen bonds. Pulps with higher content of sodium carboxylates show higher degrees of swelling [13].

The hornification tendency is also dependent on the lignin content of the pulps. Lignin acts as a spacer between the fibrils. The loss of lignin results in irreversible formation of hydrogen bonds [14].

Methods and Materials

SAXS measurements were performed with the SAXSess small-angle X-ray scattering instrument from Anton Paar GmbH and a PW3830 laboratory X-ray generator (40 kV, 50mA) with a long-fine focus sealed-glass X-ray tube (CuK_α wavelength of $\lambda = 0.1542$ nm) from PANalytical. Detection was performed with the 2D imaging-plate reader Cyclone® by Packard BioScience.

ISEC measurements were done according to Brederick and Blüher [15] with water (0.05% NaN_3) as the eluant, 150x4 mm columns and RI detection.

WRV was determined according DIN 53 814, Cuen viscosity according to SCAN CM 15:88, copper number according to Tappi 430 om – 94, COOH determination according to Philipp et al. [16], and brightness according to ISO 2470: 1999. The new CCOA method for the investigation of carbonyl groups was used as described by Röhrling et al. [17]. Molecular weight distribution was determined by SEC (size exclusion chromatography) with MALLS (multi angle laser light scattering) detection in LiCl/DMAc solution [18].

Pulp behavior during acetylation [19] was determined by an internal method based on manufacturing 2.5 acetate. Viscose

preparation and characterisation was performed according to a modified method of Treiber et al. [20] and has been tested by means of filterability.

Never-dried beech magnesium bisulfite pulp was used for this study. The wet pulp was dried 12 h at room temperature (25°C), 105°C, 130°C, and 160°C. In addition one portion was freeze-dried under vacuum.

Results and Discussion

SEC was used to compare the effect of the drying procedure on the molecular weight distribution. The results shown in Figure 1 indicate an overlap of the possible hornification effect by a thermally induced degradation of pulp. The cuen viscosity, and consequently also the cuen DP, decreased (Table 1).

Sample	Cuen viscosity [mL/g]
Air-dried	581
105 °C	546
130 °C	489
160 °C	350

Table 1. Cuen viscosity of dried samples.

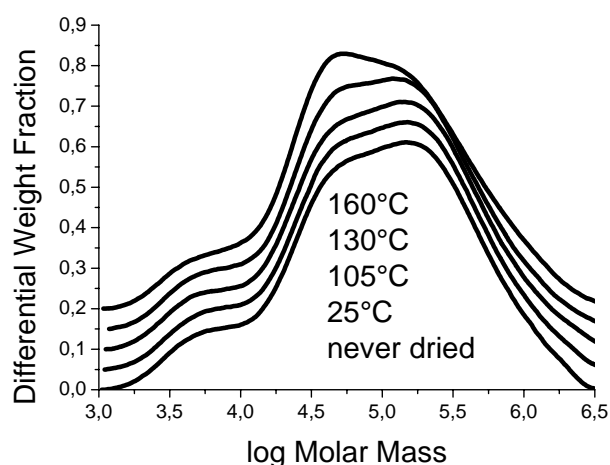


Figure 1. Molecular weight distribution of beech magnesium bisulfite pulp after different drying procedures.

The maximum of the molecular weight distribution is shifted to lower values, while a slight increase of high molecular weights

was observed. This result seemed to be the consequence of a slightly decreased quality of the solution state caused by thermal degradation.

The content of carboxyl groups decreased while the content of carbonyl groups increased especially for the pulp dried at temperatures above 100°C (Table 2).

This can be attributed to the cracking of cellulose chains by thermal degradation. The amount of reducing end groups increased and functional side groups were generated. The same trend was observed with brightness values, which decreased from 91%ISO for the wet pulp to 79%ISO for the sample dried at 160°C. This pulp showed already a yellowing effect being visible to the naked eye.

Sample	COOH [$\mu\text{mol/g}$]	C=O [$\mu\text{mol/g}$]
Never-dried	-	24.5
Air-dried	30.9	25.6
105 °C	30.5	27.5
130 °C	28.2	29.7
160 °C	27.6	37.3

Table 2. Content of functional groups.

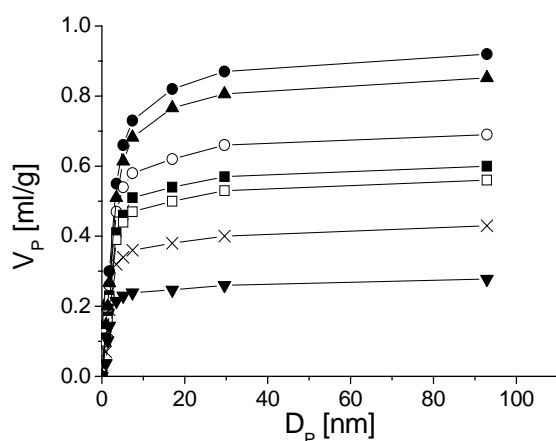


Figure 2. Pore volume versus pore diameter, beech magnesium bisulfite pulp. —●— never dried pulp; —▲— freeze dried pulp; —○— air dried pulp; —■— pulp dried at 105 °C; —□— p. dried at 130°C; —X— pulp dried at 160°C; —▼— pulp dried at 160°C (2nd time after re-wetting).

ISEC is a powerful tool to gain information about the pore structure of pulps and fibers. The effect of pore collapse along with the decrease of pore volume is clearly shown in Figure 2.

As expected, freeze-drying lead to the lowest reduction of pore size and pore volume. The formation of hydrogen bonds, which are stable during drying, seemed to be partly inhibited.

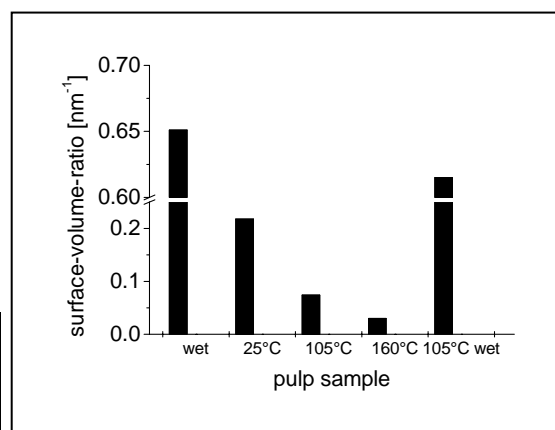


Figure 3. Surface to volume ratio of different cellulose samples (wet, air-dried, dried at 105°C, dried at 160°C).

From the small-angle X-ray data the surface-volume ratio [21] was determined, which is a characteristic property of each investigated sample. Some parameters of the sample can be directly calculated from the scattering curve. The second momentum Q of the scattering function is independent of structural details and is only influenced by the average square of the electron density fluctuation. According to Porod [22] it is therefore called the invariant of the system. The intensity at zero angle increases upon formation of aggregates, simultaneously the scattering curve decreases more quickly at higher angles, which causes the second momentum to be constant.

Thus the surface-volume ratio depends on three parameters:

- (1) Guinier extrapolation
- (2) Measured scattering curve
- (3) Porod extrapolation.

The impact of the measured scattering curve is predominant, so that the error made by

the extrapolations does not have a pronounced influence on the result.

The tendency of the surface to volume ratios showed a decrease of the accessibility of the cellulose surface with increasing drying temperature. Large differences between wet sample and air-dried were mainly attributed to different water content. Due to storage under the same conditions the amount of water in the dried samples was on the same level.

The cellulose dried at 105°C and moistened afterwards did not reach the same value of surface to volume ratio than the original wet one. This is a strong indication of the irreversible closure of pores during drying. Due to this effect the reactivity of cellulose decreased, too.

Pulp properties in acidic and alkaline media were determined by acetylation and viscose processability (Table 3).

Sample	wet	Air-dried	105°C	160°C (2 nd time re-wetted)
Acetylation yellowness	n.v.	0.589	0.593	0.888
Acetylation turbidity	n.v.	296	367	1030
Viscose filter value	327	317	315	108
Viscose ball fall [s]	56	58	44	11

Table 3. Acetylation and viscose processability.

The suitability of the pulps for viscose application has been tested by the determination of the filterability according to the method of Treiber. Ratios of more than 300 report a good performance. The influence of thermally induced degradation is also reflected by the ball fall values. Already for the sample dried at 105°C the viscosity and thus the degree of polymerisation of the dissolved xanthogenate was visibly decreased. Concerning the higher degradation, the ball fall value of 11 s for the sample dried at 160 °C was far outside the normal range. The high acetylation yellowness and the high turbidity in combination with the observed

non-dissolved pieces of pulp and gel particles showed a negative influence of the thermal degradation.

Conclusion

Depending on drying conditions two overlapping phenomena were observed: Hornification and thermal degradation. The so-called hornification is known as the irreversible closure of cellulose pores during drying. The temperature-dependent thermal degradation was determined by SEC. As expected, hornification outbalanced at room temperature, whereas drying causes a decrease of pore size and pore volume. Only freeze-drying can prevent the pore collapse. SAXS and ISEC results were in good accordance. Both of these methods are useful to investigate changes in pore size. The reactivity of pulp, both in acid and in alkaline media, was decreased caused by hornification and thermal degradation.

Acknowledgements

The authors thank Ursula Mais (Lenzing, Austria) as well as Thomas Rosenau (Vienna, Austria) for helpful discussion and Alexander Bergmann (Graz, Austria) for the support during SAXS measurements. We thank the laboratory technicians of pulp lab in Lenzing for their good work.

References

- [1] C. G. Schwalbe, Einige Betrachtungen über Holzzellstoffkochung, insbesondere die Sulfitzellstoff-kochung. *Zellstoff Papier* 1, 11-15 (1921).
- [2] E. Gruber, Ch. Schneider, J. Weigert. Möglichkeiten der Beurteilung des Verhornungszustandes. *PTS-Symposiumsband: Papierfaserstoff-Technik* 5, 5-1 - 6-16 (1999).
- [3] D. Klemm, B. Philipp, T. Heinze, U. Heinze, and W. Wagenknecht, *Comprehensive Cellulose Chemistry* Vol. 1, Wiley-Verlag Weinheim, 1998.

- [4] E. Gruber, J. Weigert, Chemische Modifizierung von Zellstoffen zur Verminderung ihrer Verhornungsneigung. *Das Papier* 52 (1998), Nr. 10A, V20-V26.
- [5] G. Jayme, Mikro-Quellungs-messungen an Zellstoffen. *Wochenbl. F. Papierf.* 75, 191-218 (1944).
- [6] K. Brederick, A. Blüher, and A. Hoffmann-Frey, Die Bestimmung der Porenstruktur von Cellulosefasern durch ausschlußmessungen. *Das Papier* 44, 648-656 (1990).
- [7] G. Jayme, G. Hunger, Die Faser-zu-Faser-Bindung des Papierblattgefüges im elektronenoptischen Bild. *Das Papier* 11 (7/8), 140-145 (1957).
- [8] R.H. Newman, J.A. Hemmingson, Cellulose cocrystallization in hornification of kraft pulp. In: 9th ISWPC., Montreal 1997, O1-1-O1-4.
- [9] E.L. Back, Thermal Auto-Crosslinking in Cellulose Material. *Pulp Paper Mag. Can.* 68 (4), T165-T171 (1967).
- [10] G. Carlsson, T. Lindström, Hornification of cellulose fibres during wet pressing. *Svensk Papperstidn.* 87 (15), R119-R125 (1984).
- [11] A. De Ruvo, M. Htun, Fundamental and Practical Aspects of Paper-Making with recycled Fibres. In: *Trans. Symp. Cambridge* (Ed.:J. Brander). 1, 195-225 (1981).
- [12] T. Lindström, G. Carlsson, The effect of carboxyl groups and their ionic form during drying on the hornification of cellulose fibres. *Svensk Papperstidn.* 85, R146-R151 (1982).
- [13] A. M. Scallan, J. Grignon, The effect of cations on pulp and paper properties. *Svensk Papperstidn.* 82, R40-47 (1979).
- [14] C. Schneider, Chemische und morphologische Veränderungen von Zellstoffen während der Bleiche und deren Auswirkung auf die technologischen Eigenschaften, PhD thesis, University of Technology Darmstadt, (2000).
- [15] K. Brederick, A. Blüher, Porenstrukturbestimmung von Cellulosefasern durch Ausschlußchromatographie, *Melliand Textilber.* 8 652-662 (1992).
- [16] B. Philipp, W. Rehder, H. Lang, Zur Carboxylgruppenbestimmung in Chemiezellstoffen. *Das Papier* 19, 1-9 (1965).
- [17] J. Röhring, A. Potthast, T. Rosenau, T. Lange, G. Ebner, H. Sixta, P. Kosma, A novel method for the determination of carbonyl groups in cellulose by fluorescence labeling. 1. Method Development, *Biomacromolecules* 3, 959-968 (2002) and J. Röhring, A. Potthast, T. Rosenau, T. Lange, A. Borgards, H. Sixta, P. Kosma, A novel method for the determination of carbonyl groups in cellulose by fluorescence labeling. 2. Validation and applications, *Biomacromolecules* 3, 969-975 (2002).
- [18] N. Schelosky, T. Röder, T. Baldinger. Molecular mass distribution of cellulosic products by size exclusion chromatography in DMAc / LiCl. *Das Papier* 53 (12), 728-738 (1999).
- [19] T.Q. Hu, B.R. James, Towards inhibition of yellowing of mechanical pulps. Part IV: Photostability of hydrogenated lignin model compounds. *J. Pulp Paper Sci.* 26 (5), 173-175 (2000).
- [20] E. Treiber, J. Rehnström, C. Ameen, F. Kolos. Using a laboratory viscose small-scale plant to test chemical conversion pulps. *Paper* 16 (3), 85-94 (1962)
- [21] J. Schurz, A. Janosi, Röntgenkleinwinkel-Studien über das Hohlraumssystem von verschiedenen Celluloseproben, *Holzforschung* 36, 307-310 (1982)
- [22] G. Porod, *Kolloid Z.* 124, 83 (1951)

A NOVEL DIAZO REAGENT FOR FLUORESCENCE LABELING OF CARBOXYL GROUPS IN PULP

Rainer Bohrn,¹ Antje Potthast,¹ Thomas Rosenau,¹ Paul Kosma¹, Herbert Sixta²

¹ University of Natural Resources and Applied Life Sciences - Vienna (BOKU),
Christian-Doppler-Laboratory for Pulp Reactivity, Muthgasse 18, A – 1190 Vienna, Austria

² Lenzing AG, R & D, A - 4860 Lenzing, Austria

The reactivity of different diazoalkane reagents was examined using the coupling reaction with methyl β -D-glucopyranosiduronic acid as a model. 9H-Fluoren-2-yl-diazomethane (FDAM), prepared from its precursor 9H-fluoren-2-carbaldehyde hydrazone by MnO₂ oxidation, was found suitable as a new labeling agent for carboxyl groups in carbohydrate materials. The reaction with methyl β -D-glucopyranosiduronic acid showed FDAM to be highly reactive

and specific for carboxyl groups. The new label will be used in pre-column fluorescence derivatization of pulp with low contents in carboxyl groups to determine these functionalities in dependence on the molecular weight distribution by a modified GPC-system with fluorescence-, MALLS- and RI-detection in DMAc / LiCl.

Keywords: Carboxyl groups, carbonyl groups, fluorescence labeling, GPC

Introduction

The reliable and accurate determination of oxidized groups in cellulosic substrates, such as reducing ends, carbonyls and carboxyls, still represents a challenging aspect of cellulose characterization. These structures are present only in the μ mol/g range, but are crucial factors in determining properties and chemical behavior of the respective cellulosic material. Oxidized groups are introduced by a variety of pulping and bleaching processes or by special treatments, such as alkalization, dissolution, irradiation or extraction of cellulose. Oxidized positions in cellulose are governing strength and performance parameters as well as aging and yellowing characteristics of pulp, paper, textiles, and other cellulosic materials.

With the CCOA method, a reliable and validated technique to analyze the carbonyl content of cellulosic materials relative to their molecular weight was placed at

disposal. The method employed pre-column fluorescence labeling in combination with GPC analysis and MALLS / fluorescence / RI detection in the solvent system DMAc / LiCl. [2, 3, 4, 5]

The determination of carboxyl groups in cellulosic substrates is even more demanding than the detection of carbonyls, especially if an approach similar to the CCOA method (covalent derivatization and GPC analysis in DMAc / LiCl) is envisioned. The unknown lactonization state of the substrates and the generally low amount of carboxyl groups are two major challenges, and so is the lack of suitable reagents. The labels to be used must fulfill several requirements: a quantitative reaction under pre-column derivatization conditions, stability under GPC conditions and optimum sensitivity, but no fluorescence interference with the MALLS setup. In this paper, studies towards a new method to quantify carboxyl

groups in celluloses relative to the molecular weight by pre-column derivatization/GPC analysis will be presented. Several approaches, derivatization reactions and reagents will be discussed in terms of their suitability. Optimization of the reaction conditions by means of carbohydrate model compounds and the preliminary procedure for pulps will be outlined; analysis results for different pulps will be presented as well. Combined with the CCOA method, the new approach is a powerful tool to analyze the oxidation state of cellulosic substrates and to report changes in this oxidation profile as a result of different conditions or treatments.

Experimental

Methyl β -D-glucopyranosiduronic acid was synthesized according to the procedure published in [1].

Labeling reagents. Synthesis and properties of the different labeling reagents will be reported elsewhere. [6]

FDAM labeling of pulps. The preliminary standard procedure for heterogeneous carboxyl-diazo-labeling (CDL) for pulp was accomplished similar to the procedure described for CCOA labeling in [3] with the following alterations: approximately 25 mg air dry pulp was disintegrated in a mixer, washed with sufficient amounts of 0.1 mol/l hydrochloric acid in order to remove cations (Ca^{2+} , Mg^{2+} , Me^{x+}). Subsequently, the pulp sample was

suspended in 3.0 ml of DMAc, and 1.0 ml of 0.125 mol/l FDAM-reagent in DMAc (9H-Fluorene-2-yl-diazomethane) added, and incubated in a water bath under shaking for 7 days at 40 °C. After labeling the pulp was filtered and washed with DMAc to remove excess diazo reagent. Prior to GPC measurement the activated pulp samples were dissolved in 2.0 ml of DMAc/LiCl 9 % (m/V), diluted and filtered through 0.45 μm single-use syringe filters (PTFE-membrane) or centrifuged (10 minutes, 5400 rpm), respectively.

GPC analysis. A modified GPC system as specified in [3] was used.

Results and Discussion

After several unsuccessful attempts to label carboxyl groups in carbohydrate model compounds according to procedures used in peptide chemistry (activation with various coupling reagents) and in fatty acid analytics, respectively, we focused our studies on different diazoalkane reagents.

The first coupling reaction was carried out with 1-(4,5-dimethoxy-2-nitrophenyl)-diazomethane. The active reagent was prepared by the oxidation of 4,5-dimethoxy-2-nitroacetophenone hydrazone with manganese(IV) oxide [7, 8]. The derivatization of methyl β -D-glucopyranosiduronic acid at room temperature produced 1-(4,5-dimethoxy-2-nitrophenyl)ethyl-(methyl β -D-glucopyranosid)uronate in 51 % non-optimized yield (Fig.1).

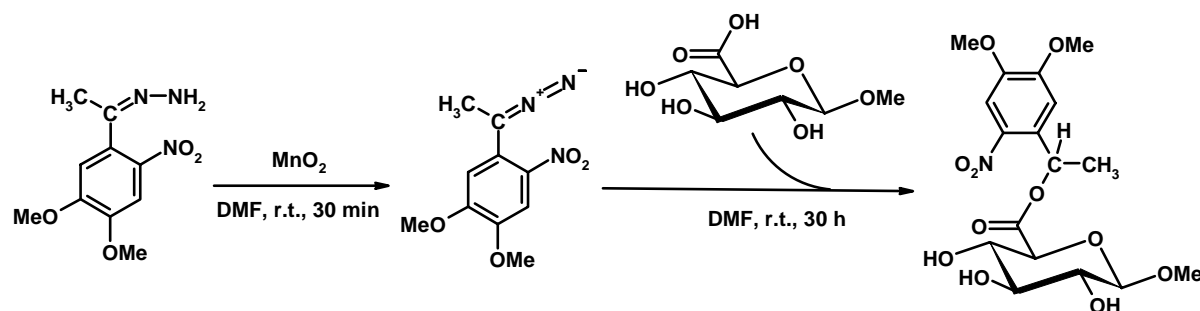


Figure 1. Oxidation of 4,5-dimethoxy-2-nitroacetophenone hydrazone and subsequent coupling with methyl β -D-glucopyranosiduronic acid.

In addition, it was attempted to determine the carboxyl content of pulp with the diazoethane derivate shown in Fig. 1. However, as expected, the low carboxyl group content rendered the UV-signal of the labeled pulp too weak to be monitored by GPC analysis with MALLS / UV / RI detection. Nevertheless, the weak UV signal of the labeled pulp demonstrated that the diazo group was in principle appropriate for labeling carboxyls in pulp. Consequently, appropriate fluorescence labels were studied and the reaction conditions were optimized.

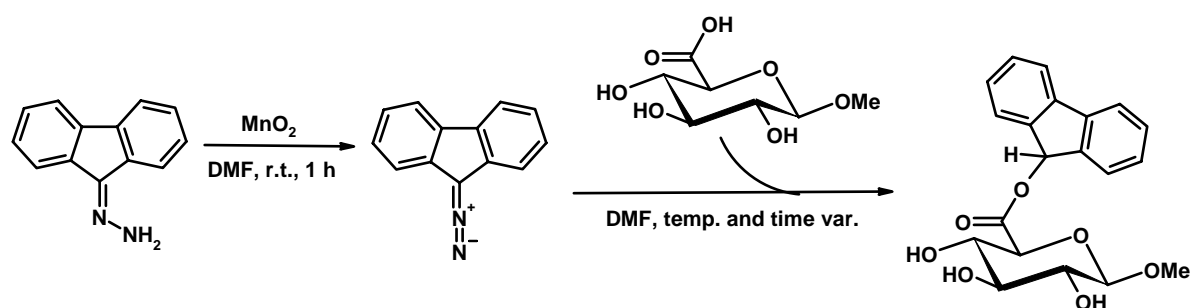


Figure 2. Formation of 9-diazo-fluorene and coupling with methyl β -D-glucopyranosiduronic acid to 9H-fluorene-9-yl-(methyl β -D-glucopyranosid)uronate.

The coupling reaction was also followed by $^1\text{H-NMR}$ (Fig.3). The decrease in the anomeric signal of the educt was accompanied by a simultaneous appearance of H(1), H(5) and H(9) signals of the product, all of these signals in non-crowded regions of the spectrum. The NMR spectrum of the reaction mixture showed that the uronic acid model was nearly completely consumed in a time period of 7.5 h at 90 °C reaction temperature.

Still, the outcome of this coupling reaction seemed unsatisfactory, and the search for an even more reactive diazomethyl reagent was continued. 9H-Fluorene-2-carbaldehyde hydrazone finally turned out

Among several reagents tested, 9-fluorenone hydrazone appeared promising, as it is readily oxidized to 9-diazo-fluorene [9]. The reaction conditions for the coupling with the model compound methyl β -D-glucopyranosiduronic acid were optimized in terms of molar reagent ratio, temperature, and reaction time (Fig.2). The product yield of 9H-fluorene-9-yl-(methyl β -D-glucopyranosid)uronate ranged between 27 % at ambient temperature and 72 % at 90°C. The yield decreased with further increasing temperature and reaction time.

to be the reagent of choice. This reagent is formed by reaction of 9H-fluorene-2-carbaldehyde with hydrazine in 92.8 % yield, along with small amounts of the corresponding aldazine (Fig. 4).

The product hydrazone was oxidized with manganese(IV) oxide to the diazo-reagent 9H-fluorene-2-yl-diazomethane (Fluorenyl-Di-Azo-Methane, FDAM). The coupling reactions with the model methyl β -D-glucopyranosiduronic acid provided the corresponding ester in a non-optimized yield of 67 % on preparative scale (Fig. 5). The coupling reaction was again optimized with regard to temperature, reaction time, and diazo reagent ratio.

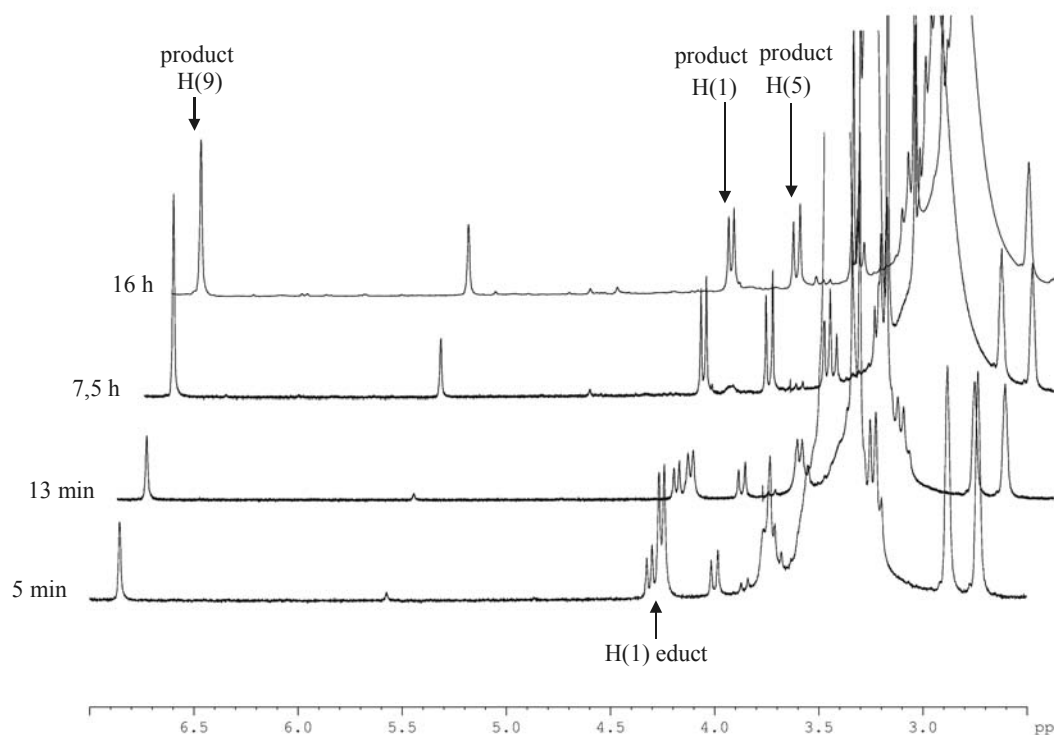


Figure 3. $^1\text{H-NMR}$ (300.13 MHz) of the reaction mixture of coupling methyl β -D-glucopyranosiduronic acid with 9-diazo-fluorene in DMF-d_7 .

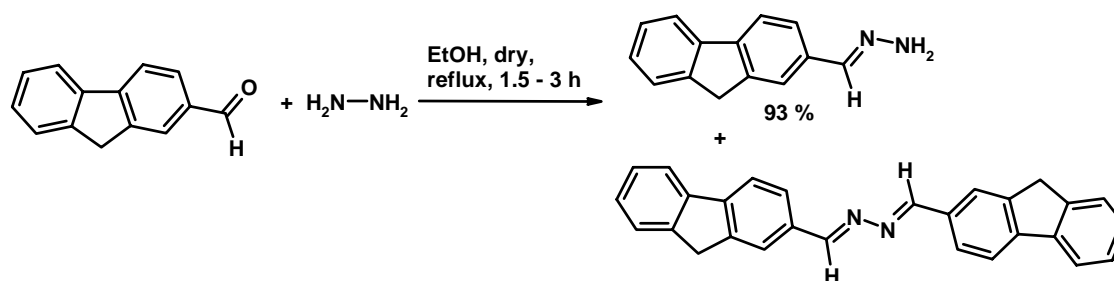


Figure 4. Conversion of 9H-fluorene-2-carbaldehyde with hydrazine to 9H-fluorene-2-carbaldehyde hydrazone and the corresponding dimeric aldazine as byproduct.

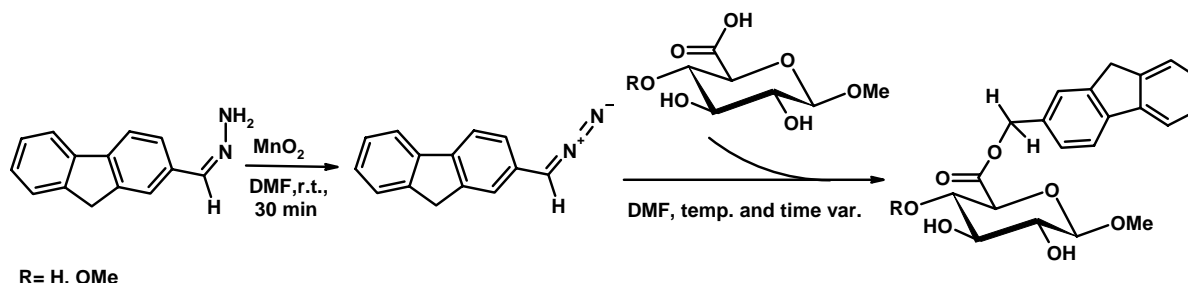


Figure 5. Formation of 9H-fluorene-2-yl diazomethane (FDAM) and coupling with carboxyl models to (9H-fluorene-2-yl)methyl-(methyl β -D-glucopyranosid)-uronate and (9H-fluorene-2-yl)methyl-(methyl 4-O-methyl β -D-glucopyranosid)-uronate.

NMR analysis of the reaction indicated a very fast conversion of the sugar acid. Already after 8 minutes at 50 °C the starting material was almost completely consumed, which was confirmed by the disappearance of the anomeric ^1H NMR signal of educt.

The kinetics of the coupling reaction between FDAM and methyl β -D-glucopyranosiduronic acid were studied by HPLC analysis with fluorescence detection. These studies confirmed the initial results, showing that the conversion was dependent on the reaction temperature, with a high initial rate (80 % yield after 4 h) and complete conversion of the starting material only after 13 days at 40 °C. Subsequent optimization was aimed at achieving quantitative conversion at shorter reaction times. Since the addition of 1 equivalent hydrochloric acid and 3.5 % (v/v) water accelerated the reaction and increased the total yield (Fig. 6), it can be concluded that the addition of the auxiliary completed protonation of the carboxyl group of the uronic acid sugar model, which is a prerequisite for the coupling. This result was taken into consideration for the development of the preliminary heterogeneous pulp labeling procedure.

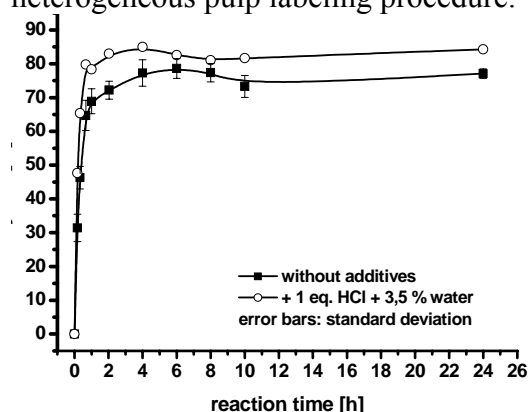


Figure 6. Kinetic studies of the coupling reaction between FDAM and methyl β -D-glucopyranosiduronic acid followed by HPLC analysis and fluorescence detection.

The results of labeling trials of a beech sulfite pulp with FDAM, which were carried out at different conditions regarding temperature, time, diazo reagent ratio, additives, pretreatment of pulp and reaction system (homogeneous or heterogeneous in terms of the state of cellulose solution during labeling) with different solvents, led to the development of a *preliminary* heterogeneous labeling procedure for carboxyl groups in pulp (CDL, Carboxyl-Diazo-Labeling).

This very simple marking procedure includes a pretreatment of pulp by disintegrating and washing with 0.1 mol/l hydrochloric acid in order to ensure the structural accessibility of the protonated acidic functionalities followed by a heterogeneous coupling reaction with FDAM in DMAc. The labeling procedure is stopped by removal of the excess diazo reagent with DMAc. Therefore the labeled pulp can be dissolved in DMAc/LiCl 9 % (m/V) without an additional time-consuming activation procedure. The solution of the FDAM-labeled pulp is diluted with DMAc, and analyzed by GPC [2, 3, 4, 5]. No cellulose degradation was observed upon heterogeneous labeling.

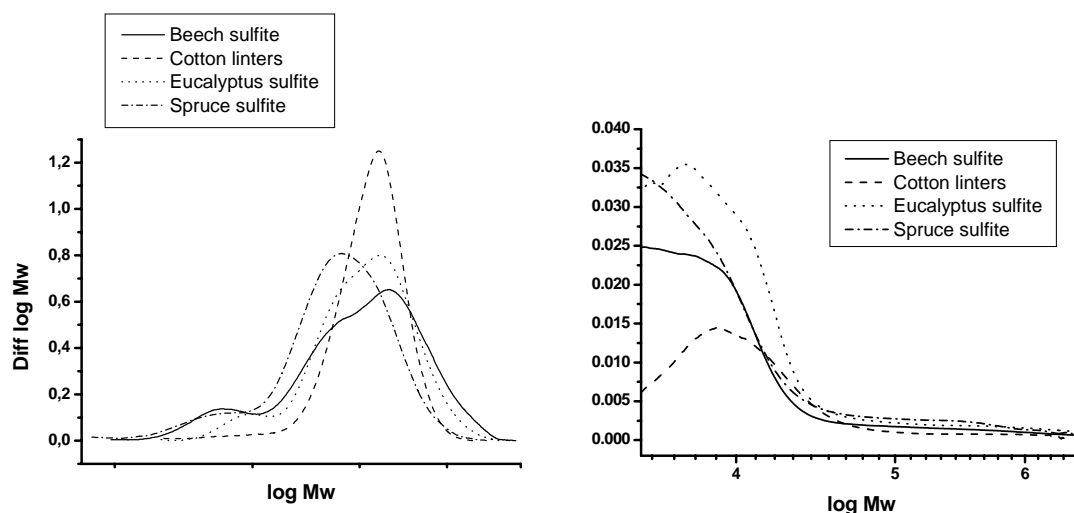


Figure 7. Molecular weight distribution of different FDAM-labeled pulps (left) and comparison of their carboxyl group profiles (right).

Fig. 7 (left) shows molecular weight distribution obtained by the measurement of four different carboxyl group labeled pulps. The comparison of the carboxyl group profiles of these carboxyl-diazo labeled pulps reveals significant differences of the carboxyl group distribution, notably in the low-molecular weight region (Fig. 7, right). The differences between the pulps can be illustrated more clearly in the pie charts as given in Fig. 8, which show the contribution of defined molecular weight regions to the total amount of carboxyl groups.

For cotton linters, more or less free of hemicellulose, the major part of the carboxyl groups can be found in the DP-range between 200 and 2000. For the sulfite pulps, roughly half of the total amount of carboxyls can be found in the low-molecular weight region below DP 100, a finding indicative of labeling the glucuronic acids of hemicellulose side chains in that region. However, also the spruce sulfite pulp, which should contain less hemicelluloses with acid side chains, exhibits a larger portion of the carboxyls in the DP > 100 range. This suggests a higher degree of oxidation for the low molecular

weight compounds through the action of hydrogen sulfite in sulfite pulping.

The high Mw region of celluloses (DP > 2000) is affected only to a rather small extent by oxidative processes generating carboxyl groups, and contains naturally only tiny amounts of hemicellulose fractions with acidic groups surviving the cooking conditions.

The labeling procedure was also tested in homogeneous solution in DMAc/LiCl (6.4 % and 2.5 % LiCl). Initial experiments indicate a slight cellulose degradation occurring during homogeneous labeling, which, however, would render this variant unsuitable. Furthermore, coupling reactions of methyl β -D-glucopyranosiduronic acid with FDAM revealed that lithium cations from the solvent mask the carboxyl groups, which are thus no longer available for coupling with FDAM. Although the homogeneous labeling procedure gives sufficiently strong fluorescence signals, it will not be used as a standard procedure for pulp labeling because of the unknown quantity Li⁺-masked carboxyl groups, the slight cellulose degradation observed, and the rather tedious working procedure.

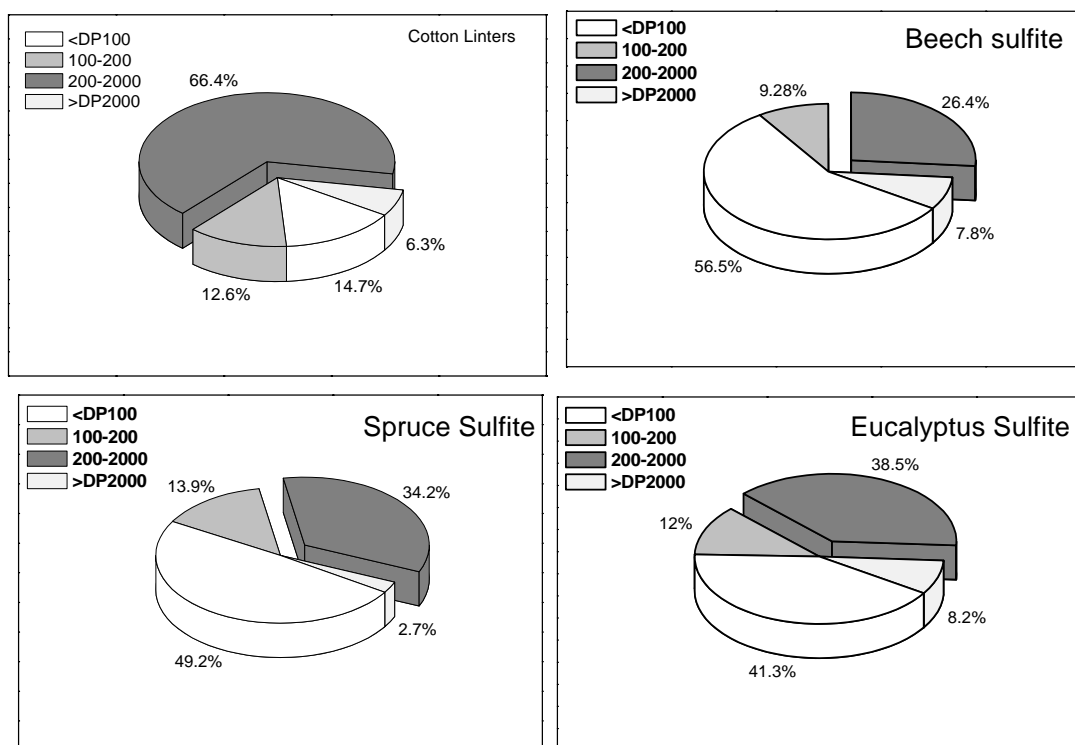


Figure 8. Contribution of defined molecular weight regions to the total amount of carboxyl groups of four different FDAM-labeled pulps.

Beyond the above applications, FDAM was also used for COOH labeling in pulps in combination with subsequent ToF-SIMS analysis (time-of-flight secondary ion mass spectrometry). ToF-SIMS images of FDAM-labeled beech sulfite pulp (approx.

24 $\mu\text{mol/g}$ carboxyl groups) and TEMPO-oxidized beech sulfite pulp (approx. 412 $\mu\text{mol/g}$ carboxyl groups) showed that in both samples the carboxyl groups are evenly distributed, albeit with different intensities (Fig. 9).

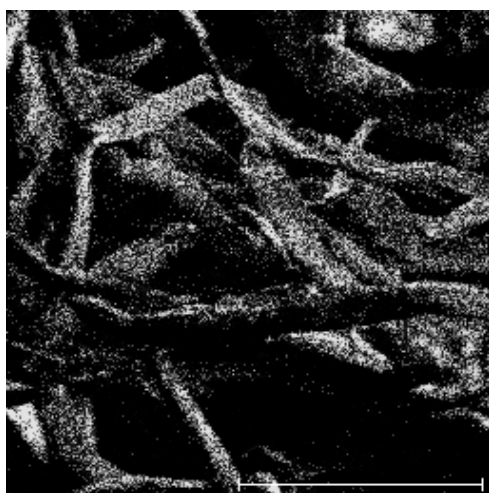


Figure 9. ToF-SIMS image of FDAM labeled beech sulfite pulp (24 $\mu\text{mol/l}$ carboxyl groups) – (left); TEMPO-oxidized beech sulfite pulp (412 $\mu\text{mol/g}$ carboxyl groups) – right. The bright spots are the marker signals [images by courtesy of Dr. P. Fardim, Laboratory of Wood and Paper Chemistry, Abo Akademi, Turku, Finland].

Conclusions

In the present work, diazoalkane derivatives showed their high potential for labeling of carboxyl groups in both carbohydrate model compounds and cellulosic pulps. Novel coupling products of methyl β -D-glucopyranosiduronic acid and different diazo reagents were prepared and comprehensively analytically characterized.

9H-Fluoren-2-yl-diazomethane (FDAM) is a novel, efficient labeling reagent for the determination of carboxylic groups in low-molecular weight carbohydrate models. Preliminary results reveal that FDAM is also a proper label for the quantitative determination of carboxylic groups in cellulosic pulps, which can be displayed as a function of the molecular weight distribution after analysis by a modified GPC system including fluorescence, MALLS and RI detection. It may also offer new possibilities to analyze hemicelluloses, either isolated or attached to the cellulose.

Further investigations into the formation of lactones in carbohydrate models and pulp samples will follow, in order to be able to guarantee complete labeling with FDAM. Subsequently, analytical parameters of the method, such as accuracy, reproducibility, limit of detection etc., will be determined, and validation as well as application to different cellulosic and non-cellulosic materials will be performed.

Acknowledgements

The authors would like to thank Dr. Andreas Hofinger for NMR-measurements and Dr. Sonja Schiehser for GPC-measurements. Financial support by the Austrian Christian Doppler Research Society and by Lenzing AG, Austria, is gratefully acknowledged.

References

1. Heyns, K., Paulsen, H. Catalytic oxidation of carbohydrates, *Advances in Carbohydr. Chem.* 17 (1962).
2. Röhrling, J., Potthast, A., Rosenau, T., Lange, T., Borgards, A., Sixta, H. and Kosma, P. Synthesis and Testing of a Novel Fluorescence Label for Carbonyls in Carbohydrates and Cellulosics. *Synlett* 5:682-684 (2001).
3. Röhrling, J., Potthast, A., Rosenau, T., Lange, T., Ebner, G., Sixta, H. and Kosma, P. A novel method for the determination of carbonyl groups in cellulosics by fluorescence labeling. Part I: Method development. *Biomacromolecules* 3:959-968 (2003).
4. Röhrling, J., Potthast, A., Rosenau, T., Lange, T., Borgards, A., Sixta, H. and Kosma, P. A novel method for the determination of carbonyl groups in cellulosics by fluorescence labeling. Part II: Validation and applications. *Biomacromolecules* 3:969-975 (2003).
5. Potthast, A., Röhrling, J., Rosenau, T., Borgards, A., Sixta, H. and Kosma, P. A novel method for the determination of carbonyl groups in cellulosics by fluorescence labeling. Part III. Monitoring oxidative processes. *Biomacromolecules* 4:743-749(2003).
6. Bohrn, R., Potthast, A., Rosenau, T., and Kosma, P. Synthesis and Testing of a Novel Fluorescence Label for Carboxyl Groups in Carbohydrates and Cellulosics. *Synlett*, in prep. (2005).
7. Wilcox, M., Viola, R.W., Johnson, K.W., Billington, A.P., Carpenter, B.K., McCray, J.A., Guzikowski, A.P. and Hess, G.P. Synthesis of Photolabile "Precursors" of Amino Acid Neurotransmitters. *J. Org. Chem.* 55:1585-1589 (1990).
8. Molecular Probes, Inc., Product Information for 1-(4,5-Dimethoxy-2-nitrophenyl) diazoethane, Generation Kit D-2516 (2001).
9. Schönberg, A., Awad, W. I., Latif, N. Experiments with Diazomethane and its Derivatives. Part XVI. Action of Diazomethanes on Perbenzoic Acid and Benzoquinone Derivatives. *305:1368-1369* (1950).

FLUORESCENT MOLECULAR PROBES FOR THE CHARACTERISATION OF FIBRE STRUCTURE AND DISTRIBUTION OF TEXTILE RESIN FINISHING ON LYOCELL

Mohammad Abu Rous¹, Avinash P. Manian¹, Thomas Röder², Irene Lichtscheidl³,
and K. Christian Schuster⁴

¹Christian-Doppler-Laboratory "Textile and Fibre Chemistry in Cellulosics"
Institute of Textile Chemistry and Textile Physics – Leopold-Franzens-University Innsbruck
Höchsterstrasse 73, A-6850 Dornbirn

²Lenzing AG, Zellstoff-Forschung, A-4860 Lenzing, Austria

³Institute of Ecology and Conservation Biology of the University of Vienna, Austria

⁴Lenzing AG, Textile Innovation, A-4860 Lenzing, Austria. Email: c.schuster@lenzing.com, (Tel: +43 7672 701 3081)

The main topic of this work is to develop a method to characterise the pore structure of cellulosic fibres applying fluorescent dyes. Furthermore, fluorescent dyes were also applied to label and quantify additives on the textile surface, as well as to visualise their distribution within the fibres and the yarns. A combination of virtual cross-sections by confocal microscopy, and real cross-sections from microtomy could deliver valuable and detailed qualitative and semi-quantitative information on the distribution of dye inside the fibre cross-section. Quantitative information

on dye distribution relative to cellulose was obtained by Raman microscopy. The fibre pore structure was probed by the optical brightener Calcofluor, approaching a fibre structure model for the influence of production and treatment parameters on the fibre structure during fibre formation and modification. Application examples in textile finishing are the distribution of chitosan and resin finishing agents in fibres and fabrics.

Keywords: *confocal microscopy, fibre, fluorescence microscopy, Raman spectroscopy*

Introduction

The typical surface morphology and the structure of Lyocell fibres are a result of the parameters of the spinning process [1],[2],[3] and have an important impact on the physical properties and the further behaviour treatment of the textile. To adapt Lyocell to the requirements of the market and to avoid technical problems in the further finishing steps, it's necessary to be able to control and to vary these properties. The classical textile tests deliver the effect of these changes on the physical and textile properties, but are not able to supply the link to the internal fibre structure. For this reason, a deep analysis

on the structure formation during the process and the following treatments is indispensable.

The use of dyes for probing pore structure has been known for long time [4],[5]. Of particular interest are rather large molecules which penetrate the fibre completely only under certain conditions, and fluorescent dyes as they can be detected in very low concentrations and in microtome cross-sections. In earlier experiments, calcofluor was found to be a promising dye.

The distribution of textile finishing agents is an important topic in development of

textile products. Uneven distribution on large scale leads to uneven dyeing. Uneven distribution of resin finishing on the fabric cross-section, yarn and fibre level (the microscopic scale) leads to poor mechanical performance. Fluorescent probes selective for textile finishing have been described. As known from earlier works [6] on cotton fabrics rhodamine B can be utilised to as a selective marker of the resin finishing agent on yarns and fabrics.

One of the main limits of conventional light and fluorescence microscopy is out-of-focus blur degrading the image. De-focused information often obscures important structures of interest, particularly in thick specimens. The out-of-focus light leads to a reduction in image contrast and a decrease in resolution. An alternative was found in confocal microscopy. The illumination in a confocal microscope system is sequential in nature. The specimen is not uniformly illuminated throughout its depth, the light being focused on a spot on one volume element of the specimen at a time. It is possible, to obtain illumination spots as small as 0.25 μm in diameter and 0.5 μm deep. Confocal microscopy applied to transparent samples could deliver highly resolved images. Virtual cross-sections can be delivered by a summation of line scans in different depths in the z-axis.

An appropriate quantification method is Raman spectroscopy, a vibrational spectroscopy which can provide multivariate information on the chemical composition of samples. Integrated in a light microscope system, confocal spectra of small objects can be obtained at a spatial resolution of about 1 μm .

Methods

Fluorescence microscopy

The fluorescence on fibres and fibre cross-sections was observed using an Olympus BX microscope equipped with a mercury burner lamp, monochromatic filters and a

digital camera system. The applied dyes on the respective substances are shown in table 1.

Extended focal images were reconstructed from several images of limited depth of focus using the *Analysis* software.

Issue	Label	$\lambda_{\text{Excitation}}$ [nm]	$\lambda_{\text{Emission}}$ [nm]
Resin-finishing	Rhodamine B	500 – 570	590 -
Chitosan	Fluoresceine Isothiocyanate (FITC)	449 – 498	510 -
Accessibility	Calcofluor	210 – 250	410 -

Table 1. Fluorescent labels

Fibre cross-sections were produced using a Reichert (model: 1140/Autocut) microtome after being embedded in a 2-hydroxyethylmethacrylate resin (Technovit7100TM, Kulzer). It was possible to prepare cross-sections down to 5 μm thickness. Cross-sections were prepared at 8 μm thickness from yarns and fibres, and 20 μm thickness from fabrics.

Confocal microscopy

The confocal observation was performed at the Institute of Ecology and Conservation Biology of the University of Vienna using a confocal laser scanning microscope (Leica TCS SP2 in combination with an inverted DM IRB microscope). The system has three lasers: HeNe (633nm/10mW, red), He/Ne (543nm/1,2mW, green) and Ar (458nm/5mW, 476nm/5mW, 488nm/20mW, 514nm/20mW, blue) [7]. FITC fluorescence was excited with the blue lines, rhodamine fluorescence using the green lines. The scans were performed at 0.5 μm of resolution.

Yarns were taken out of the fabrics and evacuated in a water-filled syringe to eliminate air pockets. The yarns were presented on a microscope slide and immersed in water.

Raman spectroscopy

The Raman measurements were performed with a HoloLab Series 5000 Modular Raman Spectrometer (HL5R) from Kaiser Optical Systems Inc. (USA) equipped with f/1.8 optics, transmission grating, multichannel CCD array detector (optimized for NIR), and a 785 nm diode laser (500 mW) coupled via single mode fibre to the microscope (approximately 80 mW on the sample). Between microscope and detector, a confocal fibre with a pinhole (silver coated) of 20 μm was used. For the measurements a 100X (0.9 N.A.) objective was used.

Cross-sections of calcofluor-dyed Lyocell fibres were prepared. The Raman intensity of Calcofluor relative to cellulose was measured.

Resin labelling with Rhodamine B [8]

Resin-finished woven fabrics of Lyocell cloth were dyed with a 10^{-4} M Rhodamine B (MW = 480) solution. The fibres were dyed for 24 h in a 10^{-3} M solution of rhodamine B in a pH 9.3 buffer solution ($\text{NH}_4\text{Cl}/\text{NH}_3$). The dye shows high affinity to the finishing resin. Unfinished fabrics showed a very weak autofluorescence. The fluorescence distribution over the cross-section is a direct representation of the resin distribution.

Dying with Uvitex BHT

Lyocell fibres were treated for various times with an aqueous 1g/L technical Uvitex BHT (Ciba, Basel, CH; an optical brightener, contains Calcofluor, molecular mass 960 Da) solution and dried at room temperature.

Chitosan labelling with FITC [9]

Chitosan-impregnated fibres were dyed with a 10^{-4} g/L fluorescein isothiocyanate (FITC) solution at pH 7 (Acetate puffer) for 1 h at room temperature, washed with

water and ethanol and dried at 60°C. FITC forms a covalent bond with chitosan through the amino groups.

Results and discussion*Observation of Chitosan distribution on cellulosic fibres*

Three types of Chitosan-containing cellulosic fibres were observed.

Chitosan on cellulosic fibres produced by various routes was labelled using the fluorescent dye Fluorescein isothiocyanate (FITC). The distribution of Chitosan on fibres and within the fibre cross-section was observed by classical fluorescence microscopy (Figure 1 – Figure 3). Confocal microscopy was used to obtain depth resolved image data. A reconstruction image over the thickness of the fibre gives an impression of the overall distribution of chitosan in the water-swollen state (Fig. 4).

Calcofluor as a fluorescent molecular probe for fibre structure analysis

The depth and the intensity of dye intrusion into fibres depend on the properties of the dye such as molecular weight, and affinity / substantivity. For a given dye, the distribution in a fibre can serve as a molecular probe for structural properties of the fibre porous system.

The substantive fluorescent dye Calcofluor (MW 960) was used as a molecular probe to explore the surface and the internal pore structure of Lyocell, viscose, modal, and cotton fibres. It's intrusion into the fibre cross-section is limited and depends on time and on the porous structure of the textile fibres. Fluorescence microscopy could deliver qualitative and semi-quantitative information about the dye penetration into different fibres.

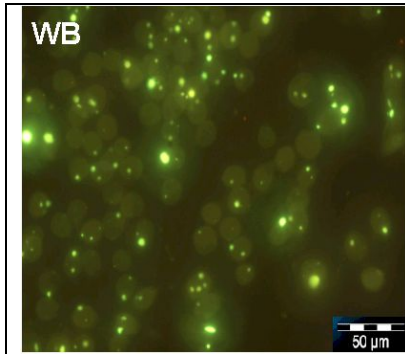


Figure 1. Cross-sections of chitosan-incorporated lyocell fibres

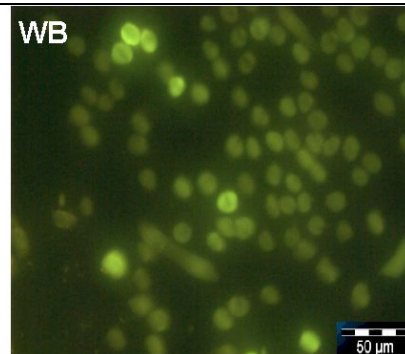


Figure 2. Cross-sections of chitosan-impregnated lyocell fibres

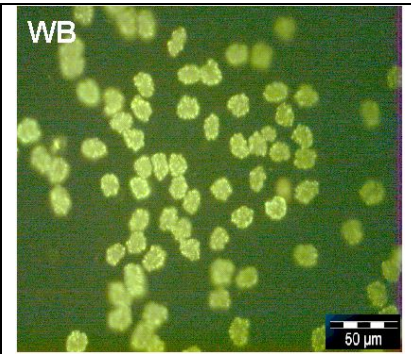


Figure 3. Cross-sections of commercial chitosan-incorporated viscose fibres (Crabyon®)

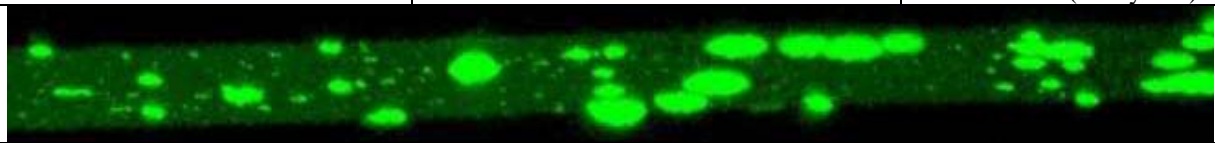


Figure 4. A reconstructed confocal image of a chitosan-incorporated Lyocell fibre in water



- Thinner skin
- Less and thinner macropores
- Appearance of core

Figure 5. Structure model of the Lyocell fibre [10]

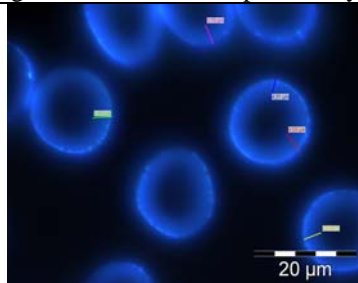


Figure 6. Calcofluor intrusion into Lyocell fibres. Cross-sections after 4 h (left) and 24 h (right)

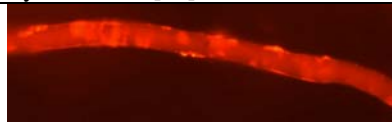
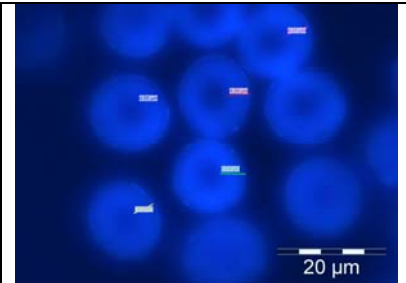


Figure 8. Resin-finished Lyocell fibre (Rhodamin B - labelled, extended focal imaging))

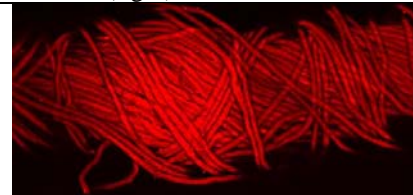


Figure 7. A resin-finished Lyocell yarn (confocal image after Rhodamin B- labelling)

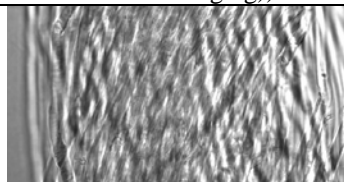


Figure 9. A comparison between a longitudinal internal view of a lyocell yarn interior, using normal light (left) and confocal fluorescence (right)

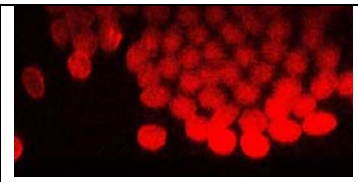
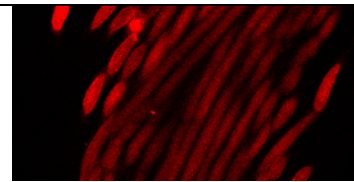


Figure 10. A confocal cross-section of a fluorescence-labelled, resin-finished Lyocell yarn

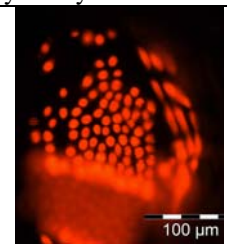
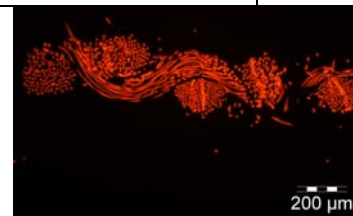
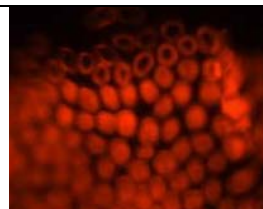
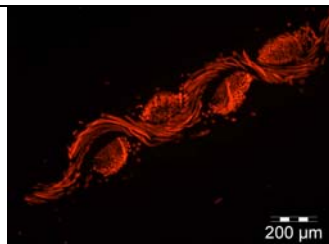


Figure 11. Microtome cross-sections of fabrics and yarns of woven fabric samples A (left) and B (right) (see text for details)

The impact of modifying the spinning and treatment parameters could be observed by the kinetics of the penetration of calcofluor. A correlation of the dye penetration kinetics with the fibre physical properties is also possible and helps to derive the relationship between fibre structure and fibre properties.

Characterisation of the fibre pore structure

Preliminary experiments applying calcofluor show that the never-dried Lyocell fibres are much more accessible to the dye than dried fibres. The intrusion of calcofluor could even reach the centre of the cross-section in some cases revealing a fairly open porous system, which collapses irreversibly after the first drying. This phenomenon wasn't observed on viscose and modal fibres, where the calcofluor dyeing remained superficial.

In earlier works [10] on cellulose crystallisation following the Lyocell process, a model of crystalline core, a porous zone and a membrane fibre skin was suggested (Figure 5). Although the model was made following experiments on the crystallisation out of dope blocks and not in the dynamic spinning process, some parallel characteristics can be seen also in the structure of Lyocell fibres.

Cross-section of fibres dyed with Calcofluor for 4 and 24 hours (Figure 6) were prepared. The fluorescence microscopy observation gave a dye distribution profile which fits with this model.

Visualising the fibre skin

The membrane skin on the fibre surface can be seen clearly after being illuminated with the fluorescent dye. The dye diffusion through the fibre inside is faster than through the fibre skin, which seems to serve as a semi-permeable membrane.

Relative quantification of Calcofluor on fibres by Raman spectroscopy

Complementary to the optical observations, the concentration of Calcofluor through the cross-section could be quantified applying Raman spectroscopy on fibre cross-section. It can be measured relatively to the cellulose amount, which serves here as an internal reference.

A comparison of the dye intensity on the fibre surface and the fibre core was made. Dried and never-dried Lyocell fibres produced under two different spinning conditions were dyed with calcofluor (Figure 14). The intrusion of calcofluor was observed scanning along the cross-sections. Calcofluor was quantified integrating its specific band of the aromatic ring system at 1600 cm^{-1} relative to the cellulose band at 1090 cm^{-1} (Figure 12).

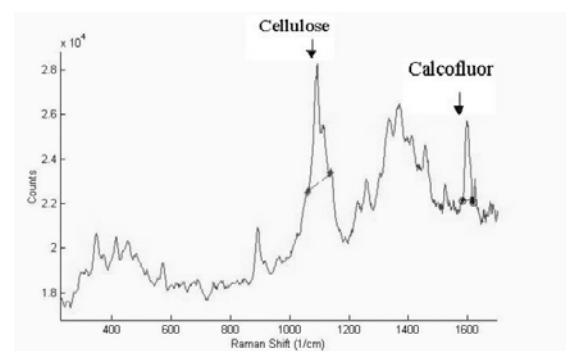


Figure 12. Raman spectrum of calcofluor on a Lyocell fibre, and bands used for quantification

It's obvious, that the kinetic of calcofluor penetration into the fibres differs depending on the spinning and drying conditions. Additionally to the qualitative and the semi-quantitative information obtained from the fluorescence microscopy, Raman spectroscopy can supply quantitative and localised information on calcofluor concentration within the fibre. Cellulose serves here as an internal reference.

Effect of caustisation (lying)

Standard and lyed (14 °Bé) CLY fabrics were dyed with Uvitex BHT for 10 min, 4

and 24 h. The penetration of dye was measured on the fibre cross-sections (Figure 13).

Although initially similar, the intrusion was deeper into the lyed than into the normal fibres. In both cases the fibre

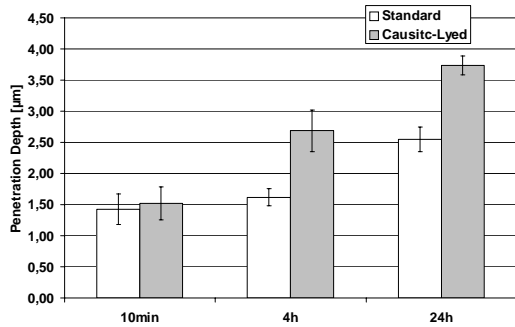


Figure 13. Time scale of the penetration of calcofluor into standard and causticised Lyocell fibres

centre couldn't be reached by the dye.

On the other hand, the fluorescence intensity was in all cases higher on the lyed than on the normal fibres.

Distribution of finishing resin

Resin-finishing on Lyocell stained with rhodamine B was observed in fluorescence microscopy of longitudinal views on fibres (Figure 8), confocal imaging (Figure 7) and fabric cross-sections. The distributions on the surface of fibres were sometimes uneven (Figure 8).

Virtual cross-sections of yarn were obtained by summing up line scans in different depths of the yarn. The conductor effect of the fibres could be eliminated, delivering highly resolved images (Figure 9).

The main problem was the depth of detection on yarns, where the decreasing signal could lead to wrong conclusion. Only the outer 3 – 4 layers of fibres could be observed accurately (Figure 10). This can be avoided combining the observations with the ones from microtomy and conventional microscopy. Any how, preparation-free virtual cross-sections were produced and gave the first approach to the distribution of fluorescent agent in the fibres.

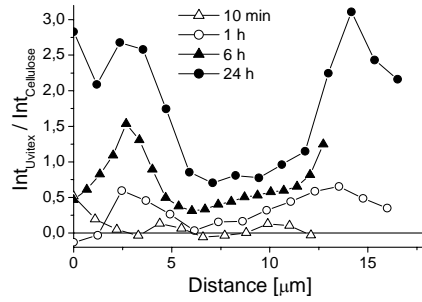


Figure 14. Raman intensity of Calcofluor relative to cellulose through fibre cross-sections over dyeing time. The rims of the fibre were at about 1 µm and 13 µm along the distance scale.

Figure 14a. never-dried Lyocell (type 1)

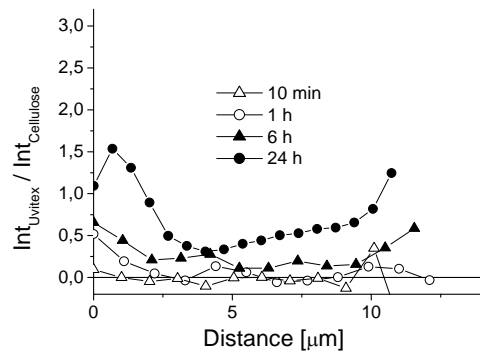


Figure 14b. dried Lyocell (type 1)

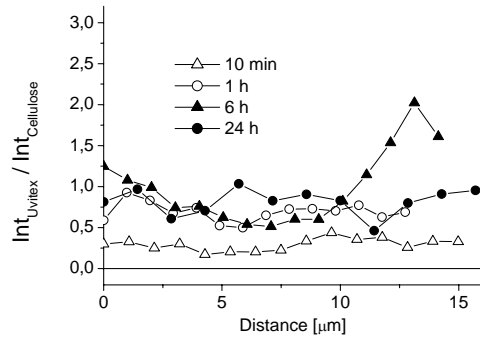


Figure 14c. never-dried Lyocell (type2)

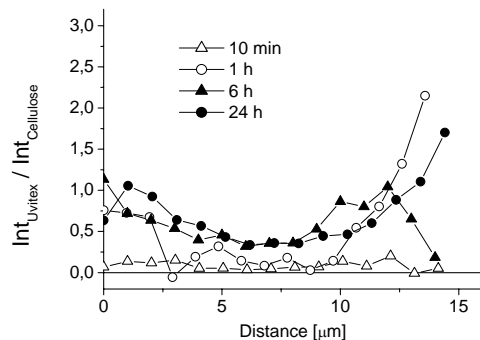


Figure 14d. dried Lyocell (type2)

Effect of drying on resin distribution

Lyocell fabrics were resin-impregnated (Fixapret ECO, BASF), dried under two different conditions and polymerised at 180°C. The samples were dried after the impregnation under the following conditions:

A: Pad - Dry at 180 °C - Cure at 180 °C for 40 s.

B: Pad - Dry at Room Temperature - Cure at 180 °C for 40 s

The samples dyed with rhodamine-B and the fluorescence images were taken on real microtome and virtual confocal cross-sections (Figure 11).

Non-finished fibres showed a very weak rhodamine B fluorescence although the cross-section. On the quickly dried sample A, the dye occurs as a ring around the fibre cross-section. The resin monomer seems either to migrate outwards in both yarn and fibre levels during the drying, or not to be able to diffuse into the fibre due to oligomer formation at the high temperature. In the second case, the diffusion is mostly limited in the more exposed zones and the monomer doesn't have enough time before the polymerisation.

On the slowly dried sample B, the fluorescence occurs through the whole cross-section. This indicates that the resin distribution remains homogenous through the whole fibre/yarn cross-section.

Correlation with serviceability: Sample B with even resin distribution had significantly better serviceability regarding crease resistance, weight loss in the Martindale abrasion test and yarn strength. Yarn elongation remained unaffected.

Acknowledgements

• Dr. Sigrid Redlinger and Gerhard Reiter (Lenzing AG) for the Chitosan fibre samples

• DI Hartmut Rűf (Lenzing AG), for the Lyocell samples

• Dr. Marina Crnoja-Cosic, Ing. Georg Kling, and DI. Karin Kämpf (all Lenzing AG) for the resin-finished samples

•Karl Reiter, Lenzing AG, for the co-operation in preparing microtome cross-sections

References

[1] S.A. Mortimer; Dissertation, Université Joseph Fourier – Grenoble I, March 1995

[2] K.C. Schuster, P. Aldred, M. Villa, M. Baron, R. Loidl, O. Biganska, S. Patlazhan, P. Navard, H. Rűf, E. Jericha; Lenzinger Berichte 82 (2003); 107 – 117

[3] K.C. Schuster, C. Rohrer, D. Eichinger, J. Schmidtbauer, P. Aldred, H. Firgo; Environmentally Friendly Lyocell Fibres, in *Natural Fibres, Plastics and Composites*; ed.: F.T. Wallenberger and N.E. Weston; Kluwer Academic Publishers Boston/Dordrecht/N.Y/London; 2003; 123 - 146

[4] K. Götze et al.; Chemiefasern nach dem Viskoseverfahren; dritte Auflage; erster Band; Springer Verlag, Berlin/Heidelberg/New York; 1967; 544 – 551

[5] X. Yu, R.H. Atalla; Powder Technology 98 (1998) 135 – 138

[6] S. Kokot, M. Matsuoka, U. Meyer, T. Zürcher; Textilveredlung 10 (1975); 127-134

[7] [http://www.univie.ac.at/IECB/cell/microscopy/confocal/\\$confocal.htm](http://www.univie.ac.at/IECB/cell/microscopy/confocal/$confocal.htm)

[8] W. Schindler, P. Drescher; Melliand Textilberichte 1-2 (1991); 67 – 77

[9] H. Onishi, Y. Machida; Biomaterials 20 (1999); 175 - 182

[10] O. Biganska; Dissertation, L'Ecole Nationale des Mines de Paris; december 2002

HIGHER PERFORMANCE WITH NATURAL INTELLIGENCE

Johann Männer, K. Christian Schuster, Friedrich Suchomel, Andreas Gürtler, and Heinrich Firgo

Lenzing AG, R&D, A-4860 Lenzing, Austria. www.lenzing.com
Tel: +43-7672-701-3488

Good comfort in wear is a challenge to the properties of textiles. Depending on the application, textiles must meet different requirements.

The cellulosic fiber lyocell (brand names: Lenzing-Lyocell® and Tencel®) consists of a nano fibril cellulosic structure. Its purity, smooth surface and outstanding moisture management properties leads to a feeling of “well-being” performance in 100% application as well as in blends. Textiles made out of lyocell provide outstanding moisture transport which promotes thermo-regulation under various climate conditions. Especially

micro fibers exhibit excellent insulation properties. Drying properties are comparable to synthetics. The smooth surface together with good moisture management leads to excellent sensory perception, which is especially important for persons with sensitive skin (e.g allergy patients or neurodermitis patients). Less growth of bacteria and less odor formation is observed, compared to synthetics. No electrostatic charge is built up.

Keywords: *Lyocell, Tencel, fibre*

Introduction

Textiles come into contact with the human body, especially the skin, at various levels of intensity. Good comfort in wear is thus a challenge to their performance. Depending on the application, though, textiles must meet different sets of requirements.

The temperature regulation of the human body is a decisive factor for comfort in wear and well-being. In warm climates and at high levels of physical activity, other properties are needed than in cold environments and when the body is at rest. In addition, the sensory perception on the skin plays an important role for the overall “feel good factor” of textiles. This is of special significance for persons with sensitive skin. Hygiene and electrostatic behavior also have an impact on comfort in wear. The diverse requirements are thus a considerable challenge for the properties of textile materials.

The cellulosic fiber lyocell (brand names: Lenzing-Lyocell® and Tencel®) can form a basis for well-being by its natural

intelligence properties. In earlier papers, we have shown some of the “feel good factors” of textiles provided by lyocell fibers especially in everyday apparel (Eichinger et al., 1998) and in home textile applications (Schuster et al., 2003; Schuster et al., 2004). In this paper, a number of examples demonstrate the “natural moisture management” of lyocell fibers in connection with temperature regulation, skin sensitivity, textile hygiene, electrostatic properties, and the contribution of these factors towards superior textile fabric structures.

The Structure of Lyocell Fibers

Fibers that are spun according to the lyocell process have a nano fibrillary cellulose structure. It consists of countless, non swelling, crystalline microfibrils. Swelling occurs in the non-crystalline regions and capillaries between the micro- and nano fibrils. Therefore, lyocell fibers can be considered as a hygroscopic nano-multifilament. This is

responsible for a superior moisture management in textiles and contribute in many

different ways towards optimizing comfort in wear.

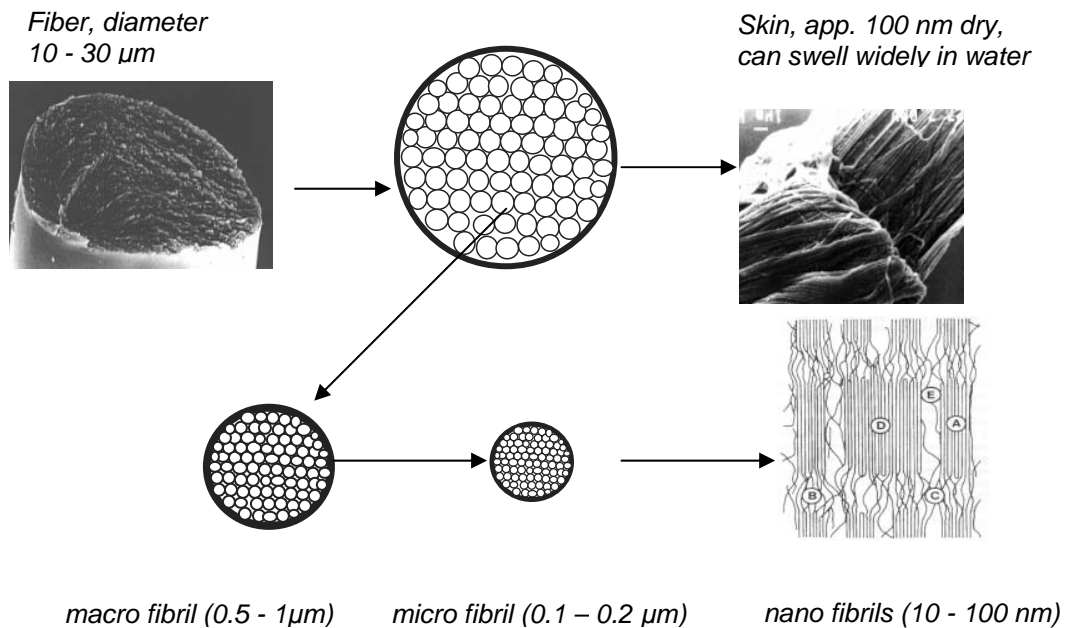


Figure 1. Model of the lyocell fiber structure (modified from Schuster et al., 2003)

Temperature Regulation of the Body at High Activity Level

Depending on the physical activity, the energy consumed by the body amounts to between 60 Watt at rest and 2000 Watt for athletes in competition sports (table 1). At high performance levels, excess heat is generated, which the body must discharge, otherwise it will overheat. The body therefore reacts by producing more perspiration.

There are about 2 million perspiration glands on about 2 m² of skin, which

distribute the water on the skin. The perspiration evaporates on the surface and cools the organism. When exercising, the body releases up to 1.8 l of water per hour.

In order to ensure an optimum temperature control of the body, it is necessary that textiles worn close to the skin facilitate an expedient transport of the perspiration at an even rate across the textile surface. Evaporation on the surface, close to the skin, then provides the necessary cooling effect and contributes as such to the temperature regulation of the body.

Physical Activity	Energy consumption [W]
rest	60 – 100
light work	120 – 300
heavy-duty work	300 – 600
light sports	600
active, competitive sports	1000 - 2000

20°C room temperature 35°C

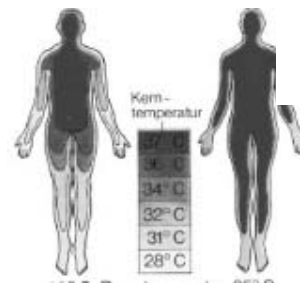


Table 1. Physical activity and energy consumption (Mich and Schönfelder, 2003)

Figure 2. Temperature distribution over the body at 20°C and 35°C ambient temperature

Various examples are presented to compare the properties and the contribution of the "moisture management" of lyocell fibers to those of other fiber materials. Water absorption, water transport and the drying behavior of knitted textiles of

comparable construction and basic processing was determined on a laboratory scale, using testing set-ups modeled on practical situations. Tab. 2 shows the standard textiles used for the following experiments.

Table 2. Standard textiles: Construction: single jersey; Processing: no resin finish, washed 1x

Material	Grammage [g/m ²]
Lyocell , 1.3 dtex	150
Cotton (bleached)	171
Polyester 1.2 dtex, filament yarn	151

Water Absorption Capacity

The absorption capacity and velocity of knitted fabrics were determined by means of a "gravimetric absorbency testing system" (GATS;

Thumm, 2000). The absorbed water quantity corresponds to the inherent absorption capacity of the material. There was no hydrostatic pressure gradient during testing.

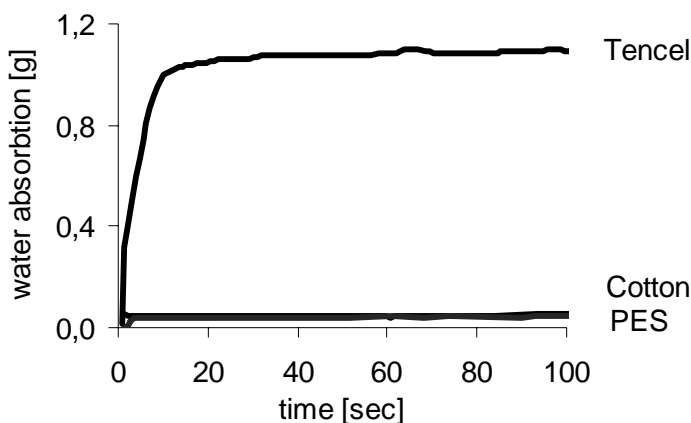


Figure 3. Comparison of the absorption capacity of lyocell, cotton, and polyester (according to GATS test) on a test area of 19.6 cm²

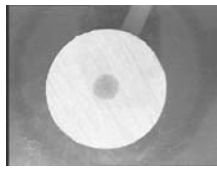
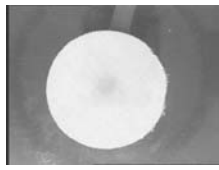
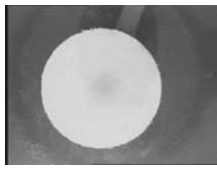
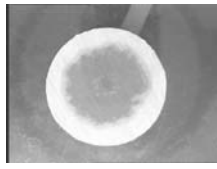

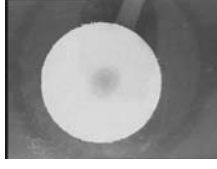
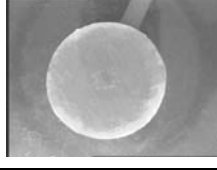
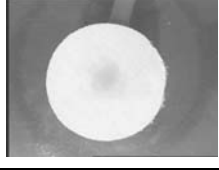
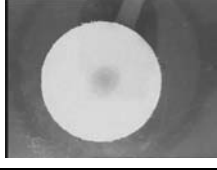
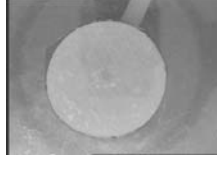
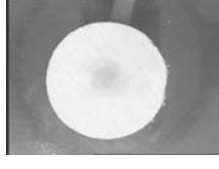
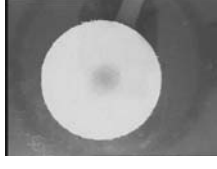
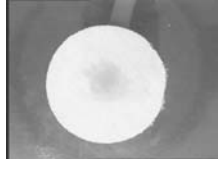
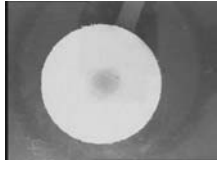
Time [sec]	Lyocell	Cotton	Polyester
1			
5			
10			
50			
100			

Figure 4. Optical presentation of the absorption capacity of lyocell, cotton, and polyester

In this comparison, lyocell shows a significantly higher water absorption capacity and – primarily – a much higher absorption velocity than cotton and polyester. On account of the homogenous moisture distribution over a large surface, lyocell can ensure an optimum evaporation on the surface of the textile material, and thus leads to an excellent temperature regulation. Within 20 seconds the

lyocell fabric reaches a maximum absorption capacity of 380% moisture, which is also absorbed in a homogenous distribution over the entire material surface. Cotton and polyester show a moisture uptake of only 16 to 19%. Even when measuring after up to 3 minutes, this level does not change to any major extent.

Moisture Distribution in Polyester and Lyocell Fibers and Fabrics

Non-absorptive fiber materials can be wetted overall upon mechanical impact by overcoming the surface tension. In case of polyester, the moisture absorbed by the textile is found between the fibers and/or yarns on the fiber surface. On account of the

nano-fibrillary structure of lyocell fibers, the moisture is transported very swiftly through the micro capillaries and absorbed inside the fibers which swell accordingly. At 100% fiber moisture, a major amount of the moisture is inside the fiber in case of lyocell without resin finishing.

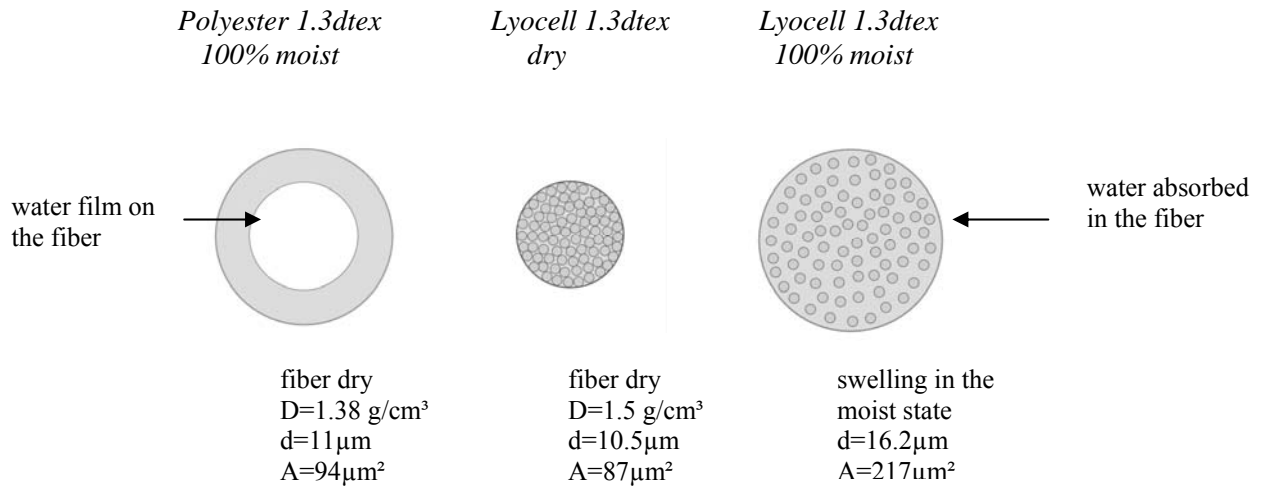


Figure 5. Model of the moisture distribution in polyester and lyocell fibers

Drying Behavior

In addition to a good moisture absorption performance, the capacity to discharge the absorbed water during drying is also an important parameter especially in sportswear. The general belief so far was that absorptive cellulose fibers have the disadvantage to dry more slowly than non-absorptive synthetic fibers. The moisture content of polyester textiles after thorough wetting and spin-drying is about 35%, depending on the construction, as compared to approximately 110%

moisture in case of lyocell. The different moisture quantities after spin-drying naturally result in a faster drying performance of the polyester materials. However, when starting from the same initial amount of moisture in the textile, no significant difference was found in the drying kinetics of polyester and lyocell materials.

Lyocell and polyester knitted fabrics with 100% fabric moisture were compared in test set-ups modeled on practical situations.

Comparison of the Dynamic and the Static Drying Behavior

The normal drying behavior under air exposure of thoroughly moistened 100% moist jersey fabrics, made of lyocell and polyester, was determined. The drying kinetics was determined both for swift and slow drying of the textiles, until conditioning moisture is reached. In the case of swift, dynamic drying, a constant air current was blown through

the textile. In the case of slow drying, the textiles were dried at ambient temperature without additional air convection.

Although in case of lyocell the moisture from the fiber must dissipate from the fiber inside to the surface and then to the air, no significant difference in drying velocity can be established between lyocell and polyester of the same initial fabric moisture.

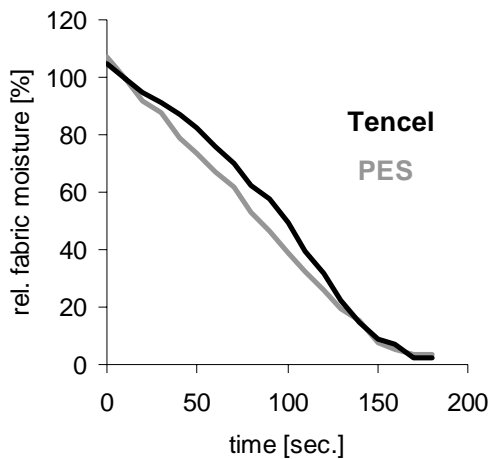


Figure 6. Swift drying with an air current of 2.5 m/s, 26°C, 18% RH through the textile

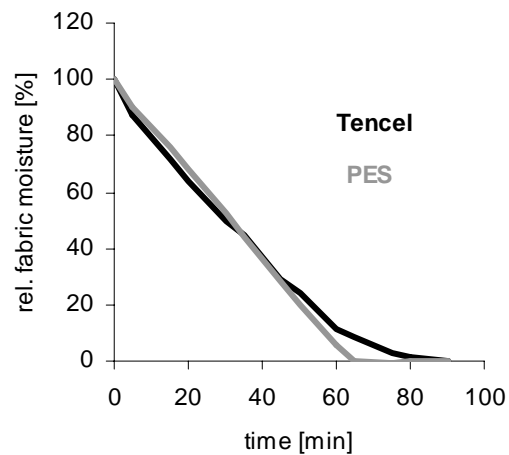


Figure 7. Slow drying without additional convection, room climate 26°, 40% RH

Comparison of the drying kinetics of moist polyester and lyocell knitted textiles. The textile were evenly wetted and set to 100% moisture in relation to the conditioning moisture. Drying is continued until conditioning moisture is reached.

Temperature Regulation of the Body in Cold Climate

In cold climate and at low physical activity the body must be protected against chilling. The insulation effect is therefore the primary target in textile performance. Since human beings dissipate moisture permanently via the skin, a sufficient water vapor transport through the textile is needed in addition to a good insulation capacity. When there are sweat impulses during higher levels of activity, the material should also show a good buffering capacity for liquid perspiration.

As a general rule, in a cold climate several textile layers are worn on the body. Conventionally, high-loft webs, made of polyester fibers, are used as effective insulation materials in the intermediate layers. This application and its requirements correspond to the materials used in quilts and sleeping bags. However, the high-loft webs used in garments are lighter (60 – 120 g/m²) than in quilts. A

winter jacket for sports activities should ensure optimum freedom of movement. The construction should be light and not too voluminous. It is mainly the insulation material used that determines the visual appearance and the volume. A requirement for high-loft webs used in garments is to offer a good insulating effect, a good water vapor transport and a high buffer capacity against moisture at a low volume.

The following examples serve to show that lyocell high-loft webs have excellent thermo-physiological properties. Especially fine denier fibers can meet these requirements in a superior fashion. When having about the same grammage (weight per unit area), but only half the web thickness, a lyocell web has much higher insulation values for standard thicknesses in comparison to polyester webs, as well as a 30% higher water vapor permeability index. The short-term water vapor absorption capacity of lyocell webs is about ten times the amount of polyester.

Table 3. Water vapor permeability index of web samples according to ISO-11092 measured at the Austrian Textile Research Institute

High-loft webs	Thickness [mm]	Grammage [g/m ²]
PES 3.3 dtex	7.3	69.1
CLY 6.7dtex	4.9	81.9
CLY 6.7dtex / 0.9dtex	4.9	87.4

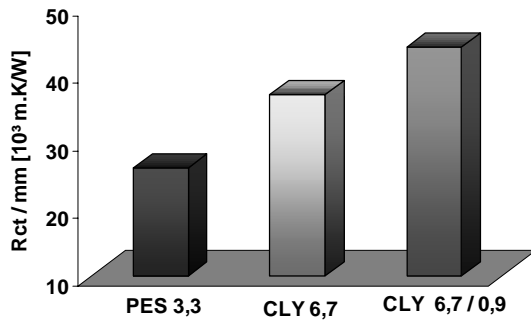


Figure 8. Thermal resistance R_{ct} , thickness standardized, acc. to ISO-11092 [$10^3.m.K/W.mm$]

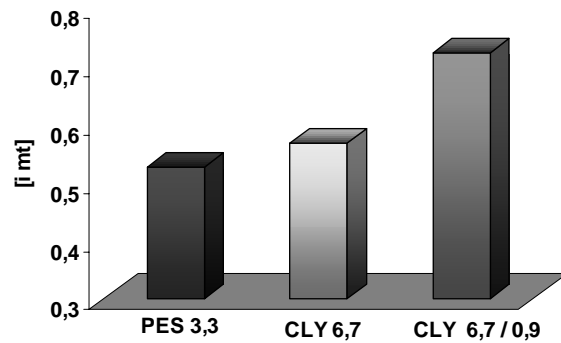


Figure 9. Water vapor transport index I_{mt} acc. to ISO-11092 [imt]

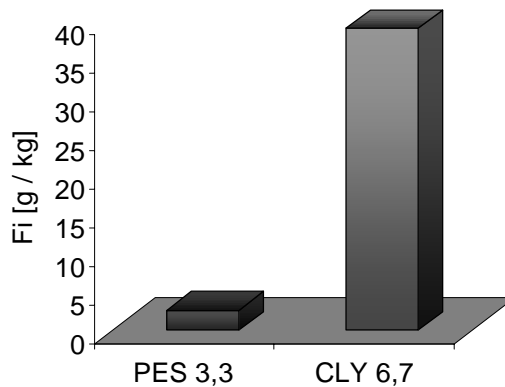


Figure 10. Short-term water vapor absorption capacity F_i according to ISO-11092 measured at the Research Institute Hohenstein [$g\ moisture/kg\ fiber$]

Skin Sensory Perception

The skin forms the surface of the human body and gets into intense contact with textiles. Receptors in the skin for temperature, changes of movement, pressure, itching irritations and pain, communicate the feeling of the skin under the impact of textiles.

A substantial number of people suffer from "wool intolerance". The scaled wool surface together with the rigid fiber ends cause an itching irritation, up to atopic eczema. In case of high friction on the skin, a mechanical-toxic contact dermatitis may be formed. Especially for persons with sensitive skin, who tend to develop pathological allergic reactions such as

neurodermitis, it is important not to cause any skin irritation. Especially under humid conditions, in case of a major perspiration discharge, the skin becomes more sensitive to irritation. Here primarily the capacity to absorb water, the moisture permeability to

the outside and the drying velocity of the fabrics are of importance.

Lyocell fibers offer an optimum comfort in wear on account of their optimum absorption capacity and their surface, which is smooth in comparison to cotton and wool (Fig. 11).

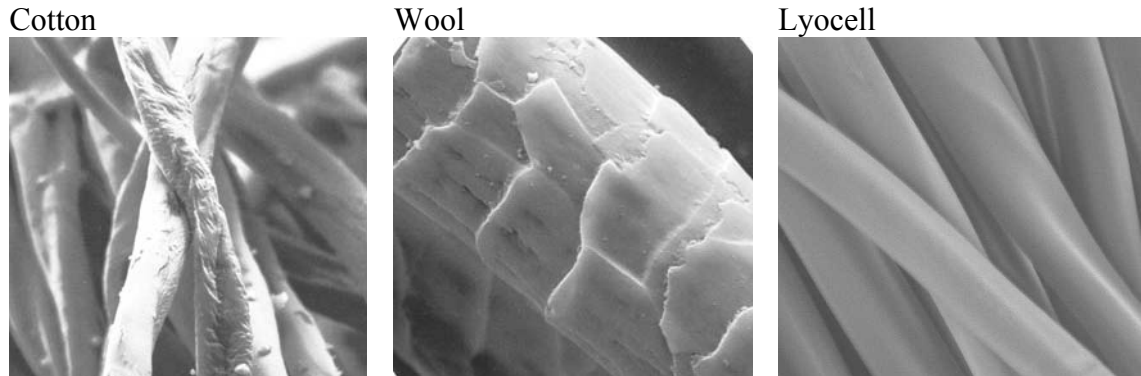


Figure 11. Scanning electron micrographs of cotton, wool and lyocell fibres

Study at the University Hospital Heidelberg

In a study conducted at the University Hospital Heidelberg, a wearing trial was conducted under the leadership of Prof. Diepgen with neurodermitis and psoriasis patients. Textiles made of lyocell were tested. The result of the study indicates that more than 80% of the test persons noted a

clear improvement of the skin-sensory and thermo-regulatory properties in the lyocell materials, as compared to the materials which they had previously regarded as having optimum characteristics.

Refer to the paper presented by Prof. Diepgen:

"Dermatological examinations on the skin compatibility of Lenzing Lyocell textiles"

Improved Comfort in Wear

Blended fabrics of polyester and cotton are mainly used for vocational clothing in order to meet the requirement of a longer service life. When textiles become humid, the friction resistance on the skin increases, which may be the primary cause of skin irritations and contact dermatitis. A two-layer material blend with synthetic fibers on the side closer to the skin is often used in functional textiles. The poor water absorption of synthetic fibers has a negative

effect on the comfort in wear, in comparison to materials with better absorption capacity.

Using lyocell fibers can considerably improve the comfort in wear of blended materials due to lyocell's good absorption capacity (as compared to synthetics) and smooth surface (as compared to cotton). The results and personal observations indicate that there is a clearly positive influence.

Skin-sensory perception properties of shirt materials of identical construction
 Source: Research Institute Hohenstein

	wet cling index i_K	skin-sensory comfort grade	wearing
100% cotton	10.9	1.7	
60% cotton 40% lyocell	8.6	1.3	

Table 4. Skin-sensory key data for shirt materials made of cotton and a cotton/lyocell blend

Comparison of the wet cling index of functional materials: R/L single jersey, plated, Polyamide on the side close to the skin / lyocell, cotton or polyester on the outside. (Ernst and Planck, 2004)

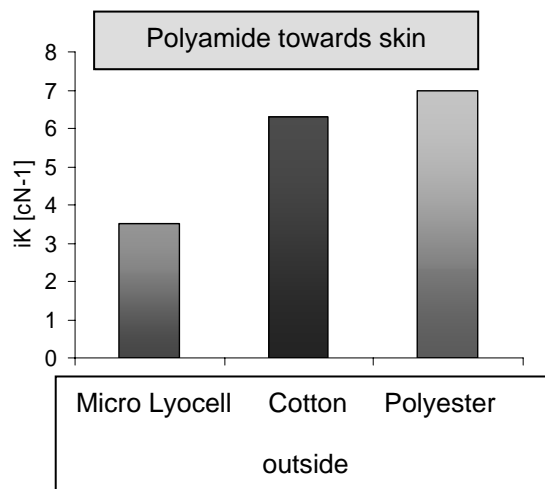


Figure 13. Comparison of the wet cling index in two-layer knitted fabrics

Practical experience with working clothes

Working clothes for medical personnel in operating theaters are currently made of cotton – polyester blends, in order to meet the high demands. The extreme temperature conditions and other stress factors in this working area frequently leads to complaints

about skin irritation and poor comfort in wear.

The medical textile company Wozabal, Lenzing, Austria, has introduced a new standard material of 70 % lyocell (Tencel®) / 30 % polyester. Doctors and nurses confirm that these blended fabrics show greatly improved wear properties compared to the conventional materials.

Textile Hygiene

A multitude of micro-organisms can be found on the skin, forming the skin flora essential for human health. In case of strong perspiration, the sweat transports these organisms into the textiles, where

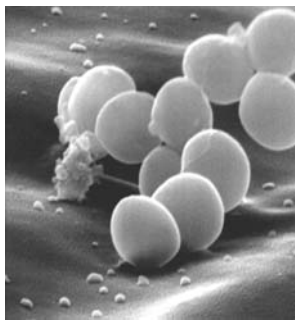
components of the sweat are decomposed by the micro-organisms. In the course of these reactions substances such as butyric acid are formed, which are perceived as the unpleasant smell of perspiration.

Assessing Bacterial Growth on Textiles

The well-known "challenge test" method to determine bacteria growth on textiles was further developed at the University of Innsbruck under the leadership of Prof. Redl. In the challenge test based on to the Japanese standard JIS1902L, *Staphylococcus aureus* bacteria is cultured in a growth medium that simulates perspiration. A known number of bacteria in growth medium is then transferred to the

textile samples in a dilution to obtain a moisture content of 50%, and incubated at 37° C for 24 hours. Then, the bacterial growth is determined.

On synthetic materials, it is found that bacterial growth is higher by a factor of 100 to 1000 as compared to lyocell. On cotton, the growth is still higher by a factor of 10, as compared to lyocell.



Staphylococcus aureus

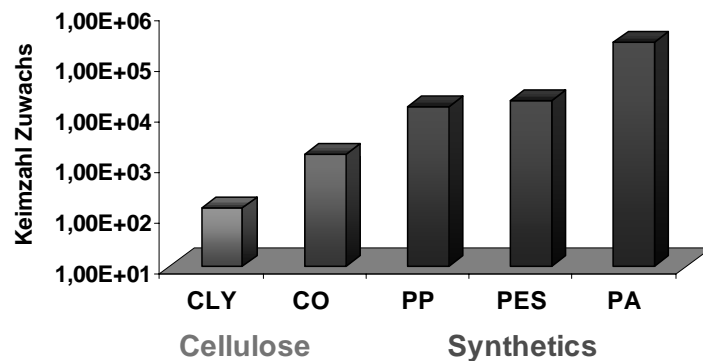


Figure 14. Increase in bacterial counts (logarithmic scale) during the Challenge Test. A comparison of cellulose fibers and synthetics (Redl, 2004)

The considerably higher growth on synthetic fibers may be regarded as the responsible cause for the well-known stronger odor formation. The clearly reduced growth on lyocell, as compared to synthetics, can be explained by the behavior of the fiber towards water (Fig. 5). The water on the surface of synthetic fibers is fully accessible to micro-organisms. In lyocell materials, the water becomes

absorbed almost entirely into the fiber and therefore offers only little life-sustaining basis for the micro-organisms. The higher growth on cotton is due to the coarser surface, to which bacteria may cling better, and to the higher content of residual components (cotton wax and harvesting residuals), which serve a additional nutrient source.

Electrostatic Charge

The surface friction of materials results in electrostatic charge, caused by a separation of the electric charge. The amount of charge built up depends on the friction intensity, the conductivity, the capacity and the ranking of the materials in the "triboelectric series".

Electrostatic charge does not only influence the processing of the fibers, but also has an impact on the wearing properties of the textiles. In practice, the unpleasant effect of

electrostatic charge is the spark that spurts via the hand to the door handle, or the hair-raising effect when taking off garments made of synthetic materials.

The electrostatic effect of textiles depends primarily upon the moisture in the fabric and thus conductivity and/or resistance. The conditioning moisture of lyocell fibers is approximately 13%. Polyester fibers are not hygroscopic and have conditioning moisture of approximately 1% and thus a considerably lower conductivity.

Electric Resistance of Lyocell and Polyester Fabrics

The conductivity of textiles depends upon their moisture contents. In standard climate with 65% RH, lyocell fabrics with 6.8×10^7

Ω show a clearly lower resistance, as compared to polyester tissues with 5×10^{13} Ω . According to the Protective Clothing Ordinance, noticeable electrostatic charging appears as of $10^9 - 10^{10}$ Ω .

	Electric contact resistance [R _{DT}] Ω	
	Climate 23°C / 25% RH	Climate 22°C / 65% RH
Lyocell	4.5×10^{10}	6.8×10^7
Polyester	5×10^{13}	5×10^{13}

Table 5. Electric contact resistance according to DIN 54345 for lyocell and polyester fabrics, source: Austrian Textile Research Institute

Triboelectric Series of Materials

The ranking in the triboelectric series helps to define the character and intensity of electrostatic charge.

+ positive charge	Human skin Human hair Polyamide Wool
neutral	Cotton Rayon (Viscose) Polyester
- negative charge	Acryl Polyethylene

Figure 15. Ranking of selected materials in the triboelectric series (Allen, 2000)

Electrostatic Charge of the Human Body from Textile Friction

The potential that is caused on the human body on account of textile friction on the skin was measured at the Austrian Textile Research Institute. For this purpose, knitted fabric materials were drawn over the shoulder under identical conditions in a standard climate, in order to simulate removal of a garment. The generated tension was measured by means of a hand electrode, which is used in a modified test

arrangement to determine the electrostatic behavior of wall-to-wall carpeting according to DIN 66095. For polyester and polypropylene a positive potential of 3000 Volt was measured. On account of the higher conductivity due to fiber moisture, cellulose has almost no charging. From a charge of 1800 to 2000 Volt and higher, noticeable sparks appear when discharge occurs on grounded objects.

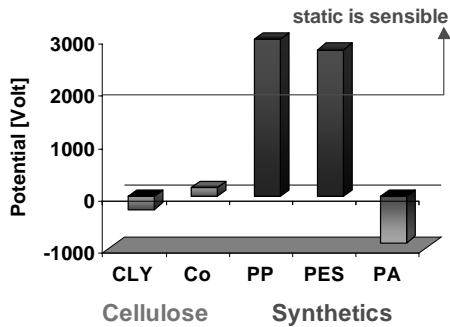


Figure 16. Electrostatic charge of the human body after a friction experiment with textiles

Source: Austrian Textile Research Institute

Acknowledgements

Special thanks to the Wozabal company, Lenzing, Austria, for results on comfort in wear; to all the colleagues in Lenzing, especially Marina Crnoja-Cosic, Rosemarie Hinterleitner, Egon Dünser, Johann Gruber, Thomas Podluczky.

References

- [1] Allen, R.C.: Triboelectric Generation, 2000
- [2] Austrian Textile Research Institute, Ing. Peter Trappl, Physiological and Electrostatic Tests.
- [3] Diepgen, T., Dermatological Examinations on the Skin Compatibility of Lenzing Lyocell textiles. Lecture & Proceedings, Int. Man-Made Fibres Congress Dornbirn, 2004
- [4] Eichinger, D., P. Bartsch, P. Schafheitle, C. Kreuzwieser, Proc. Int. Man-Made Fibres Conference Dornbirn, 1998
- [5] Ernst, M., / Planck, H.: Garment-Physiological Investigations on the Construction of Functional Knitwear.

Summary

The nano-fibrillary fiber structure of lyocell and the resulting ability to perfect moisture management, the smooth surface and the purity of the fiber, which is due to the environmentally friendly production process, result in superior properties regarding wearing physiology. Lyocell, a basic textile material, satisfies the requirements for the temperature regulation of the human body, for skin sensitivity, hygiene and electrostatic behavior, on account of its natural construction and the associated properties, when compared to other fiber materials.

Lyocell is a textile fiber which – both in 100% applications and as partner in textile blends – has a clearly positive influence on the comfort in wear of textiles

ITV Denkendorf, Maschenkolloquium, June 2004

- [6] Michna, H., M. Schönfelder, Technical University of Munich, Chair for Sports and Health Promotion: Physiology Lecture, winter semester 2003/2004
- [7] Redl, B., University of Innsbruck, unpublished results
- [8] Research Institute Hohenstein: unpublished textile physiology measurements
- [9] Schuster, K. C., H. Firgo, F. Haussmann, and J. Männer, D. Eichinger, Lecture, Int. Man-Made Fibres Congress Dornbirn, 2003
- [10] Schuster, K.C., H. Firgo, F. Haussmann, and J. Männer, Proc. of the Textile Institute 83rd World conference, Shanghai, May 2004, 422 - 426
- [11] Schuster, K.C., P. Aldred, M. Villa, M. Baron, R. Loidl, O. Biganska, S. Patlazhan, P. Navard, H. Rűf, and E. Jericha, Lenzinger Berichte 82 (2003), 107-117
- [12] Thumm, S., International Textile Bulletin Jan. 2000, p.60

HOME TEXTILES WITH FEEL GOOD FACTOR DERIVED FROM WOOD

K. Christian Schuster, Heinrich Firgo, Fritz Haussmann, and Johann Männer

Contribution to the Textile Institute 83rd World Conference, Shanghai, China, 23.-27. May, 2004
Lenzing AG, Dept. of Textile Innovation , A-4860 Lenzing, Austria, Europe. c.schuster@lenzing.com,
h.firgo@lenzing.com

Well-being indoors is becoming more and more important. Textiles can improve the indoors climate substantially. In home textiles, Lenzing Lyocell® is particularly suitable to generate comfortable sleeping conditions in beds, and to balance the room climate. Also in clothing textile applications, Lenzing Lyocell® contributes to well-being

by its properties of cool, smooth and dry feeling, and the natural ability to minimise growth of microbes. Even for persons with sensitised skin, Lenzing Lyocell® offers improved comfort.

Keywords: *fibre, home textiles, lyocell*

A Healthy indoor environment AS an important well-being factor

More people than ever spent most of their time indoors. Therefore, the indoors environment is of increasing importance for quality of living. Formerly, natural materials like wood, clay and natural fibres were used a lot in building, often helping to produce a comfortable room climate. Today, unnatural building methods and the excessive use of artificial materials can lead to an extremely unhealthy climate in our homes and offices. Therefore, the factors influencing the well-being of dwelling become more and more important, as studied in the new science discipline “biology of housing” or “physiology of dwelling”.

Not only building materials and furniture can add to a healthy housing environment, but also textiles influence strongly our indoors well-being , i.e. on

- micro-climate, room-climate (temperature, humidity)
- sensorial comfort
- hygiene (dust mites, mildew, bacteria, pollutants)
- optical appearance (design, colours...)

Feelgood factors for the indoor environment
Most of us spent about one third of their lifetime in bed. Therefore, the “physiology of the bedroom” is a major well-being factor. The textile components for bedding play an important role in this context. For this purpose the complete Lenzing Lyocell® bed derived from wood is available:

- Duvets - Filling and covers
- Pillows - Filling and covers

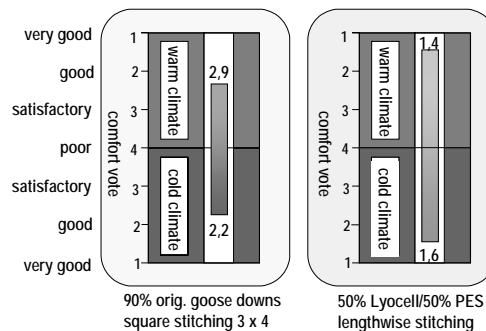


Figure 1. Duvets - comfort votes (Umbach. 2003)

- Bed linen, fitted sheets
- Mattress tickings and mattress fleeces
- Pyjamas

Lenzing Lyocell®: In Summer Cool and Dry, in Winter Warm ?

Lenzing Lyocell® as a filling fibre offers a very broad comfort range in duvets (Umbach, 2003). Compared to a goose down (90%) filled duvet, the range of comfort in a lyocell/polyester (50%/50%) filled duvet is larger not only in the in a warm climate, but also in a cold climate. So, Lenzing Lyocell® filled duvets are good to very good in summer and winter. The comfort votes (1 – very good, 5 – poor) were calculated from textile physiological measurements. We approach here an explanation for this outstanding behaviour.

Textile Physiological Measurements

Filling	µCL Y	CLY	CLY/ PES	PES	Wool	Down
I _{mt}	0,70	0,58	0,53	0,36	0,58	0,50
R _{ct} /mm	30,5	25,2	23,0	15,8	21,5	19,1

Table 1. Water vapor permeability (I_{mt}) and thermal resistance (R_{ct}) of duvets with various fillings (Measurements at the Hohenstein Institutes, Germany)

Table 1 shows for Lyocell Fill ® better water vapour transport properties than PES fillings. Fibre blends like CLY/PES and CLY/PLA (polylactate) show fairly good performance. Lyocell Micro® even excels the natural materials wool and goose down. At comparable thickness of duvets, Lyocell Fill® has better thermal insulation properties than PES, wool and even goose down.

Micro-climate in Bed Tested with Test Persons

A comparative study was done in 3 different beds using various fibre materials (Helbig, 2003) with test-persons who tend to sweat more than the population average. Lenzing Lyocell® exhibited the driest climate in the sleeping cave and close to the body (Table 2). When the temperature-humidity index (NWS–USA, web) is calculated as a measure for the apparent (felt) temperature,

taking into account that humid air is felt warmer than dry air in this temperature range, the apparent temperature in a Lenzing Lyocell® bed is lower and closer to the body temperature due to the lower humidity.

		Standard bed	PES bed	Lenzing Lyocell® bed
Beds	Mattress: Fabric / Filling	Cotton / PES	PES /	CLY blend / CLY blend
	Bedlinen Duvet / Pillow: Filling / Cover	Cotton / PES / Cotton	PES / PES /	µCLY / CLY FILL / µCLY
Results	Humidity in sleeping cave (%)	50,8	48,5	43,5
	humidity close to the body (%)	47,5	44,5	39,3
	Temperature close to body (°C)	36,3	36,1	36,6
	Apparent T close to body (°C)	42	42	39

Table 2. Beds used for sleeping trials, and results

Water Vapour Absorbing Lenzing Lyocell® Water Vapour Absorption of Lyocell

The water vapour absorption of Lyocell is similar to wool over the whole range of relative humidities, and clearly exceeds cotton (Figure 2). In comparison, polyester shows a very poor moisture absorption capability. This feature will have a great influence on the room climate when Lenzing Lyocell® textiles are used.

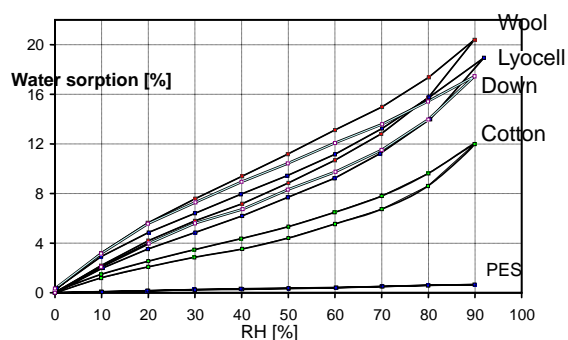


Figure 1. Water vapor absorption isotherms

Effect of Home Textiles on the Room Climate

Especially modern “low energy – high insulation” building techniques can lead to humidity problems. Human water vapour production is not a negligible factor in cool rooms (e.g., sleeping rooms), if no water absorbent material is present.

Too high air humidity in a cool sleeping room may lead to an uncomfortable sleeping climate, water condensation on cold surfaces and therefore can cause mildew growth, and enhanced growth of dust mites. An example for the development of humidity in a closed room over night is given in Figure 2. At a low air exchange rate, the humidity exceeds the

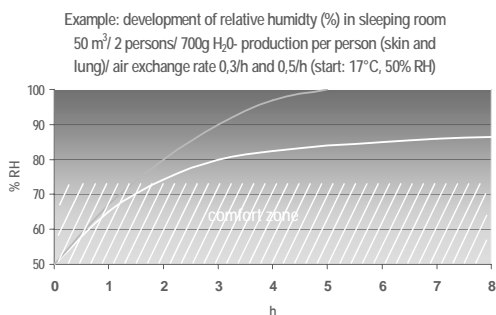


Figure 2. Calculated humidity in a bedroom over night. Air exchange rates top: 0,3 / h, bottom: 0,5 / h

comfort zone after only a few hours. Later, the humidity reaches 100 %, leading to condensation somewhere in the room.

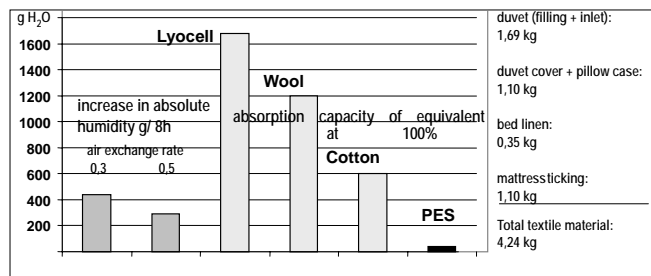


Figure 3. Humidity balance in a bedroom as Figure 2

Lenzing Lyocell® beds can help to prevent this problem (Figure 3): A complete Lyocell bed contains about 4 kg of textile material, which can absorb the respective amounts of moisture. In case of Lyocell, the increase in absolute humidity is easily buffered by the absorption capacity of the bed. A polyester bed is not able to absorb the excess moisture.

When the bedroom is equipped with a Lenzing Lyocell® containing carpet, the moisture buffering in the room will further be improved.

Heat of Sorption as a Feel-Good Factor?

Why are Lenzing Lyocell® duvets in summer cool and in winter warm? A key may be found in the heat of sorption of water vapour. For wool, it is well described that heat of sorption plays a major role in the heat buffering capacity of textiles (Morton et al. 1962). Literature data suggest this also for Lyocell (Mizutani et al., 1999).

We measured sorption isotherms at two temperatures (20 °C and 36 °C). The difference in vapour sorption at a certain relative humidity is a direct measure for the heat of sorption. In medium humidity, for Lyocell the difference is similar to wool, at high humidity even higher.

From these data, the differential heat of sorption can be calculated (Morton et al. 1962). The overall heat released when a fabric is transferred from low to high humidity air includes the heat of condensation of the respective amount of moisture. The total heat released correlates roughly with the moisture regain. However, there are exceptions; some Lyocell types show very high heat of sorption.

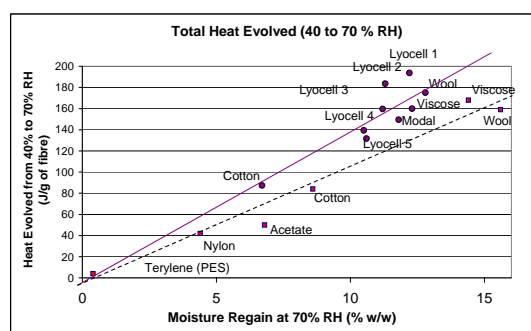


Figure 5. Total heat evolved when various fibres are transferred from 40 to 70% rH. ●, our data

A hypothesis can be formulated:

In winter, in cold conditions at low starting humidity the fibres recycle latent heat from moisture by absorption of water vapour released from the body. The cooling effect of de-sorption mainly takes place in the upper region of the duvet, therefore it does not affect the body temperature very much (direction of convection is upwards).

In summer, in warm conditions and at high starting humidity the body is cooled by the energy needed for desorption of water in the lower region of the duvet. The high water vapour permeability index of Lenzing Lyocell® results in permanent good cooling by insensitive (not noticeable) perspiration.

Feelgood factors in clothing textile applications

Cool Feeling

The well-known “cool” feeling of Lenzing Lyocell® can be quantified by the Alambeta method (Hes, 2002). The measured values of thermal absorptivity correlate with a cool feeling or touch of textiles; a higher thermal

absorptivity means a cooler feeling of the fabric. Lyocell feels cooler than cotton. This is explained in a first approach due to the higher moisture content of Lyocell at a given relative humidity.

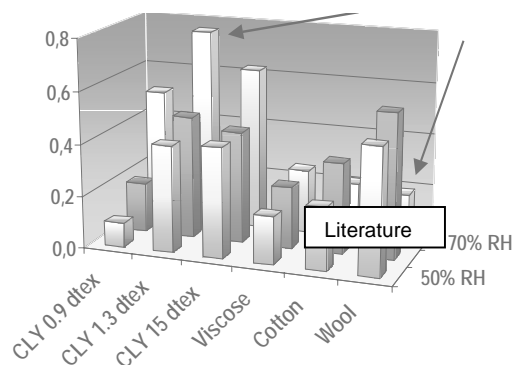


Figure 6. Difference in vapour sorption at 20°C and 36°C and 50, 60 and 70% rH

Bacterial Growth and Odour

It is generally accepted that unpleasant odour of worn textiles is mainly produced by decomposition of sweat by bacteria. Therefore, a reduction of bacterial growth

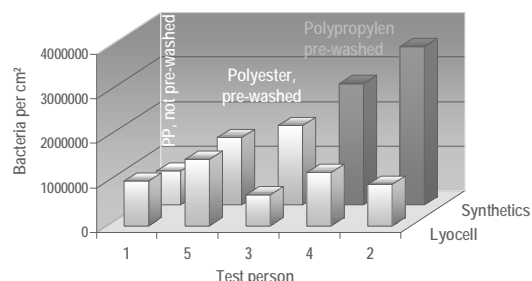


Figure 7. Bacterial growth on T- shirts in a wearing trial

on a textile will lead to lower odour development. One approach to this problem is antibacterial finishing of textiles.

In a comparative wearing trial, test persons wore T-Shirts sewn together from halves of commercial T-Shirts of varied materials. The exercise was 4 hours fast walking at moderate temperature (15 to 18 °C). The T-shirts halves were analysed for bacterial growth by extraction and DNA analysis.

Lenzing Lyocell® T-shirts showed lower bacterial growth than corresponding polyester and polypropylene sports wear, leading to less odour formation. 4 of the 5 synthetic materials samples were pre-washed (5 times at 95 °C); the exception is the non pre-washed PP material, indicating that this contains a antibacterial finishing, though this was not declared on the package. The antibacterial activity of the commercial shirts was confirmed by the challenge tests.

Lenzing Lyocell®: Smooth, Cool, and Dry Relief for patients suffering from neurodermitis and psoriasis

A clinically supervised study was conducted by Prof. T. Diepgen, University of Heidelberg/Germany. 60 Patients suffering from Neurodermitis and Psoriasis tested commercially available Lenzing Lyocell® textiles: 100% Lyocell bedding (duvets, covers, bedlinen, sheets), and clothing from 70% Lyocell / 30% Cotton (T-shirts, Polo-shirts, Pyjamas). As a control, patients used their own clothing and their own bed textiles. A generally accepted “objective standard” is not available, as neurodermitis and psoriasis are complex syndromes with individually differing symptoms. Adult patients have individually optimised their textile use for decades, providing the toughest possible control.

		Acceptance of Lenzing Lyocell® textiles		
Patients with	Total	Worse	Equal	Better
Neurodermitis	14	0	2	12
Psoriasis	19	1	1	17

Table 3. First results of wearing trials with lyocell textiles, as compared to the patient's usual textiles

The test period were conducted over one week for each set of textiles. Development of the symptoms was evaluated by initial and final diagnosis, and daily protocols.

The preliminary results of 33 patients show that the Lenzing Lyocell® textiles help nearly 90 % of the patients to a great improvement in the symptoms. Details of the study have been published in the meantime by Diepgen and Schuster (2004)

A fibre structure model for Lyocell

From the results of earlier structure characterisation approaches, and the water swelling and vapour sorption behaviour of Lyocell, the individual fibre can be considered as a hygroscopic nano-multifilament: It consists of countless hydrophilic, non swelling, highly crystalline micro- or nano- fibrils. Swelling occurs in the non-crystalline but highly ordered regions, capillaries and voids between the fibrils.

Conclusions

- Bedding materials of Lenzing Lyocell® lead to pleasant micro climate in bed and exhibit a very broad comfort range: dry and warm in winter, dry and cool in summer
- Home textiles made of Lenzing Lyocell® derived from wood can add to a dry, comfortable and healthy room climate

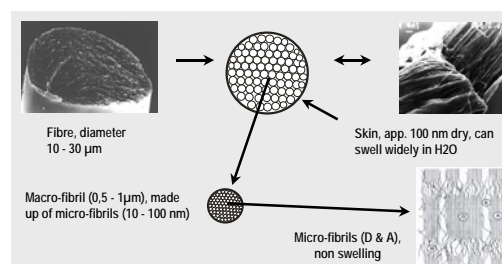


Figure 8. A fibre structure model for Lyocell

- Regulation of air humidity restricts growth of dust mites and mildew
- Lenzing Lyocell® brings hygiene into our homes: Less growth of bacteria and less odour formation
- Clothing textiles made of Lenzing

Lyocell® have extremely good sensorial properties: cool, smooth and dry

References

- Diepgen, T., and Schuster, K.C., Dermatological examinations on the skin compatibility of Lenzing Lyocell textiles . 43rd International Man-made Fibres Conference, Dornbirn, Austria, Sept. 2004
- Helbig, K., 42nd International Man-made Fibres Conference, Dornbirn, Austria, Sept. 2003
- Hes, L., World Congress of the Textile Institute, Cairo, March 2002
- Morton, W.E.; Hearle, J.W.S.; 'Physical Properties of Textile Fibres' , Chpt. 8-Heats of Sorption, 1962, pp. 178-185. 3rd ed., The Textile Institute, 1997
- Mizutani, C; Tsujii, Y; Bertoniere, N; Textile Res. J., 1999, 69(8), 559
- National Weather Service, USA (<http://www.crh.noaa.gov/arx/heatindex.html>)
- Umbach, K.H., Lenzing AG customers' meeting, Fuschl, Austria, May, 2003

Acknowledgements

The authors wish to thank Dr. Peter Aldred, Dr. Satoko Okubayashi of the CD Laboratory for Chemistry of Cellulosic Fibres & Textiles, Dornbirn, Austria; Prof. Bernhard Redl and Linda Teufel, University of Innsbruck; Dr. Sigrid Redlinger, Lenzing AG, and the Christian Doppler Research Society, Vienna

TREATMENT OF CELLULOSIC FIBERS WITH SUPERCRITICAL CARBON DIOXIDE

Gregor Kraft¹, Christoph Muss¹, Christian Adelwöhrer², Thomas Rosenau², and Thomas Röder¹

¹Lenzing AG, R&D, A-4860 Lenzing, Austria, E-mail: g.kraft@lenzing.com

²University of Natural Resources and Applied Life Sciences - Vienna (BOKU),
Christian-Doppler-Laboratory for Pulp Reactivity, Muthgasse 18, A – 1190 Vienna, Austria

Supercritical carbon dioxide has become a tool for various applications and different substrates. The introduction of active substances into cellulosic fibers with the usage of supercritical carbon dioxide is of interest in this study. Particularly, the distribution of D-panthenol all over the cross sectional area of the cellulosic fiber after the treatment with supercritical carbon dioxide was investigated closely.

The impregnation and incorporation of D-panthenol was not successful for example by bathing or steaming, even when never dried Lyocell fibers are treated in a solution of the active components.

Therefore further experiments were performed with supercritical carbon

dioxide at NATEX Prozeßtechnologie, Ternitz, Austria.

We could determine only a small increase of the absorption abilities of Lyocell fibers by supercritical drying. Contrary to our expectations there was no benefit with regard to the water retention. The incorporation of D-panthenol in cellulosic fibers, however, could be performed successfully with this method, which could be confirmed with Raman spectroscopy.

Keywords: *Lyocell fibers, Viscose fibers, supercritical drying, supercritical carbondioxide, D-panthenol*

Introduction

The treatment of different compounds with supercritical carbon dioxide started as a pure laboratory method. Within the last years it has reached a high acceptance and has been implemented in different technical processes. The probably most common application is the extraction of natural essences, particularly the production of decaffeinated coffee and tea.

The impregnation of wood products with supercritical carbon dioxide has been established recently. Furthermore, cellulosic

material has been treated with it mostly for extraction and dyeing¹⁻³).

This new technology has the advantage of working without any additional solvent. Additionally there formed no waste products, which have to be disposed, by applying this method. In other words, the supercritical carbon dioxide treatment could be a key technology for an environmental friendly industrial process.

The main focus of this investigation was on fibers produced by the NMMO process⁴).

This method simplifies the production of cellulosic fibers by dissolving the cellulose in NMMO without any chemical modification of the cellulose. The feature of the NMMO process is a closed water circuit with an extremely high recovery rate of the solvent. Additionally, the NMMO is a biodegradable, nontoxic substance.

This study investigates the application and incorporation of D-panthenol, a widely used substance especially for wound healing⁵⁾, in cellulosic fibers with supercritical carbon dioxide and its final distribution over the fiber cross-section. Therefore the treated fibers were scrutinized by Raman spectroscopy.

Supercritical drying of Lyocell fibers

The adsorption of the water is a significant ability of the fiber, which is correlated to its pore structure. Unfortunately, the originally existing fiber pores collapse during the conventional drying process. Consequently, the water retention decreases during this process.

It is known from aerogels, that the original porosity does widely remain unchanged when supercritical drying after solvent exchange is performed. Normally, the water is replaced by acetone to avoid the collapse of these pores during the supercritical drying. Therefore, it should also be possible to increase the absorption abilities of Lyocell fibers clearly by the supercritical drying process.

The investigations, done by P. Aldred⁶⁾, showed an increase of 30% in the water retention of Lyocell fibers comparing supercritical CO₂ drying to the conventionally oven dried Lyocell fiber.

The verification of these results principally confirmed the results mentioned before.

We also found an increase of the water retention ability of approximately 20% compared to a conventional oven dried fiber

performed on a Lyocell fiber with different properties.

Primarily, this is a very encouraging result. If the water retention ability of the supercritical dried fiber is compared with a never dried or air dried fiber the experiment, however, gives fairly disappointing and unexpected results.

The increase of the relative adsorption capacity from 102% in case of air dried up to only 106% by supercritical drying and is therefore only marginal (Fig. 1).

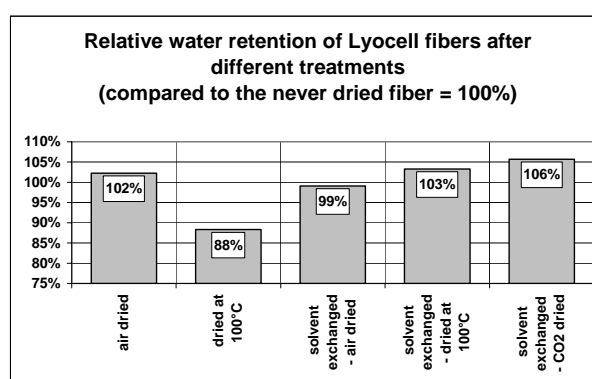


Figure 1. Relative water retention of Lyocell fibers

Incorporation of biological active substances into a cellulosic fiber

Introducing the technique of supercritical fluids can very likely increase the number of incorporable compounds in an environmental friendly way. The usage of supercritical carbon dioxide may open the door for several compounds, especially biologically active, hydrophobic substances, which are so far not utilizable by the classical incorporation technologies.

Naturally there is an overwhelming choice of active compounds available like plant extracts, vitamins, perfumes/scents or even flame retardants.

The analysis of these complex natural products is anything but simple. Therefore we started the investigations in that field by using pure active substances like D-panthenol. This compound was selected

because of its rather simple structure and the fact that it can be easily determined and well observed by Raman spectroscopy.

The Raman measurements were performed with a HoloLab Series 5000 Modular Raman Spectrometer (HL5R) from Kaiser Optical Systems Inc. (USA) equipped with f/1.8 optics, transmission grating, multichannel CCD array detector (optimised for NIR), and a 785 nm diode laser (500 mW) coupled via single mode fibre to the microscope (approximately 80 mW on the sample). Between microscope and detector, a confocal fiber with a pinhole of 20 μm was used. With the 100X objective the lateral resolution was about 1-2 μm .

Raman was used to track the concentration distribution of D-panthenol within a single cellulosic fiber. This method allows determining the active component within the cross section of a single fiber. Figure 2 shows the selected measurement points over the cross section of a Lyocell fiber after the supercritical incorporation of D-panthenol.

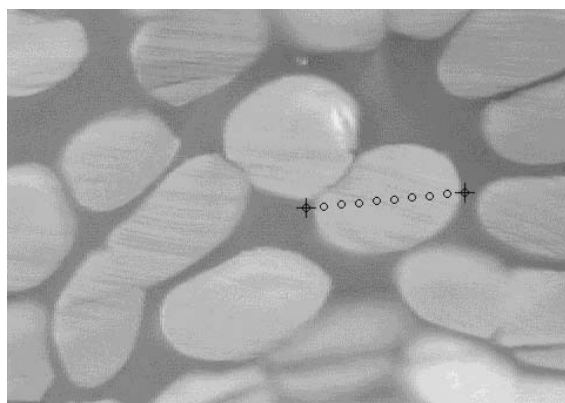


Figure 2. Selected measurement points within one fiber.

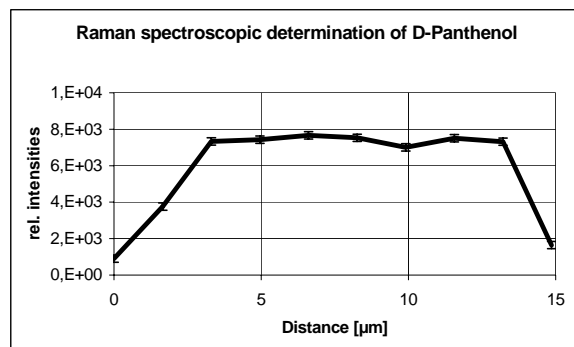


Figure 3. Distribution of D-Panthenol along the cross section of a single Lyocell fiber

The result of the Raman microspectroscopic investigation of the treated fibers showed that the incorporation of D-panthenol was successful. This, however, is depending on certain characteristics of the used fibers. Figure 3 shows the D-panthenol distribution across the processed Lyocell fiber. This is indicated by the relative intensities of the correlated Raman bands between $795.6 - 820.2\text{cm}^{-1}$. The amount of the active substance is clearly lower at the edge of the fiber cross section than it is in the center of the fiber. We assume that the substance is washed off at the end of the treatment, when the supercritical fluid is removed from the autoclave.

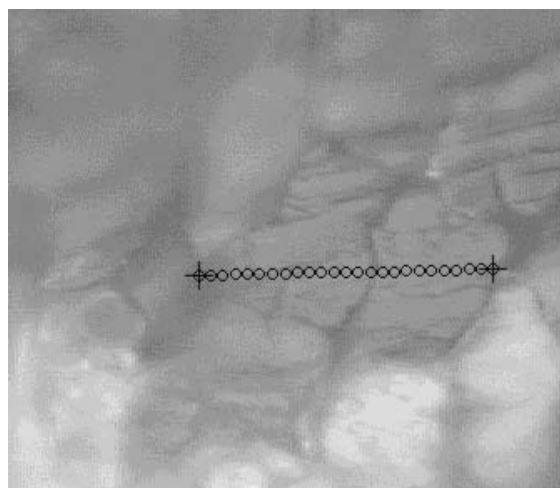


Figure 4. Selected measurement points within the cross section of two ZS-Viscose fibers

The incorporation can not only be performed with Lyocell fibers but the experiments can be transferred to a common ZS-Viscose fiber as well and gives similar results (Figure 4 & 5).

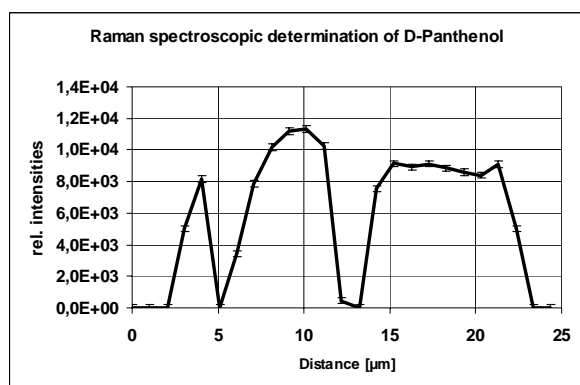


Figure 5. Relative intensities of the corresponding Raman band of the selected measurement points showed in figure 4 (ZS-Viscose fiber)

Principally, it is possible to incorporate active substances into a cellulosic fiber by using the supercritical carbon dioxide technology.

The permanence of the incorporated active compound is a key criteria for the practical use. It is necessary to investigate if the incorporated substance will be washed out or can resist the common laundry.

A practical test performed in a commercial washing machine (40°C) gave the following results. The fibers contained no more D-panthenol after washing. This raised the question if this behavior is specific for D-panthenol, or universal for all possible incorporated compounds. Further experiments will be necessary to answer to this question.

Alternatively, there might be an opportunity to impregnate or even incorporate the fibers with D-panthenol by treating never dried fibers with aqueous D-panthenol or Ca-pantothenate solutions, respectively.

Surprisingly, only a very small amount of D-panthenol / panthothenate could be found in

the fiber. The highest concentration of the active substance, is located on the surface but cannot be determined quantitatively with the Raman analysis. Furthermore steaming was applied to the fiber, which is normally a useful way to impregnate Lyocell fibers. It, however, was not successful in this case. So far our conclusions are that the only way to incorporate D-Panthenol into a cellulosic fiber is the supercritical carbon dioxide treatment.

Economical aspects

The easy removal of D-panthenol from the fiber during one washing cycle predestined this product for a single use application. This one time usage could be an interesting application in the medical field of wound healing. Furthermore a slow release of the active substance could be an additional benefit for this application. First trials performed at BOKU showed a slow release effect of D-Panthenol out of the fiber, but clearly more experiments are necessary. Unfortunately, the expected costs of the supercritical incorporation of the active compounds are still in the range of €2 per kg fibers, which is far too expensive for an economically application. This process can only become interesting for industrial usage, when high value products can be manufactured or the process itself will be optimized and therefore becomes cheaper.

Acknowledgements

I want to thank Mr. E. Lack and Mr. M. Sova from NATEX Prozesstechnologie, Hauptstr. 2, A-2630 Ternitz, Austria, for performing the supercritical CO₂ experiments.

References

- [1] Lindstroem, Eva et al.; "Treating cellulose fibers with supercritical fluids for fibers with reduced content

- of wood extractives and increased absorption rate and products comprising the fibers therefrom”, EP1205598
- [2] Schlenker, Wolfgang et al., Process for dyeing cellulosic textile material with disperse dyes, US5298032
 - [3] Schollmeyer, E. et al., Färbeverfahren, DE3906724
 - [4] Firgo H., Eibl M., and Eichinger D., Lyocell an ecological alternative, Lenzinger Berichte 1995, 75, 47-50
 - [5] Hagers Handbuch der Pharmazeutischen Praxis, 4. Aufl., 9. Bd., Berlin: Springer 1933-1995
 - [6] Aldred, P., internal report, 2003